University of Nottingham

UK | CHINA | MALAYSIA

Department of Mechanical, Materials

& Manufacturing Engineering

Study on flame retardancy and interfacial properties of plant fiber reinforced epoxy resin composites

Liyue Zhang

Student ID：20319752

Supervisors：

Prof. Xiaosu Yi

Prof. Ping Cui

October 9th, 2024

Abstract

With the exacerbation of environmental deterioration and resource crisis, reducing energy consumption and mitigating environmental impacts have become a consensus aims for ecological industry and sustainable social development. As representative products of green manufacturing technology, green composites not only have a reputation for their renewable fabrication and environmental friendliness, but also feature advantages such as low price, lightweight, and high specific strength, which make them promising candidates for application in various important end-uses including aerospace, construction, and transportation with a growing trend. Unfortunately, plant fiber-reinforced epoxy resin composites are beset by poor interfacial compatibility between the plant fabric and epoxy resin due to the hydrophilicity of plant fiber and the hydrophobicity of epoxy resin. The phenomenon of lamination and fracture is easy to occur when the material is subjected to load under the poor interfacial compatibility, which restricts the further development and application of the plant fiber reinforced epoxy resin composites. Additionally, the high flammability, due to the presence of flammable fibers and epoxy resin, is another obstacle in the development of the composites and limits their applications. Consequently, studying on how to effectively improve the flame retardancy of the composites has become a goal pursued by industry

and researchers. Regrettably, there are difficulties in establishing a balance between flame retardancy and interfacial performance.

In this way, multi-functional modifier that can simultaneously improve mechanical and thermal performance is significant for composite production. On the basis of reviewing the research progress on flame retardants and interface modification of epoxy resin composites, and aiming at addressing the fire risk and poor interface compatibility of plant fiber/epoxy resin composites, this thesis designed and synthesized three kinds of modifiers for flame retardant plant fibers from the perspective of compound design. The effects of different modifiers on the flame retardancy and mechanical properties of the composites were studied, with the aim of achieving plant fiber-reinforced epoxy resin composites with both flame retardant properties and satisfactory mechanical performance. In addition, TG-IR, SEM, and Raman spectroscopy were used to study the flame retardancy mechanism. The application of the three modifiers to the flame retardancy and interfacial properties of plant fiber-reinforced epoxy resin showed remarkable innovation. The specific information for each part of the work is as follows.

To begin with, inspired by the chemistry of mussel, an interfacial modifier named FPD was designed and synthesized through one simple step, which were attached by three functional groups (i.e., catechol, N-H bond and DOPO). Due to the innate properties of each functional group,

FPD played multiple roles: adhere to the ramie fiber through catechol, cure with the epoxy resin from -NH-, provide antiflaming property from DOPO. Moreover, the compatibilizer between ramie fiber and epoxy resin was also improved by changing the polarity of ramie fiber. All of the above functions were proved by means of water contact angle (WCA), atomic force microscope (AFM) and scanning electron microscopy (SEM) *etc*. After solidification, the ramie fiber-epoxy composites demonstrated superior performances in terms of good mechanical properties and excellent flame retardant property. With the addition of 30 wt.% FPD, the tensile strength and modulus of the ramie/epoxy composite showed an improvement of 37.1% and 60.9%, flexural strength and modulus of the composite were improved by 8.9% and 19.3% comparing with no addition composite. Moreover, the composite could achieve the goal for V-0 rating in the UL-94 test and limiting oxygen index (LOI) value was 34.6% when the addition of FPD reached 30 wt.%. This work provided us with efficient methods for fabricating nature fiber/epoxy composites with good properties.

Secondly, a combined modifier consisting of a water-soluble benzoxazine (HGB) with high carbonization and phytic acid (PA) containing phosphorus elements and acid groups was devised to treat the regenerated cellulose fabric (SF). The treated fabric (F-SF) not only could realize self-extinguishing from the fire which helps to avoid the

wick effects, but also exhibited an optimized interfacial property of composites. After being combined with an intrinsic flame-retardant epoxy resin (F-EP), the composite material (F-SF/F-EP) achieved a V-0 rating in the UL-94 test and an excellent LOI value of 33.8% due to the flame-retardant effect in both the gaseous phase and condensed phase. Simultaneously, benefiting from the improved interfacial compatibility, both tensile modulus and impact strength were enhanced from 9.82 GPa and 6.58 MPa to 11.29 GPa and 7.21 MPa, respectively, compared with untreated SF/EP composite, especially the interlaminar shear strength (ILSS) dramatically increased by 21.7%.

Finally, in view of the damage of phytic acid to ramie and Suncell fabric found in the last chapter, imidazole phytate was synthesized via a simple one-step strategy to replace phytic acid. Imidazole phytate retained the high phosphorus content of phytic acid, changed the strong acidity of phytic acid, and caused less damage to the mechanical properties of plant fiber. At the same time, as the accelerator of epoxy resin curing, imidazole can reduce the curing temperature and curing time of epoxy resin, shows high thermal stability and good compatibility with EP matrix. Like last chapter, PAIM and arbutin benzoxazine to form an expansive flame retardant in order to make the composite material achieve flame retardant effect and maintain its mechanical properties to a certain extent. The modified fabric was further used to reinforce

DGEBDB composites through a vacuum bag-assisted compression molding process, which could improve interfacial adhesion and fire safety of the regenerated cellulose fabric/epoxy composite in the simultaneous. After combining with an intrinsic flame-retardant epoxy resin (F-EP) and benefiting from the improved interfacial compatibility, both the tensile modulus and impact strength were enhanced from 9.82 GPa and 6.58 MPa to 11.33 GPa and 7.26 MPa compared with untreated SF/EP composite, especially interlaminar shear strength (ILSS) dramatically increased by 19.7%, from 11.41 to 13.66 MPa. Simultaneously, the composite material (F-SF/F-EP) achieved a V-0 rating in the UL-94 test and an excellent LOI value of 34.3% compared to pure composits. The pHRR of F-SF/F-EP achieved about 834.9 kW/m^2, which is decreased by 44.9% relative to 459.9 kW/m^2 of SF/EP due to the flame-retardant effect both in gaseous phase and condensed phase.

This work provided an integrated strategy for synchronously enhanced interfacial compatibility and fire-proof performance of plant fiber-reinforcement composite.

Keywords

Plant fiber reinforced composites, Ramie fiber reinforced epoxy-resin composites, Ramie fiber, Protocatechualdehyde, Co-curing agent, Suncell fabric water-soluble benzoxazine, Interfacial properties, Flame retardant, Self-flame retardant epoxy resin

List of publications

Journal Papers：

1. **Zhang, L.**; Liu, J.; Dai, J.; Zhang, X.; Liu X.; Liu X.; Yi X. Preparation and Application of a Multifunctional Interfacial Modifier for Ramie Fiber/Epoxy Resin Composites. *Polymers.* 2023, 15, 3800. DOI: 10.3390/polym15183800
2. **Zhang, L.**; Liu, J.*; Liu X.; Dai, J.; Liu X.; Yi X*. Water-soluble bio-based modifier towards epoxy/cellulose fabric composite with simultaneous enhancement of flame retardancy and interface adhesion. *ACS Applied Polymers Materials.* DOI: 10.1021/acsapm.4c00338
3. **Zhang, L.**; Liu, J.*; Dai, J.; Liu X.; Liu X.; Yi X*. Achieving all-day freshwater harvesting by designing Janus film combining photothermal conversion and radiation cooling technology. (accepted by Chemical Engineering Journal)
4. **Zhang, L.**; Liu, J.; Dai, J.; Liu X.; Liu X.; Yi X. Non-destructive Modification of Cellulose-based Fabrics in Aqueous Phase for Flame-Retardant Green Composite. (reviewing by Polymer International)
5. Liu, J.; **Zhang, L.**; Shun, W.; Dai, J.; Peng, Y.; Liu, X. Recent development on bio‐based thermosetting resins. *Journal of Polymer Science.* **2021,** *59* (14), 1474-1490.
6. Chen, Q.; **Zhang, L**.; Zhang, J.; Habib, S.; Lu, G.; Dai, J.; Liu, X. Bio-based polybenzoxazines coatings for efficient marine antifouling. *Progress in Organic Coatings.* **2023,** *174*, 107298.
7. Hu, J.; **Zhang, L.**; Chen, M.; Dai, J.; Teng, N.; Zhao, H.; Ba, X.; Liu, X. Synthesis of Hyperbranched Flame Retardants with Varied Branched Chains' Rigidity and Performance of Modified Epoxy Resins. *Polymers-Basel.* **2023,** *15* (2), 449.
8. Chen, M.; Dai, J.*; **Zhang, L**.-Y.; Wang, S.-P.; Liu, J.-K.; Wu, Y.-G.; Ba, X.-W.; Liu, X.-Q. The Role of Renewable Protocatechol Acid in Epoxy Coating Modification: Significantly Improved Antibacterial and Adhesive Properties. *Chinese Journal of Polymer Science.* 2024, 42, 63–72.
9. Wuliu, Y.; Liu, J.*; **Zhang, L.**; Wang, S.; Liu, Y.; Feng, J.; Liu, X. Design of bio-based organic phase change materials containing a "safety valve". *Green Chem.* **2021,** *23* (21), 8643-8656.
10. Zhu, X.; Liu, J.; Yang, K.; **Zhang, L**.; Wang, S.; Liu, X., Structurally engineered 3D porous graphene based phase change composite with highly efficient multi-energy conversion and versatile applications. *Composites Part B: Engineering* **2024,** *272*, 111233.

Patents:

1. 益小苏，**张力月**，孟润生等，一种含磷的水溶型阻燃剂及其制备方法。申请号：202110839793.6 审中-公开

2. 益小苏，**张力月**，孟润生等，一种含磷的溶剂型阻燃剂及其制备方法。申请号：202110838356.2 审中-公开

3. 刘小青，**张力月**，代金月，一种复配型植物纤维阻燃改性剂及其应用。已授权，授权号：CN115613358B

Book Chapter:

Chapter 7: Intrinsically flame-retardant bio-based epoxy thermosets and composites of Non-halogenated Flame- Retardant Technology for Epoxy Resin Thermosets and Composites.

Acknowledgements

First of all, I would like to thank my supervisors, Prof. Xiaosu Yi, Prof. Ping Cui, Prof. Xiaoling Liu and Prof. Xiaoqing Liu from NIMTE sincerely. They have provided me the opportunity to study for my research project, appreciate their generous support, guidance and encouragement to my work and life. I have learned a lot of knowledge, experience and wisdom from them.

Also, I want to thank the support from the staff in composite team, Xiaoye Cong, Saihua Li *etc*., have helped me a lot about my research work. My sincere thanks also extend to my colleagues in campus, Zhao Liu, Chenhao Dong, Dongyuan Hu, Minqiang Jiang, Lu Tong, etc., for their support in lab work. I really appreciate the support from staffs in NIMTE as well. Xinbei Zhu, Yingkang Zhu, Jingkai Liu, Mingxuan Chen, Ming Mu, Zeqi Yu, Linghui Gong, Yehua Jiang, Weiwei Zhao, Jiamei Liu, Guangmeng Chen.

At last, I must thank my parents, they have given me the confidence and support to complete my Ph. D. work.

Abbreviations

AFM: Atomic force microscopy

APP: Ammonium polyphosphate

ATH: Aluminum hydroxide

CCT: Cone calorimeter test

COPR: Carbon monoxide production rate

DDM: 4, 4′- Diamino diphenylmethane

DGEBDB: a kind of self-flame retardant epoxy resin prepared in our own lab

DOPO: 9, 10- dihydro-9, 10-oxa-10-phosphaphenanthrene 10-oxide

DPDDM: a kind of co-curing agent for epoxy resin reported in previous work

EP: epoxy resin

F-EP: flame retardant epoxy resin

FR: flame retardant

FRPC: Fiber reinforced polymer composites

HGB: a water-soluble benzoxazine synthesized in this thesis

HRR: Heat release rate

IFR: Intumescent flame retardant

ILSS: Interlaminar shear strength

IM: imidazole

ISO: International Standard Organization

LOI: Limiting oxygen index

LCA: life cycle assessment

MCC: Micro-scale combustion calorimeter

MTH: magnesium hydroxide

NFRP: Natural fiber reinforced polymer

PA: Phytic acid

PHRR: Peak heat release rate

PSPR: Peak smoke production rate

R_{800}: char yield at 800 °C

RF: ramie fabric

RTM: resin transfer molding

SEM: Scanning electron microscopy

SF: Suncell fiber

SPR: Smoke production rate

T_{d10}: 10% weight loss temperature

TGA: Thermogravimetric analysis

THR: Total heat release

T_{max}: maximum weight loss temperature

TSP: Total smoke production

TSR: Total smoke release

TTI: time to ignition

wt.%: weight percent

List of Contents

List of Figures

List of Tables

Chapter 1 Introduction and literature review

1.1 Introduction

1.1.1 Research background

In recent years, fiber reinforced polymer composites (FRPC), with their excellent designability, easy processing, low density, high specific strength, high specific modulus, fatigue resistance, corrosion resistance and good damping and vibration damping properties, have occupied an increasingly important position in the field of materials and have been gradually applied in aerospace, electronics and electrical, transportation, construction and building materials and other fields, which have played an extremely important role in the national economy and construction[1-2]. At present, commonly used reinforcement materials in the market are mostly high-performance synthetic fibers such as carbon fiber, glass fiber, aramid fiber and so on. However, these fibers have the disadvantages of high processing energy consumption, high density, high price, high pollution and non-renewable[3]. Furthermore, the exhaustion of fossil fuels, raising awareness of the environmental crisis and promoting sustainable practices, has generally compelled scientists and inventors to transition to producing environmentally friendly, biodegradable, and recyclable FRPC[4].

Therefore, in order to cope with the energy crisis and protect the environment, the environmental effects of synthetic fibers might be significantly decreased by using biodegradable and renewable fiber materials such as plant fibers in their manufacturing. Compared with inorganic synthetic fibers, plant fibers are renewable, biodegradable, and rich in variety, with good environmental compatibility, and are less energy-consuming to process, which is in line with the requirements of green environmental protection and sustainable development[5-7]. The composite materials formed by using plant fiber reinforced polymers are environmentally friendly[8-9]. The composite materials reinforced with plant fibers have attracted extensive attention from both domestic and international materials industries, becoming a research hotspot in the field of composite materials. They show promise for a wide range of potential applications such as aerospace, construction and transportation, and even natural fiber-reinforced composite products are gradually replacing glass fiber-reinforced composites in some fields[10-11].

Moreover, the majority of the raw ingredients for fiber-reinforced composites come from agricultural goods. Because of this, their use offers a method for waste disposal, reducing the amount of agricultural residues, and preventing environmental contamination from burning such residues. It also provides a cost-effective alternative for rural and

agricultural areas in underdeveloped nations[12-13]. In this way, the implementation of plant fiber-reinforced polymer composites is advantageous not only for the environment but also from an economical viewpoint.

Regrettably, they encounter certain challenges in practical applications. Plant fibers typically contain hydrophilic substances such as cellulose, while many matrix materials are hydrophobic. One of the challenges associated with plant fiber reinforced composites is the mismatch and poor adhesion between hydrophilic natural fiber surfaces and hydrophobic polymers. The adhesion and compatibility between the fibers and the matrix play a significant role in determining the mechanical properties and durability of the composites. Poor compatibility between fibers and substrates can lead to ineffective interfacial bonding, uneven distribution of fibers in the matrix and the formation of voids during processing. Furthermore, a lack of good interfacial fiber/matrix adhesion can reduce the effective stress transfer from the continuous phase to the fibers that carry loads, compromising the mechanical properties of the composite.

Another key issue with plant fiber reinforced composites is their susceptibility to fire. Plant fibers and polymers are inherently flammable, and their use in composites can pose a fire hazard. Moreover, adding

plant fiber to polymer results in the "wick effect"[14], which means that plant fibers act as conduits, providing mass and heat transfer pathways for the combustion of low carbonization rate polymers. Flame retardancy is crucial for ensuring the safety and fire resistance of these composites. The inherent high flammability and the release of large amounts of smoke and heat during combustion greatly constrain their further utilization in specific fields such as electrical and electronic industries industry applications and development. In this context, improving the flame retardancy of the composites is one of the urgent problems to be solved in the development of this industry.

1.1.2 Research gap and objectives

On the basis of above statement, in the field of plant fiber reinforced epoxy composites, significant research has been conducted on enhancing mechanical properties and flame retardancy. Unfortunately, there remains a notable gap in achieving a balance between interfacial performance and flame retardancy of plant fiber reinforced epoxy composites. Previous studies have often focused on individual aspects, such as mechanical strength or flame resistance, without a comprehensive analysis of their combined effects. On the one hand, introducing interface modifiers may not affect the flame retardant

performance since most modifiers have no flame retardant effect. On the other hand, the addition of flame retardants can destroy the mechanical properties of the composite. Therefore, realizing green, lightweight, strong, tough and flame-retardant plant faber reinforced epoxy resin composites poses challenges and has recently attracted significant attention. Moreover, it is of great scientific significance and considerable application value to carry out the research of multifunctional solubilizers with both flame retardancy and interface enhancement.

The current work aims to address the challenge that most traditional methods are limited by the inability to improve both mechanical and thermal properties. In this thesis, ramie fiber in Chapter 2 and the regenerated cellulose fabrics (trademark: Suncell) in Chapters 3 and 4 were chosen as the reinforcement. As for the polymer, epoxy resin—one of the best and most widely established commercial classes of thermoset polymer resin—was selected as the matrix of composite. Accordingly, the objective of the current study is to design and synthesize multifunctional modifiers that can meet the above requirements and contribute to the development of fire-safe and high-performance materials. Those approaches not only contribute to the existing body of knowledge but also offer practical insights for developing more sustainable composite materials. At the same time, this

work revealed the flame retardant mechanism by investigating the flame retardancy of plant fiber reinforced epoxy composites. Additionally, the mechanical performance and interfacial properties between the plant fibers and epoxy matrix were also investigated. This includes examining the effects of fiber surface treatments, such as chemical modifications or coatings, on enhancing the adhesion and compatibility between the fibers and the matrix. Through a comprehensive investigation of flame retardancy and interfacial properties, the study aims to provide insights into the optimization of flame retardant formulations and interfacial modifications, leading to the design and fabrication of sustainable composites with improved fire resistance and enhanced mechanical properties.

1.1.3 Thesis outline

This thesis consisted of five chapters.

Chapter 1 reviewed the overall background of this research.

In Chapter 2, inspired by the mussel, a multifunctional modifier was successfully designed and synthesized in a single step to simultaneously improve the mechanical and thermal performance of ramie-reinforced epoxy resin composites. It can be successfully introduced and firmly adhered to the ramie fabric, both the hydrophobic property and N-H were

integrated into ramie fabrics, enhancing the compatibility between fibers and epoxy resin. Thus, FPD can play a bridging role in enhancing the interfacial properties of ramie epoxy composites. The flexural strength, tensile strength, and modulus all increased, from107 MPa, 70 MPa, 4670 MPa, and 4212 MPa for RFEPC-0 to 116.5 MPa, 96 MPa, 5570 MPa, and 6779 MPa for RFEPC-3. In addition, the fire safety of modified RFEPC was also improved by forming compact and continuous char layers and facilitating the release of non-flammable gases, which enabled RFEPC-3 to achieve a UL-94 V-0 rating.

In Chapter 3, a water-soluble combined modifier composed of bio-based benzoxazine (HGB) and Phytic acid (PA) were successfully applied in the simultaneous improvement of interfacial adhesion and fire safety of the regenerated cellulose fabric/epoxy composite. Specifically, HGB was facilely synthesized through one step with confirmed structure and excellent purity. Then it was combined with PA to modify the regenerated cellulose fabric in the water solution phase via simple impregnation, which exhibited a self-extinguishing behavior after ignition. The modified fabric was further used to reinforce DGEBDB composites through prepreg preparation and a vacuum bag-assisted compression molding process. Results indicated that F-SF/F-EP well balanced its mechanical modulus and roughness due to the optimized interface,

reflected in the 14.9% and 9.6% improvement compared with SF/EP, respectively. Meanwhile, owing to the higher interface stress transfer efficiency, F-SF/F-EP possesses an ILSS of 13.89 MPa, outperforming that of SF/EP, F-SF/EP, and SF/F-EP with 11.41, 12.42, and 12.77 MPa, respectively. Besides, both the flame-retardant modified fabric and intrinsically fire-resistant epoxy matrix contributed to a V-0 classification in the UL-94 test and 33.8% of the LOI value of F-SF/F-EP composite, which was mainly achieved by the avoidance of the wick effect in the fabric phase, barrier effect in the gaseous phase, and inhibition effect in the condensed phase.

In Chapter 4, a curing accelerator (PAIM) was successfully synthesized and the chemical structure was carefully characterized to reduce the effects of phytic acid on the mechanical properties of fiber. Here, PAIM and benzoxazine (HGB) were used to develop a flame retardant coating on Suncell fabric to improve the interfacial behavior between fiber and epoxy resin matrix. The flame-retardant Suncell fabric reinforced epoxy resin composites were prepared with PAIM/HGB treated ramie fabrics as reinforcement. The flame-retardant coating on the fabric surface endowed the composites with a self-extinguishing ability, and the treated composites achieved UL-94 V-0 rating during the vertical flame tests and 34.3% of the LOI value. In consequence, the

interfacial adhesion of the treated composites was enhanced by almost 19.7%. Moreover, its tensile properties and toughness were improved compared to the untreated composites.

Chapter 5 summarized the research results and proposes possible future research topics on the basis of the current work.

1.2 Plant Fiber reinforced polymer composites

1.2.1 Introduction of plant fibers

Plant fibers (Figure 1-1), derived from renewable sources, such as jute, hemp, flax, and kenaf, have gained attention as potential reinforcements for polymer composites due to their low cost, low density, strength, flexibility, sustainability, and biodegradability[15-18]. Plant fibers come from various sources, including the stem, leaf, or seed of plants.

Figure 1-1. Several common natural fibers.

Here are some common types of plant fibers[19-20]:

Cotton: cotton fiber is obtained from the seed of the cotton plant, which is the most widely used natural textile fiber[21]. It is soft, breathable, and widely used in the textile industry for clothing, bedding, and other fabric-based products. Cotton fiber reinforced composites, which can make up to 80% of overall fiber by weight, have been widely used as thermal and acoustic insulators[6].

Jute: jute is an agro-based plant, mostly farmed in India, China, and Bangladesh (Figure 1-2). Jute fibers are long, coarse, and strong, making them suitable for applications such as rope, twine, sacks, and packaging materials, household textiles and even construction materials[22].

Hemp: hemp fibers are known for their strength, durability, and environmentally-friendly characteristics. They are used in textiles, ropes, paper, and even composite materials for green building applications[23].

Figure 1-2. Hemp (cannabis sativa) plants grown in the wild (left); close up of the leaves of the same hemp plants (right)[24].

Flax: flax fiber also known as linen, is highly durable and have excellent moisture-wicking properties. They are used in textiles, home furnishings, and industrial applications.

Bamboo: bamboo is one of the fast-growing plants with high yields that can be harvested year after year[25-27]. There are over 1200 species in it, grouped into 50 genera. Bamboo fibers provide a more opulent appearance and are soft, flexible, robust, breathable, have been widely used in paper, textile, construction, and composite manufacturing industries[28]. Due to its unique qualities, bamboo fiber is becoming a very popular material for reinforcement[29-30].

Ramie: ramie also called Chinese grass, is one of the most important non-wood fibers (Figure 1-3). Until now, ramie fiber has been extensively chosen as a reinforcement for composite components due to the capability of meeting the requirements of manufacturing fiber-reinforced

polymer such as low density (1.5 g/cm^3) and high tensile modulus (61.4~128 GPa).

Figure 1-3. Ramie plants grown in the wild (left); close up of the leaves of the same ramie plants (right).

Natural fibers are mostly composed of cellulose, hemicellulose, and lignin[31-32]. Cellulose is a linear polymer made up of glucose units, which is the primary structural element that provides a natural fiber with strength and stability. Although cellulose is rapidly hydrolyzed by acid to produce water-soluble carbohydrates, it is resistant to powerful alkalis. A branching polymer composed of several polysaccharides is called hemicellulose. Hemicellulose is much more hydrophilic, soluble in alkali, and readily hydrolyzed in acids than cellulose; however, it contributes less to the fiber's stiffness and strength. The physical and mechanical properties of some natural fibers are summarized in Table 1-1. Natural fibers usually exhibit variations in their properties due to differences in their chemical compositions, which might result in unanticipated properties.

Table 1-1. Mechanical properties of different natural fibers compared to conventional reinforcing fbers[1, 5, 15, 33-34].

Fiber		Density (g cm^{-3})	Tensile Strength (MPa)	Young's Modulus (GPa)	Elongation at break (%)
Eco-friendly sustainable Nature Fibers	Cotton	1.5-1.6	287-597	5.5-12.6	7-8
	Jute	1.44	393-773	10-30	1.5-1.8
	Flax	1.54	345-2000	27-85	1-4
	Hemp	1.47	368-800	17-70	1.6
	Kenaf	1.2	240-930	14-53	1.6
	Ramie	1.5-1.56	400-1000	27-128	1-4
	Coir	1.25	220	6	15-25
	Abaca	1.5	980	-	-
	Sugar palm	1.5	421.4	10.4	9.8
	Baggase	1.2	20-290	19.7-27.1	1.1
	Sisal	1.33	600-700	38	2-3
	Pineapple	1.5	170-1627	82	1-3
	Banana	1.35	355	33.8	5.3
	Bamboo	0.6-1.1	140-230	11-17	-
	Henequen	1.4	500	13.2	4.8
	Nettle	1.51	650	38	1.7
Conventional fibers	E-glass	2.5	2000-3500	70-77	4.5-4.9
	S-glass	2.5	4570	86-90	4.5-4.9
	Carbon	1.8-1.9	3400-5400	230-440	1.4-1.8
	Aramid	1.45	3400-4000	130-185	2.5

Natural fibers exhibit variability in quality and consistency properties due to factors such as species, growth conditions, and harvesting methods. This variability can lead to inconsistency in composite performance and make it challenging to achieve uniformity in manufacturing processes. In this regard, regenerated fiber, which is a

type of fiber extracted or synthesized from natural plant material by chemical or physical methods, presents a better alternative to natural fiber. Common types of regenerated plant fibers include artificial cellulose fibers, such as artificial cotton, hemp, and bamboo fibers. These fibers are extracted from natural plant, such as cotton, flax, and bamboo, using chemical dissolution or mechanical methods. The cellulose is chemically treated to dissolve it into a solution, which is then passed through a spinneret where it is extruded into a specific liquid medium. Once in the liquid medium, the cellulose solution solidifies to form fibers. The solidified fibers are cured by chemical or heat treatment to stabilize the fibers and achieve the desired properties; several common regenerated fibers are shown in Figure 1-4. Compared with natural fibers, artificial plant fibers usually have higher strength and stiffness, which can improve the mechanical properties of composite materials. At the same time, the manufacturing process of artificial plant fibers can be accurately controlled, and consistent fiber properties can be obtained to meet the specific application needs. Therefore, they can serve as a replacement for natural fibers in composite reinforcements. Thus, they offer better performance and sustainability in some aspects.

Figure 1-4. Several common regenerated fibers.

1.2.2 Introduction of plant fiber reinforced polymer composites

Fiber reinforced polymer composites (FRPC) are a class of composite materials made of a polymer matrix reinforced with fibers. The fibers provide high tensile strength and stiffness, while the polymer matrix contributes to the overall toughness and resistance to impact. By combining the special qualities of the reinforcing fibers and the polymer matrix, these composites can exhibit a material with improved mechanical performance compared to the individual components. The combination of stiff and strong reinforcing fibers with the ductile and flexible polymer matrix results in a composite material that exhibits improved mechanical properties including high strength, stiffness, impact resistance, and fatigue resistance.

Fiber reinforced polymer composites are known for their lightweight nature, corrosion resistance, and ability to be tailored to specific design

requirements[35]. In most cases, these composites exhibit superior material properties that traditional engineering materials (e.g., metals) cannot provide at low weight. Overall, fiber reinforced polymer composites offer a lightweight, high-strength alternative to traditional materials and have the potential to revolutionize various industries by providing improved performance, durability, and design flexibility. Due to their unique combination of properties, fiber reinforced polymer composites are used in various industries including aerospace, automotive, construction, wind energy, marine, and sporting goods. There are more than 40,000 industrial composite products in various sectors including energy, transportation, medical and construction. The use of composites is increasing daily, particularly in industrial applications. For example, in airplanes, approximately 50% of the aircraft's mass is designed from composite materials including wings, tail, and fuselage. Other applied materials used include: aluminum alloys (20%), titanium alloys (15%), steel (10%), and other materials (5%)[36-37].

There are two main types of fibers used in fiber reinforced polymer composites: synthetic fibers and natural fibers. Synthetic fibers, such as carbon fibers, glass fibers, and aramid fibers, are manufactured through chemical processes and offer exceptional strength, stiffness, and other desirable mechanical properties. Natural fibers, on the other hand, are

derived from renewable resources such as plants (e.g., jute, hemp, and flax) and have gained attention due to their eco-friendliness, low cost, reduced environmental impact, and biodegradability. Plant fiber-reinforced composite materials are composite materials composed of plant fibers as the reinforcing phase material. In terms of the polymer matrix, the most commonly used are thermosetting plastics (e.g., epoxy resin (EP), vinyl ester, polyester) and phenol formaldehyde resins. The most well-known commercial thermosetting resin is epoxy resin, which is also a frequently used matrix for composite materials. Because of its exceptional qualities, such as high transparency, excellent electrical and mechanical performance, favorable solvent and chemical resistance, and superior adhesion to substrates, epoxy resin has drawn a lot of attention as an advanced resin used in the electrical, electronic, and aerospace industries[38-39].

Compared with synthetic fibers, plant fibers have many advantages, including their abundance, light weight, high strength, renewability, environmental friendliness, availability, and low cost[40-41]. Plant fibers can be employed as reinforcing materials to compensate for material strength without sacrificing recyclability. When used as the reinforcing phase, plant fibers can provide material strength and stiffness while reducing the composite's density[41]. What’s more, such composites offer

greater efficiency, as evidenced by their life cycle assessment (LCA), compared to traditional engineering materials, and represent a promising alternative for future sustainable industries[4, 42]. The comparison of LCA of bio-composites and glass FRP composites can be reviewed in this context (Figure 1-5), which reveals the following: a) natural fiber composites have a lower environmental impact than glass-based materials; b) an increase in natural fibers content could reduce the use of base fibers; c) the final product could be lighter, thus contributing to fuel efficiency; d) recycling could be more extensively applied to biobased parts in other applications[43]. Based on the above analysis, the use of plant fibers to partially replace man-made fibers can improve the environmental sustainability of the composite materials industry[1, 11, 43-45].

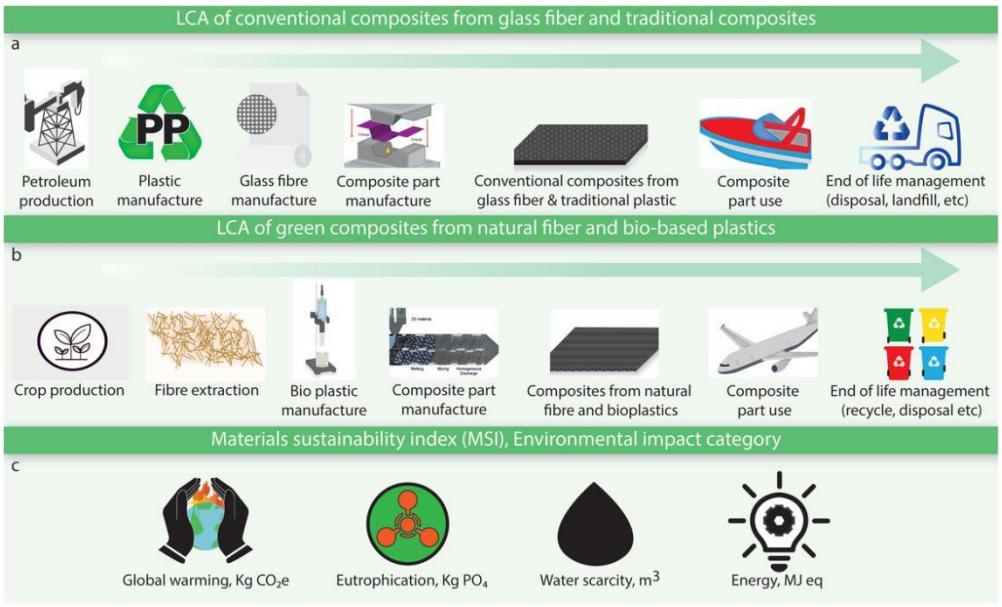

Figure 1-5. Simplified LCA study approach for a) conventional composites from glass fibers and traditional plastics, b) green composites from natural fibers and bio-based plastics, and c) environmental impact category for materials sustainability index (MSI)[1].

1.2.3 Application of plant fiber reinforced polymer composites

Natural fiber reinforced polymer composites have gained significant attention as sustainable alternatives to traditional composites. These composites combine the benefits of natural fibers, such as low cost, renewability, and low environmental impact, with the inherent advantages of polymer matrices. Plant fiber-reinforced composite materials have wide-ranging applications in various fields. Here are several common application areas (Figure 1-6):

1. Automotive industry: natural fiber reinforced polymer composites are widely used in the manufacturing industry for interior components, such

as lightweight door panels, dashboard trims, and seat backs. These composites offer weight reduction, improved fuel efficiency, reduced emissions and enhanced sustainability compared to traditional materials[46]. Later examples include floor mats for Mitsubishi motors composed of PLA and nylon fibers, and interior components that blend bamboo fibers with a plant-based resin called polybutylene succinate (PBS)[47].

2. Construction and building materials: plant fiber-reinforced composite materials are employed extensive applications in the construction and building materials industry. For instance, eco-friendly flooring, wall panels, roofing materials, and doors/windows can be manufactured using plant fiber-reinforced composite materials, offering excellent strength, and resistance to moisture and weathering, and sound insulation properties.

3. Packaging industry: natural fiber reinforced polymer composites are utilized in the packaging industry for applications like disposable containers, trays, and packaging inserts. These composites offer biodegradability, lower environmental impact, and a sustainable alternative to conventional plastic packaging materials[22].

4. Electronics products: plant fiber-reinforced composite materials are also used in the manufacturing of electronic products. Thin and

lightweight phone cases, laptop shells, and flat-screen TV casings can be made using plant fiber-reinforced composite materials, offering both aesthetic appeal and mechanical performance[48-49].

5. Aerospace industry: although less common than in other industries, natural fiber reinforced polymer composites have begun to find applications in the aerospace sector. These composites are used in non-structural interior components such as cabin panels, overhead compartments, and luggage bins. Due to their lightweight and high strength characteristics, plant fiber-reinforced composite materials can be used to manufacture structural components for aircraft and spacecraft, reducing overall weight and enhancing fuel efficiency[50].

6. Consumer goods: natural fiber reinforced polymer composites are used in various of consumer goods, including furniture[18], luggage, home accessories, and sporting goods. These composites provide a combination of aesthetics, durability, and sustainability, making them suitable for eco-friendly product designs.

7. Marine industry: natural fiber reinforced polymer composites are employed in the marine sector for boat interiors, decking, and furniture. and hull components. The composites offer improved resistance to moisture, reduced weight, and enhanced durability in saltwater environments. They offer advantages such as high strength-to-weight

ratio, resistance to water and corrosion, and design flexibility, leading to improved performance and fuel efficiency[51].

8. Furniture and home decoration: natural fiber reinforced polymer composites are utilized in the manufacturing of furniture, flooring, and interior decor items. These composites offer aesthetic appeal, strength, and eco-friendliness, contributing to sustainable design practices[52].

9. Sporting Goods: natural fiber reinforced polymer composites are used in the production of sporting goods such as bicycles, skateboards, and helmets. These composites provide lightweight, high strength, and enhanced impact resistance, contributing to improved performance and durability.

In summary, plant fiber-reinforced composite materials offer the advantages of renewability, lightweight high strength, and environmental friendliness, making them suitable for diverse applications in various fields. As technology advances and research deepens, the application potential of natural fiber reinforced polymer composites is continually expanding as research and development focus on optimizing their properties, processing techniques, and cost-effectiveness. Plant fiber-reinforced composite materials are expected to replace traditional materials in more areas, contributing to sustainable development. Overall, the wide range of applications for fiber reinforced polymer

composites demonstrates their versatility, offering solutions in industries where high strength, light weight, corrosion resistance, and durability are valued.

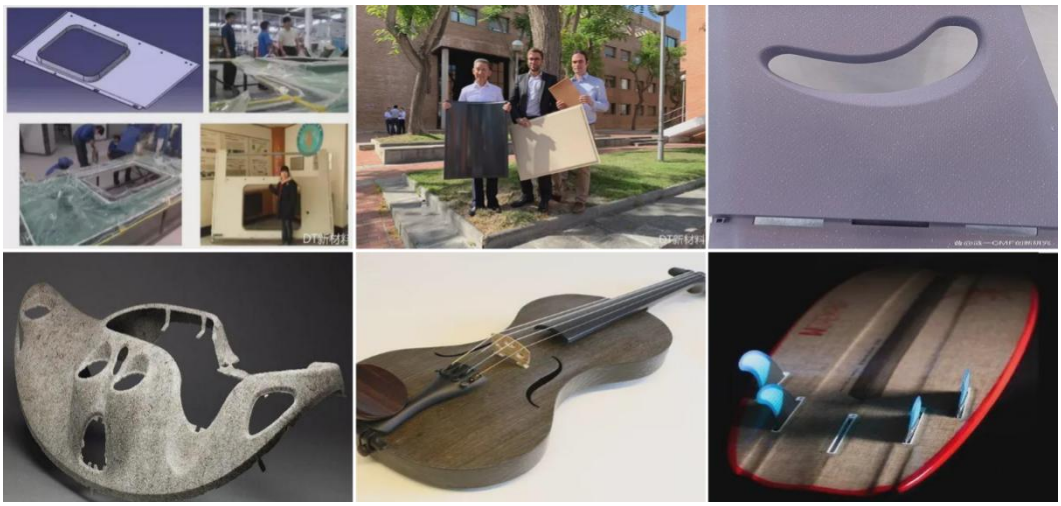

Figure 1-6. Application examples of plant fiber composite materials.

1.2.4 Limitations of natural fiber reinforced polymer composites

While plant fiber reinforced polymer composites provide numerous advantages, they also present certain limitations that must be taken into account when considering them for various applications. These limitations can affect the overall performance of the composites in different engineering sectors. Here are some of the challenges associated with them:

Poor interfacial performance

Plant fiber reinforced composite materials are emerging as a promising class of engineering materials due to their renewability,

biodegradability, and relatively low density. However, the widespread application of such composites is constrained by insufficient interfacial performance. Interfacial performance refers to the interaction between the fibers and the matrix. The interfacial properties between the plant fibers and the resin matrix critically impact the performance of the composites, directly affecting their mechanical properties and durability. Good interface strength helps effectively transfer stress from the matrix to the reinforcement, thereby significantly reducing stress concentration and greatly improving mechanical performance.

The inadequacy in interfacial performance of plant fiber reinforced composites primarily stems from the mismatch in surface properties between the fibers and the resin matrix. This leads to poor compatibility and consequently insufficient bonding capacity of the plant fibers as the reinforcing phase with the resin matrix, resulting in low interfacial bond strength. Specifically, there is a notable difference in chemical and physical properties between plant fibers and most thermoplastic or thermosetting resin matrices. Plant fibers, composed of natural polymers such as cellulose, hemicellulose, and lignin, contain an abundance of polar hydroxyl groups (-OH). These polar hydroxyl groups endow plant fibers with high polarity and hydrophilicity, whereas most thermoplastic and thermosetting resin matrices are made from non-polar or

low-polarity polymers, such as polypropylene (PP), polyethylene (PE), and epoxy resin (EP). This polarity difference in chemical properties increases the interfacial tension between the plant fibers and the matrix, making it challenging to form effective chemical bonding, which significantly reduces compatibility with epoxy resin matrices. In addition, plant fibers usually have higher surface roughness and irregular shapes, while plastic matrices are relatively smooth. These differences could increase mechanical interlocking to some extent, but in most cases, the surface characteristics of plant fibers are not conducive to forming strong interfacial bonds. In plant fiber reinforced composites, weak interfacial bonding between fibers and the matrix can lead to insufficient load transfer, reducing the mechanical performance of the composite. Furthermore, fiber pull-out, breakage, and matrix damage often occur initially at the interface, further highlighting the importance of interfacial bond strength. Additionally, due to the hygroscopic nature of the fibers, changes in environmental humidity can cause dimensional mismatch between the fiber and the matrix, leading to stress concentration and interfacial delamination. Ideally, chemical reactions between plant fibers and resin matrices should form covalent bonds to enhance interfacial bond strength. However, due to the uneven distribution of active sites on plant fibers and challenging reaction conditions, the formation of

covalent bonds is typically not ideal. Even with the use of coupling agents and other surface-active agents, it is often difficult to achieve uniform and stable interfacial chemical reactions.

Therefore, to improve the interfacial compatibility of plant fiber reinforced composites, a series of measures need to be taken. Effective surface treatment methods can significantly address these issues, thereby enhancing the overall performance of the composites and broadening their application scope. Future research should focus on developing new surface treatment technologies and a deeper understanding of the interfacial interaction mechanisms to lay the foundation for the design and preparation of high-performance plant fiber reinforced composite materials.

High flammability

In addition to the poor interfacial performance, the inherent flammability of both plant fibers and epoxy resin matrices contributes to the high combustibility of the composites made from them[53-54]. Specifically, plant fibers such as flax, hemp, bamboo fibers, bagasse, and wood fibers are essentially composed of natural polymers like cellulose, hemicellulose, and lignin, which are prone to thermal degradation at elevated temperatures. Cellulose and hemicellulose are

flammable polysaccharides that begin to degrade at temperatures typically between 250-350 °C, while lignin, with its complex aromatic structure, has relatively higher thermal stability but is also combustible. When plant fibers are exposed to a flame or high-temperature environments, they rapidly undergo pyrolysis, releasing combustible gases and forming a char layer. This process can lead to fires, emitting substantial heat and toxic fumes that pollute the environment and pose life-threatening risks to humans life, including potential asphyxiation or death[55-56]. Such risks significantly limit the application of these composites in fields like aviation, transportation, and electrical equipment, especially in applications where fire resistance is a critical requirement[57-58].

Furthermore, in plant fiber composites, the interaction between the fibers and the matrix has an important effect on the overall combustion performance of the material. Thermoplastic or thermosetting polymer matrices may demonstrate higher thermal stability within the pyrolysis temperature range of plant fibers. However, due to differences in interfacial bonding performance, once the fibers begin to degrade, cracks can form at the interface, leading to accelerated release of internal gases and further propagation of the flame.

The flammability of plant fiber composites is determined by their natural polymeric constituents and thermal decomposition characteristics. The flammability of plant fibers can induce a wick effect within the composite material, leading to easy ignition when exposed to external heat and flame sources. The "wick effect" (Figure 1-7) in fiber reinforced composite materials occurs when the fibers act like the wick of a candle, igniting and directing the flow of combustible material. The surface of the material becomes molten after being heated, and then the molten liquid will move along the fiber to the place with high temperature. After moving to the top of the fiber, it will vaporize into combustible small molecules and burn. The combustion heat will further promote the matrix material to melt and move towards the flame, which will make the combustion continue. Therefore, in fiber reinforced composite materials, the fiber has a promoting effect on the combustion of the material, making it more challenging to achieve flame retardancy. In the process of flame retardant research on fiber reinforced composite materials, it is not only necessary to determine the flame retardant and flame retardant method according to the properties of the matrix material, but also to consider the elimination of the "wick effect" of the fiber in order to better play the flame retardant effect.

By improving the interaction between fibers and the matrix, enhancing the interfacial performance of the composite, and employing various flame-retardant techniques, the resistance to combustion can be effectively increased, broadening the safety and practicability of their applications. At present, a lot of research has been done on the flame retardancy of fiber reinforced composites. Yuling Xiao et al.[59] synthesized polymeric compatibilizer (PPC) and directly compounded with 3-aminopropyltriethoxysilane modified GF, polyamide 6 (PA6) to prepare fire retarded glass fiber reinforced polyamide 6 (GFPA6) containing aluminium diethlyphosphinate. When GFPA6 burns, the addition of PPC leads to more continuous and dense carbonaceous char on GF surface, which weakens the “wick effect” and improves the flame retardant efficiency. Future research should continue to explore more efficient and environmentally friendly flame retardants and develop new composite designs to optimize the burning behavior and flame retardancy of the materials.

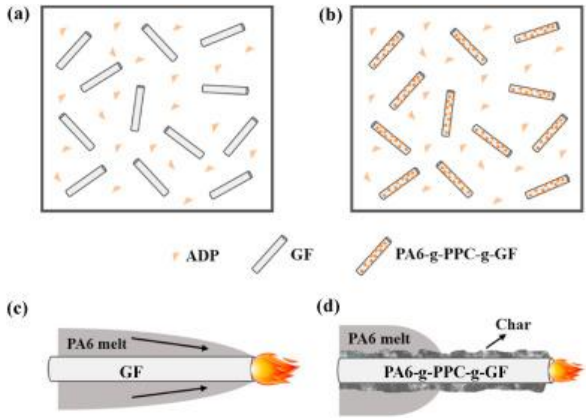

Figure 1-7. The flame retardant distribution of (a) bulk and (b) both bulk and interface; interfacial flame behaviors of PA6 melt in (c) bulk and (d) interfacial regions[59].

1.3 Study on how to improve interfacial compatibility of plant fiber reinforced polymer composites

Interface compatibility plays a vital role in optimizing both the manufacturing process and the mechanical properties of the composite. However, the surface hydrophilicity and low reactivity of the fibers greatly limit their interaction with the polymer matrix[60-62].

Consequently, poor wetting performance and shear failure can occur, often resulting from inevitable defects and inefficient stress transfer[63-64]. Generally, the extent of interfacial adhesion depends on the polarity differences between two phases, which inspired researchers to modify the surface of plant fibers. Up to now, various methods have been reported for improving the interfacial bonding through the pre-treated fiber materials, broadly categorized into twofold[65]: physical treatment

(such as plasma[66] and corona[67]) and chemical modification (including esterification[68], alkaline treatment[69], silanes[70], isocyanates[71], and so on). The former activates the surface through physical energy, while the latter modifies surface groups by using additional chemical substances.

1.3.1 Physical modification

The physical modification can change the structure and surface properties of the fiber and improve the physical adhesion between the fiber and the resin matrix. Common physical modification methods include heat treatment, steam blasting treatment, radiation treatment, plasma treatment and so on.

Heat treatment

Heat treatment is a commonly used method for the pre-treatment and modification of plant fibers. Cellulose fibers contain both free water, which can be removed by drying, and bound water, which is difficult to eliminate. Water is detrimental to composite formation because the temperature increase during the blending process will cause evaporation within the plant fibers, leading to the creation of pores and internal stress defects in the composite material. The natural fiber was heat treated in a nitrogen atmosphere below 240 °C, and the treatment effect was better[72-73].

Steam blasting

The basic principle of steam blasting treatment is to use high-pressure water vapor in a closed container to cause swelling of cellulose, destroy the supramolecular structure of cellulose, and increase the degree of intramolecular hydrogen bond fracture. Bo Lei[74] applied this technique to sisal fiber and analyzed the changes in chemical components and morphological structure of sisal fiber before and after blasting treatment by chemical analysis and other methods. Additionally, mechanical stretching can alter the structure and surface properties of the fiber, facilitating mechanical crosslinking.

Plasma treatment

Plasma treatment has been widely used to modify the surface of polymers such as polyene, polyester and reinforced fibers, so as to improve the wettability and adhesiveness. Low-temperature plasma offers benefits such as high strength, low reaction temperatures, minimal penetration, ease of operation, and environmental friendliness. The energy of the particles in the low-temperature plasma is slightly higher than the chemical bond energy in natural fibers, enough to break or recombine the chemical bonds.

1.3.2 Chemical modification

Different from the physical modification, the chemical modification method is to change the chemical structure of the surface of the plant fiber, so as to improve the mechanical performance of the composites. The common methods are alkali treatment, graft copolymerization, interfacial coupling modification, etc.

Alkali modification

Alkali treatment is an ancient fiber modification method. It is the most widely used method in natural fiber surface treatment due to its low cost and high efficiency and has been widely used. An appropriate alkali treatment concentration can remove impurities and oils from the surface of ramie fiber, make the surface smoother, reduce the fiber diameter, increase the length-to-diameter ratio, improve the orientation, and thus enhance the strength of the fibers. alkali treatment dissolves some small molecular impurities such as pectin, hemicellulose, and lignin in natural fibers, and reduces the rotation angle of microfibers to improve molecular orientation, thus enhancing the adhesion between fibers and resins. During alkali treatment, some hydroxyl groups on the cellulose surface react with alkali solution, which reduces the number of hydroxyl groups on the plant fiber surface, thereby reducing its surface polarity,

improving hydrophobicity, reducing the polarity difference between plant fiber and epoxy resin, and increasing the compatibility and bonding strength of the two phases. In this way, the mechanical properties of plant fiber/epoxy resin composites were improved. Abir Saha[48] treated pineapple leaf fiber with a 5% NaOH solution and the results revealed that the treatment has improved the material characterization as well as mechanical properties.

Graft copolymerization modification

Graft copolymerization is an important fiber modification method. Through this method, a coordination complex or covalent bond can form between the coupling agent, fiber and matrix polymer, so that the interface adhesion can be changed. After cellulose graft copolymerization modification, the fiber not only retains the inherent properties of cellulose, but also adds new properties to the synthetic polymer branch chain.

Acetylation modification

Acetylation constitutes a chemical modification process involving the employment of an appropriate catalyst, predominantly acetic acid, to displace hydrogen atoms present within the hydrophilic hydroxyl moieties of cellulose molecules. This modification is instrumental in

diminishing the hydrophilic propensity of natural fibers, consequently enhancing their resistance to moisture uptake. As a result, the dimensional stability and environmental degradation resilience of both the individual reinforcing fibers and the resultant fiber-reinforced composites are significantly improved. Empirical evidence suggests that acetylated fiber composites demonstrate superior performance across all levels of fiber incorporation. The acetylation process is known to facilitate the establishment of robust covalent bonds, the removal of noncrystalline fractions in fibers, the alteration of surface characteristics/topography, the change of fiber surface free energy and the improvement in the efficiency of stress transference at the interface, resulting in a notable augmentation of the tensile strength and Young's modulus in the acetylated fibers[75-76]. In an investigative study by Seena et al.[77], the impact of acetylation on the attributes of banana-fiber-reinforced phenol formaldehyde composites was scrutinized, revealing that both the tensile strength and modulus, as well as the impact resistance, were substantially enhanced when compared to composites comprising untreated banana fibers.

Silane coupling agent modification

However, many of the afore-mentioned treatments can sacrifice the mechanical properties and structural integrity of the fibers, as they may improve the fiber/matrix interface properties at the expense of the properties and structural integrity of the fibers. At present, the silane coupling agent has been proven to be a traditional and excellent non-damaging surface modifier. The coupling agent has bifunctional groups in its chemical structure and can play a "bridge role" in the composite material, that is, one end of the coupling agent molecule reacts chemically with the surface of the fiber, and the other end reacts chemically with the matrix or becomes physical entangled, thereby improving the interface compatibility between the fiber and the matrix[78]. In silane treatment, the interaction between silane coupling agent and natural fiber is mainly carried out through hydrolysis, self-condensation, adsorption and chemical grafting[79]. The capacity of the fiber and polymer to bind at the interface can be enhanced once the natural fiber is modified by the coupling agent, which prevents fiber swelling. Although the cost of silane coupling agent treatment is higher than that of alkali treatment, it has been applied more and more because of its remarkable effect in improving the mechanical properties of composite materials[80]. Fui Kiew Liew et al.[25] investigated the effects of 3-aminopropyl

triethoxysilane (APTS) coupling agent and poly(ethylene-co-glycidyl methacrylate) (EGMA) copolymer on thermal, mechanical, and morphological properties of hybrid composites. The results showed that the tensile strength and Young's modulus of the treated hybrid composites exceeded 150% and 330%, respectively. A low water absorption rate in the treated hybrid composites was also observed. M. Asim[16] used silane-treated PALF and KF for the fabrication of PALF/KF/PF hybrid composites, and the results indicated that the treated PALF/KF/PF composites exhibited higher tensile, flexural and impact strength than their untreated counterparts.

Other modification methods

In recent years, numerous papers have been published regarding the use of adhesion promoters/compatibilizers for green plastic composites[81]. The modification of the fiber surface through chemical substitution of apolar groups for polar hydroxyls has been shown to be one effective method of enhancing the mechanical properties of composites made of natural fibers. Introducing nonpolar groups onto the fiber surface aiming for hydrophobic modification has been shown to be one of the most appealing methods, benefiting from its designability and efficiency, which are typically achieved by chemically grafting the terminations or by

directly coating with an interfacial agent compatible with the polymer matrix[82]. For example, *Elisa Zini*[83] grafted PE glycol onto flax fibers, enhancing the mechanical characteristics of PLA composites supplemented with flax fibers. Compared to chemical treatment, coating methods that offer higher reproducibility can improve the surface friction coefficient without damaging the fiber morphology and are gradually becoming widely accepted.

Another strategy to improve fiber matrix adhesion is to add a compatibilizer that acts as an adhesion enhancer. Interface modification with compatibilizers: compatibilizers are additives specifically designed to improve the interface compatibility between natural fibers and polymer substrates. They can enhance interfacial adhesion by reducing interfacial tension, promoting dispersion, and improving fiber compatibility with the matrix. A mussel-inspired coating strategy has attracted much attention due to its ease of implementation and general universality[84-86], which some are convinced to be a potential way to modify the matrix in interfacial functionalization[87-88]. Chen et al.[2] fabricated polyethyleneimine/catechol-modified PET fiber-reinforced composites inspired by mussel, and the analysis revealed that the interfacial property was significantly improved compared to the untreated PET-reinforced composite[89]. Unfortunately, research focusing on new

compounds with mussel-inspired multifunctional abilities to produce fiber-reinforced composites is still rare.

However, the introduction of interface modifiers may not affect the flame retardant performance since most modifiers have no flame retardant effect.

1.4 Study on combustion theory and flame retardancy of plant fiber reinforced composites

To study the flame retardancy of fiber reinforced composite materials, we must first have a clear understanding of its combustion process and flame retardancy mechanism, and essentially delay or prevent the process or elements of the combustion reaction to achieve the purpose of flame retardancy.

1.4.1 Combustion process

The combustion of fiber reinforced composites is a very complex physical and chemical process. In recent years, research has identified four elements of polymer combustion, namely a heat source, air (oxygen), fuel, and free radicals[61, 90]. These four aspects make up the fire tetrahedron of composite combustion, as shown in Figure 1-8. The combustion process of composite materials involves the combustion reaction of combustible components within the materials in response to

heat or external heat source[91]. In general, the combustion process of composite materials can be divided into three stages: heating stage, decomposition stage and combustion stage[92].

Heating stage: when exposed to a heat source, the composites material begins to absorb heat energy, and its temperature gradually rises. During this stage, the combustible components of the composite, such as the resin matrix or the added combustible agent, begin to undergo thermal decomposition, releasing flammable gases and vapors.

Decomposition stage: as the temperature increases, the combustible components in the composite continue to decompose, producing more combustion products. These products may be volatile organic compounds, gases, or solid char. At the same time, the non-combustible components in the composite, such as the fiber reinforced phase and inorganic fillers, may undergo thermal decomposition or melting.

Combustion stage: the combustion reaction begins when the combustible material produced in the decomposition stage reaches its flammability limit and meets oxygen. This leads to the formation of a flame and releases a large amount of heat energy and combustion products such as smoke, carbon monoxide, carbon dioxide, and water vapor. At the same time, the flame further heats the surrounding material, leading to the spread of fire and sustained combustion.

As can be seen from the entire combustion process, thermal decomposition is a very important step. Various combustible gases are produced by the thermal decomposition of composite materials, and the free radicals generated during the combustion process are highly reactive; in the case of not obtaining energy from the outside, it can react with the outside molecules, even without external energy, they can react with surrounding molecules and generate new free radicals, thus forming a chain reaction of combustion. The combustion chain reaction of polymer is generally carried out according to the free radical chain reaction shown in Figure 1-8, including three elementary reactions: chain initiation, chain growth and chain termination. Therefore, inhibiting the generation of free radicals can achieve the goal of flame retardant of polymers[91].

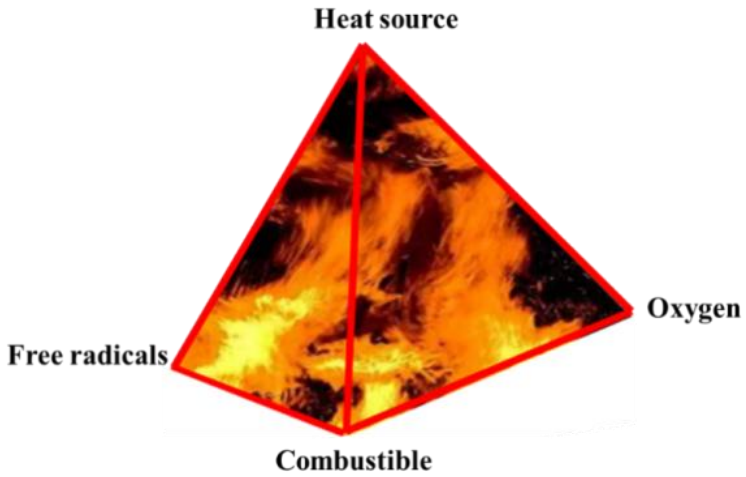

Figure 1-8. Schematic diagram of the fire tetrahedron model.

1.4.2 Flame-retardant mechanism

The flame retardant mechanism refers to the process whereby flame retardants interfere with the combustion reaction through chemical or physical means, thereby slowing down or inhibiting the combustion process, reducing the spread rate of the flame and heat release. Following the above analysis of the combustion process and mechanism of polymer, it can be concluded that to achieve the flame retardancy, the combustion cycle of the "fire tetrahedron", as shown in Figure 1-8, must be desrupted, that is, by inhibiting one or several elements of combustion, the goal of flame retardancy is achieved. It mainly includes the following aspects:

(1) Termination of the free radical chain reaction: some flame retardants can react with ·OH and ·H generated during the combustion process, generating active free radicals in the gas phase decomposition, thereby terminating the combustion chain reaction and altering the degradation mode of the polymer to achieve the purpose of flame retardancy.

(2) Endothermic cooling: adding flame retardants with a high specific heat capacity allows them to undergo an endothermic decomposition reaction at high temperatures, absorbing heat, reducing the system’s temperature, delaying the thermal degradation rate of the polymer, and

ultimately rendering the heat required to maintain polymer combustion insufficient to achieve flame retardancy.

(3) Dilution and coverage: non-flammable gases such as water, ammonia, carbon dioxide, hydrogen halide, and nitrogen released during the polymer combustion process can dilute the concentration of flammable gases and oxygen around the combustion substance, reduce the oxygen supply of the flame, thereby slowing the combustion reaction rate and reducing below the ignition limit. Additionally, they can form a high-density gas layer that covers the surface of the material, providing heat and oxygen insulation[93].

(4) Formation of a barrier layer: in the process of composites combustion, a thick barrier layer forms on its surface to provide physical isolation, reduce heat transfer and gas diffusion, thus inhibiting the combustion reaction and achieving flame retardancy. The formation of this barrier layer is mainly in the following three ways: a) During the combustion process, the flame retardant forms a foam-like protective layer on the surface of the composite, which prevents heat and air from entering the material and flammable gas diffusion to the outside, achieving a flame retardant effect. b) The thermal degradation products of the flame retardants can promote the dehydration of the polymer into charcoal, thus forming a protective dense carbon layer on its surface to

prevent the further spread of the flame. c) The flame retardant decomposes before the composite reaches its decomposition temperature, generating a viscous glass or ceramic-like substance that covers the surface of the composite and acts as a barrier layer.

1.4.3 Development status and trend of flame retardants

In recent years, as composite materials have been widely applied in various fields, many high-end technology sectors have set increasingly stringent fire safety standards, which provides a broad arena for the development of flame retardant materials. More importantly, with heightened awareness of environmental protection and the continuous introduction of strict laws and regulations, there is a demand not only for materials and products to be flame retardant but also environmentally friendly, posing an unprecedented challenge to product designers and manufacturers. Therefore, the development direction of flame retardants is mainly to meet the requirements of industrial development while also adhering environmental protection standards, which encompasses the following aspects.

No halogenation trend[94]

Halogen flame retardants are compounds containing halogen elements (fluorine, chlorine, bromine or iodine). Early halogenated flame

retardants are commonly employed as commercial flame retardants due to their significant flame retardancy effect despite being added in small amounts. Halogenated flame retardants primarily function in the gas phase to retard flames. Specifically, halogen flame retardants, under thermal decomposition, generate active free radicals that can interrupt or reverse the gas phase combustion chain reaction, terminate the combustion, and ultimately serve the purpose of flame retardancy in the gas phase. Although halogen-based flame retardants have considerable flame retardant effects, they also release corrosive and toxic gases such as halides and halogenated dibenzodioxins, and dibenzofurans during combustion, which seriously affect human life and health and cause environmental pollution[95-96]. Therefore, the development of halogen-free flame retardants has become an inevitable trend, more and more scientific researchers are keen to participate in green halogen-free flame retardant research, and have achieved remarkable results[97-98].

Suppressing smoke and reducing toxic gas trend

Smoke and poisonous gasses are the primary causes of fire deaths, as they suffocate victims during real fires, rather than the victims burning[99]. According to statistics, 80% of fire deaths are due to asphyxiation from smoke and hazardous gases emitted during burning.

Therefore, "smoke suppression", "flame retardancy", and "reducing toxic gases" are interrelated topics. Consequently, reducing the amount of smoke and toxic gases released during material combustion has been a key research topic in the flame retardant field in recent years[100].

Synergistic flame retardant trend

In actual applications, single-component flame retardants typically have various drawbacks or flaws, and it is difficult to meet the increasingly high flame retardant requirements when used alone. To enhance the overall performance of flame retardant materials, compounding technology combines the benefits of two or more flame retardants, achieves complimentary performance, and reduces their required dosage[101]. For example, employing synergistic flame retardancy (such as the combination of phosphorus and nitrogen) can obtain better flame retardancy with a lower addition amount[102-103].

1.4.4 Research of halogen-free flame retardants and applications

Currently, the main halogen-free flame retardants for epoxy resins include phosphorous flame retardants, nitrogen flame retardants, inorganic metal hydroxides, halogen-free expansion flame retardants and inorganic nano flame retardants[104-105]. The following describes the

application and research progress of the above five flame retardants in composite materials.

Phosphorus based flame retardant

Among halogen-free flame retardants, phosphate-based flame retardants are a major class and are characterized by low toxicity, low smoke, and high efficiency[106-107]. Phosphorous flame retardants are considered to be the most efficient flame retardants available and can inhibit the spread of flames by slowing the combustion rate, forming a carbonized layer, or inhibiting the combustion reaction chain. These flame retardants act by releasing phosphate during combustion, absorbing heat, or forming a phosphating layer[108-109]. Phosphorus-containing flame retardants can be divided into two categories: inorganic and organic. Inorganic phosphorus flame retardants mainly include red phosphorus, ammonium polyphosphate and water-soluble inorganic phosphate[110]. Organic phosphorus compounds include phosphate esters, phosphite esters, phosphonates, organophosphorus salts and phosphorus oxide. Under normal circumstances, phosphorous flame retardants mainly play the role of condensed phase flame retardancy. It has been found that materials produce more char under the influence of phosphorous flame retardants,

thereby reducing the amount of fuel generated, primarily through the condensed phase by altering the thermal degradation mode and promoting the formation of carbon and coating layer. However, there are also many phosphorous flame retardants that contain both condensed and gaseous phases[111]. Phosphorus-containing flame retardants can decompose into phosphoric acid during combustion, which further dehydrated to produce metaphosphate, and then polymerizes to form poly-metaphosphate. The strong acidity of polyphosphoric acid can promote the dehydration and carbonization of the material, thereby reducing the amount of fuel generated, forming a carbon layer that isolates air and heat, thus playing an effective flame retardant role[112]. Some phosphorous flame retardants will form PO· during combustion, which can react with ·OH and ·H generated by combustion in the following free radical reactions to inhibit combustion. For instance, multiple H_3PO_4 molecules decompose to produce HPO_2· and PO·, among other products. The PO· radicals can react with ·H to form HPO and terminate the combustion chain reaction, acting as a vapor phase flame retardant[113-114].

So far, 9, 10-dihydro-9-oxygen-10-phosphophenanthrene 10-oxide (DOPO) and its derivatives have proven to be one of the most effective flame retardants, receiving increasing attention from academia and

industry[115-116]. The molecular structure of DOPO contains phosphoheterophenanthrene ring, characterized by its non-coplanar, large volume structure, and polar molecule. The cyclic O=P-O bond provides greater thermal and chemical stability compared to typical non-cyclic organophosphates, enhancing its flame retardancy. At the same time, DOPO has active P-H bonds in its molecular structure, and can react with compounds containing active double bonds (such as olefins, aldehydes, etc.) and epoxides to obtain reactive or additive flame retardants. To prepare highly effective flame retardants, many DOPO-based derivatives have been synthesized by combining phosphaphenanthrene with other groups including triazine[117], silsesquioxane[118], pentaerythritol[119-120], maleimide[121-122], and triazine-trione[123-124]. A novel flame retardant (TGIC-DOPO) was designed and synthesized by Qian et al.[125] via ring-opening addition reaction between phosphaphenanthrene and triazinetrione groups. The produced EP/DMT composites with 12 wt% TGIC-DOPO passed UL-94 V-0 rating and had a LOI value of 33.3%. In addition, compared to neat EP, the peak heat release rate dropped by 50.2%. TGIC-DOPO demonstrated flame retardant effects in both gaseous and condensed phases during combustion. Chen et al.[126] successfully synthesized a novel flame retardant, poly(piperazine phosphaphenanthrene)

(DOPMPA), using DOPO and piperazine. The DOPMPA was applied to improve flame retardancy of epoxy resin (EP). The EP/DOPMPA sample had a high limited oxygen index (LOI) value of 34% and passed the UL-94 V-0 grade when the addition content of DOPMPA in EP was 13 wt.%.

Nitrogen based flame retardants

Common nitrogen flame retardants mainly include melamine, melamine salt, urea and triazine compounds. Compared with phosphorous flame retardants, nitrogen flame retardants have lower flame retardancy efficiency, and their flame retardancy mechanism is in the vapor phase flame retardancy, that is, non-combustible gases such as nitrogen, ammonia and nitrogen oxides generated by thermal decomposition at high temperatures, can effectively dilute oxygen and combustible gases in the air. At the same time, nitrogen flame retardants absorb a lot of heat when they decompose, delaying combustion. In addition, nitrogen flame retardants are often combined with phosphorus flame retardants through physical or chemical means to form an intumescent flame retardant system that achieves efficient flame retardancy[127].

Metal hydroxide

Hydroxide flame retardants mainly refer to compounds containing hydroxides (such as aluminum hydroxide). Hydroxide flame retardants offer advantages such as low toxicity, low smoke production, low volatile cost and abundant available resources. At present, magnesium hydroxide (MTH) and aluminum hydroxide (ATH) are more extensively researched and utilized. The flame retardant mechanism is primarily endothermic decomposition at high temperatures, which generates water molecules and metal oxides[128]. The heat absorption of decomposition and water phase transition will delay the temperature rise of the condensed phase matrix and reduce the release of combustible gas products. The released water vapor will dilute the concentration of combustible gas and oxygen in the gas phase and inhibit the gas phase combustion. The metal oxide forms a non-combustible thermal insulation protective layer over the substrate surface, thereby providing flame retardant and smoke suppression effects. Researches have demonstrated the flame retardant (FR) potential of zinc borate (Zb) and $Mg(OH)_2$ for sawdust fiber and rice-husk fiber reinforced with polypropylene (PP) matrixes. They investigated that Zb is a decent FR, but $Mg(OH)_2$ has an even greater ability to reduce the rate of burning[129]. In another research work, $Mg(OH)_2$ and Zb were employed with APP as synergists in a sisal/PP composite[130].

However, due to the large required amounts and poor compatibility with the matrix, it is necessary to employ ultra-fine or chemical synthesis methods to obtain ultra-fine, or even nanoscale, aluminum hydroxide (ATH) and magnesium hydroxide (MTH), which can enhance the interfacial effect with the matrix and achieve the purpose of using reduced amounts while improving the flame retardant performance[131]. In addition, the flame retardant effect is closely related to its filling amount. The flame retardancy increases with the amount of flame retardants, however, in order to achieve the UL-94 V-0 combustion grade, the filling amount must be 70 wt.% or more, and such high levels certainly affect the material's mechanical properties, processing, and compatibility, greatly limiting the application of inorganic flame retardants. Therefore, it is necessary to mix them with other flame retardants to reduce the amount of inorganic flame retardants while still meeting the flame retardant requirements.

Inorganic nano flame retardants

With the rapid development of nanotechnology, the increasing research on the application of nanoparticles in polymer flame retardant provides a new way. Compared with traditional flame retardant systems, the excellent performance of nanomaterials with very low addition

amount to achieve significant flame retardant effect has been paid attention to by researchers in the field of flame retardant.

Nanomaterials can be divided into three types according to their dimensions: (1) One-dimensional materials: there are layered compounds where only one-dimensional is on the nanoscale, while the other two dimensions can be hundreds or even thousands of nanometers in length or width. Examples include layered silicates, layered double hydroxides (LDH)[132-133] and graphene (GNS); (2) Two-dimensional materials: Nanotubes are nanoscale in two-dimensions but can extend to hundreds or even thousands of nanometers in the third dimension, such as carbon nanotubes (CNT)[134] and GO; (3) Three-dimensional materials: Materials that are nanoscale in all three dimensions, such as nanoparticles etc.

As for the flame retardant mechanism of CNTs in polymers, the current recognized mechanism is the barrier effect of CNTs forming a network structural protective layer in the condensed phase. Specifically, because CNTs form a three-dimensional network structure when added to polymer material, the resulting carbon layer structure is very tight. This prevents the feedback heat generated by gas phase combustion from transferring to the polymer interior and the internal pyrolysis gas from

diffusing into the gas phase combustion zone, thus improving the flame retardant performance of the material.

Some previous literatures have revealed the potential flame retardancy of GO for polymers[135]. However, its weak compatibility with polymer matrices seriously restricts its flame retardant efficiency, which remains a significant challenge for future research[136-137].

When the nanomaterials are uniformly dispersed in the epoxy resin matrix, the two phases can obtain a large internal interface contact area. The nanoscale effect of nanomaterials can enhance the interface between nanoparticles and the matrix, thereby improving the flame retardant efficiency and other properties. Wu et al.[138] studied the effect of CNT films on the flame retardancy of epoxy (EP) resin/bismalayamide/carbon fiber composites. The results show that CNT films can effectively reduce the heat release rate (HRR) and smoke emission during the combustion of composites.

Inrumescent flame retardants

Intumescent flame retardant (IFR) is a flame retardant with nitrogen, phosphorus and carbon as the core components, which is mainly composed of three parts: carbon source (carbonizing agent), acid source (dehydrating agent) and air source (blowing agent)[139-141]. Intumescent

flame retardants, which are halogen-free, produce low smoke, and are environmentally friendly, are considered superior to traditional flame retardants[142-143]. The requirements for each component are as follows: (1) Acid source: the acid source, which dehydrate the carbon source, is typically an inorganic acid or salts that can generate acid in situ upon heated, such as phosphoric acid and polyphosphate APP). The acid must be released below the decomposition temperature of the carbon source[144-145]. (2) Carbon source: the carbon source is fundamental to forming the carbon layer, and its effectiveness is affected by the carbon content and the number of active hydroxyl groups. Polyhydroxyl compounds with high carbon content can be used as carbon sources; common examples include starch, pentaerythritol (PER), and its dimer and trimer, as well as neopentanediol. (3) Air source (blowing agent): the air source can decompose at an appropriate temperature to produce numerous inert gases. The air source is mainly carbon compounds containing nitrogen in the structure, such as urea, melamine (MEL) and melamine urate (MC). The flame retardant mechanism of IFR operates when heat causes the acid source within the intumescent flame retardant system to catalyze the dehydration of the carbon source into carbon, and the gas released by the gas source promotes the formation of a fluffy, porous, and relatively closed carbon layer. The foam carbon

layer is not easily combustible and can weaken heat conduction, gas diffusion is also prevented. In the condensed phase, it can insulate against oxygen and heat, thereby providing an excellent flame retardant effect.

However, the addition of flame retardant would disturb the adhesion between fiber and matrix, so it is a big challenge to develop a fire resistant biocomposite that will maintain its level of mechanical performance.

The primary aim of the present research is to design and synthesize multifunctional modifiers that can fulfill a set of critical requirements with the ultimate goal of contributing to the development of materials exhibiting both superior performance and fire safety.

Three kinds of multifunctional modifiers were designed and synthesized in this context, named FPD, HGB and PAIM, respectively. They can potentially enhance the adhesion and compatibility between the fibers and the matrix, thereby improving the overall performance of the composites. After treated， the also exhibit enhanced flame retardant properties. This research could pave the way for the development of safer and more efficient materials for various applications.

Chapter 2 Study on the preparation of epoxy resin co-curing agent FPD as well as mechanical and flammability properties of FPD coated ramie-epoxy resin composites

2.1 Introduction

This chapter addresses the efficient use of renewable resources, a practice increasingly emphasized due to resource shortages and worsening environmental pollution. Unlike glass fibers and carbon fibers, plant fibers serve as environmentally-friendly reinforcements of composite. Particularly, ramie fiber might satisfy the requirements of reinforced fiber because of its lower specific density (1.5 g/cm^3) and competitive tensile modulus of 61.4-128 GPa, which is close to E-glass fiber (70 GPa) and higher than that of flax, jute, and sisal fibers (27.6, 13-26.5 and 9.4-22.0 GPa)[60, 146-148]. In terms of polymer, epoxy resin represents the most widely utilized matrix due to its excellent dimensional stability, superior chemical resistance, and mechanical qualities[38]. Hence, ramie fiber reinforced epoxy resin composite is undoubtedly promising.

As we know, each type of composite possesses its own benefits and drawbacks. On the one hand, the high flammability of both plant fiber and epoxy resin as well as the “wick effect” restrict their use to industries

with strong fire safety rules[149-150]. To this end, flame-retardant compounds must be incorporated into composites by integrating flame retardants into polymer or fibers[151-152]. Up to now, 9,10-Dihydro-9-oxa-10-phosphaphenanthrene-10-oxide (DOPO) has been shown to be one of the most efficient flame retardants and has gained increasing attention in both academia and industry[153-154]. To avoid impairing mechanical performance, which can be caused by the direct inclusion of flame retardant and to consider the characteristics of epoxy resin, synthesizing a new compound containing DOPO and an imino group to be incorporated into the epoxy resin as a curing agent is a potential solution[155-157]. On the other hand, hydrophilic natural fibers could not be inherently compatible with hydrophobic epoxy resin, which would lead to weak interfacial adhesion between the fiber and the matrix[158] and further result in poor mechanical for composites[8, 105, 159-160]. In many applications, surface modification including alkali treatment, surface oxidation, chemical grafting, plasma irradiation, and ultraviolet grafting is widely employed to improve the adhesion[161-162] or mechanical interlocking[163]. However, most of the above treatments may sacrifice the fiber's mechanical properties and structural integrity[2]. At present, silane coupling agents as a traditional and excellent damage-free surface modifier were proven in research[164]. However, all these methods were

constrained by the fact that they could not improve mechanical and thermal properties simultaneously[159]. In this way, a multi-functional modifier, which could match the above requirement, is necessary.

Based on the above analysis, the ideal modifier that may satisfy these requirements should contain at least three functional structures including catechol, N-H, and DOPO. Specifically, catechol can adhere the ramie fabric similarly to mussel and the N-H cure the epoxy resin during curing process, and the two special structures could form chemical links between the reinforcement and matrix to enhance the interfacial performance. In addition, DOPO can endow the compound flame-retardant characteristic. In fact, a chemical compound named DPDDM, which contains these three structure was reported before (Figure 2-1)[156]. Nevertheless, it was utilized as a co-curing agent for epoxy resin and cannot dissolve in any organic solvent except DMF due to its strong rigidity, which indicates that it cannot achieve the adhesion function of catechol and be used for the modification of composite materials.

In this chapter, a novel compound soluble in low-boiling solvent (tetrahydrofuran) was designed and synthesized successfully. Moreover, the hydrophobicity of ramie fabric after being modified by FPD was improved, and the compatible was also promoted in the process of

making the composite, furthering the interfacial properties of the obtained composites facilitated. Concurrently, the composite also displayed outstanding fire safety performance. This work offers an effective approach to fabricate strong interfacial and flame-retardant ramie-reinforced epoxy composites.

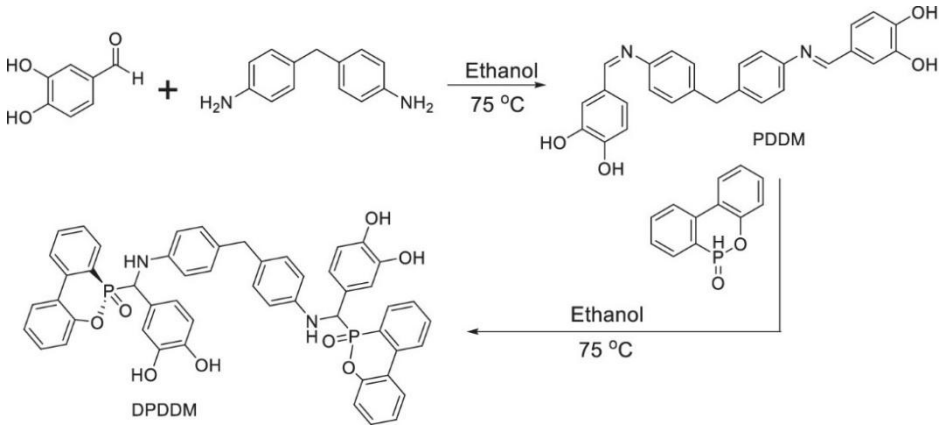

Figure 2-1. The synthesis route and structure of DPDDM[156].

2.2 Materials and methods

2.2.1 Materials and chemicals used

Ramie fabric was purchased from Hunan Huasheng Dongting hemp Industry Co., Ltd, the areal density is 135.1 g/m^2, and 3,4-dihydroxybenzaldehyde, aniline, polyethyleneimine (PEI), and 4,4'-diaminodiphenylmethane (DDM) were obtained from Aladdin Reagent Co., China. The 9,9-Bis(4-aminophenyl)fluorene was purchased from Shenzhen Star Kaiyue Biotechnology CO., Ltd., China. Diglycidyl ether of bisphenol A (trade name DER-331, abbreviated as

DGEBA, viscosity less than 1 Pa·s) with epoxy value around 0.51–0.53 mol/100 g was purchased from Dow Chemical Company. The 9,10-dihydro-9-oxa-10-phosphaphenanthrene-10-oxide (DOPO, 98%) was bought from Guizhou Yuanyi Mining Group Co., Ltd., China. Tetrahydrofuran and ethyl alcohol was acquired from Sinopharm Chemical Reagent Co., Ltd. All the materials were used as received without any further purification.

2.2.2 Synthesis of FPD

Synthesis of 4,4′-(9H-fluorene-9,9-diyl) dianiline and 6,6′-((((9H-fluorene-9,9-diyl)bis(4,1-phenylene))bis(azanediyl))bis((3,4-dihydroxyphenyl)methylene)) bis (dibenzo (c,e)(1,2)oxaphosphinine 6-oxide) (FPD) was according to the synthetic procedure showed in Figure 2-2. In a 250 mL three-necked flask equipped with a reflux condenser, a magnetic stirrer, and nitrogen atmosphere, 9,9-Bis(4-aminophenyl)fluorene (17.4 g, 0.05 mol), and 3, 4-dihydroxybenzaldehyde (13.8 g, 0.1 mol) were dissolved in 300 mL ethanol. The mixture was heated up to 80 °C and kept at this temperature for 12 h. After that, DOPO (21.6 g, 0.1 mol) was added and continued to react for 12 h at 80 °C; then, it was cooled to room temperature and the aqueous solution was added dropwise into hot

water. The product was filtered and washed with hot water for three times. Then, it was dried at room temperature for 24 h under a vacuum and a light-yellow solid powder (FPD) was obtained (yield: ~85.7%). ^{1}H NMR (DMSO-d6, ppm): δ = 9.2-8.5 (O-H), 8.3-6.4 (Ar-H and N-H), 5.2 (N-H), and 5.16 and 4.67 (C-H).

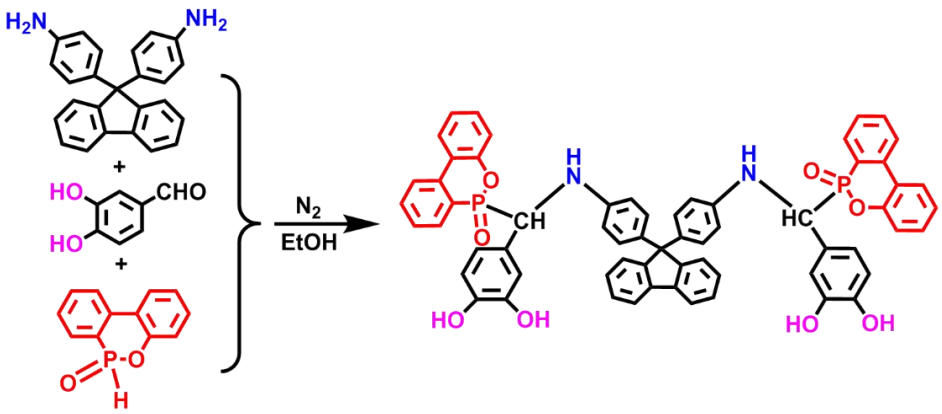

Figure 2-2. Synthesis illustration and chemical structure of FPD.

2.2.3 Fabrication of FPD on ramie fabric by mussel inspiration

According to the adhesion mechanism of dopamine, which is polymerized in an alkaline solution and deposited on the surfaces of various materials, for catechol, it would be polymerized and deposited with polyamine in an alkaline solution. In addition, to study the effect of different FPD addition levels on system performance, FPD was methodically added to the composite system at 10 wt.%, 20 wt.%, and 30 wt.% for the composites weight, corresponding to 12 g, 24 g, and 36 g. The phosphorus content was calculated to be 1.70%, 3.38%, and 5.04%,

respectively. Based on literature research[125-126], a phosphorus content of 5.04% is typically sufficient for flame retardancy of composites. Experiments were then conducted to validate this. Additionally, the epoxy resin amount curable by FPD was calculated, and the required DDM amount was determined based on the total epoxy resin in composites system. In this way, ramie fabric was first immersed in an aqueous solution of 1 mg·mL^{-1} for 20 min to deposit a layer of PEI to provide -NH_2 on the surface of ramie[165]. After being washed with deionized water, the PEI-coated fabric was squeezed to remove the adsorbed water and then dried in an oven for 4 h at 65 °C. Then, the FPD modification of the ramie fiber producer occurred in a THF solution containing various contents of FPD, adjusting the pH value to 8.5 with NaOH solution, and then immersed the fiber until the THF volatilized. After completion of the reaction, the FPD-grafted ramie fabric was washed with methyl alcohol and dried in an oven, the flame-retardant fabric was obtained and named RF-1, RF-2, and RF-3, respectively, and the pristine ramie fabric was named RF-0.

2.2.4 Preparation of ramie-epoxy resin composites

For fabrication of each composite, twelve layers of four kinds of ramie fabrics measuring 150 mm× 150 mm were cut and dried in a convection

oven. The epoxy resin (DER-331) was mixed with the hardener (DDM) and the transparent mixture was obtained; then, the composite material was prepared by a vacuum-assisted resin transfer molding process. The curing reaction was conducted at 90 °C for 2 h, 110 °C for 2 h, and then 130 °C for 2 h. The laminates were obtained after natural cooling to room temperature. The resin content was kept at 55-60 wt.%. The schematic diagram of the preparation process of composite materials was shown in Figure 2-3. The composites that obtained FPD-treated ramie fiber with different loading were marked as RFEPC-0, RFEPC-1, and RFEPC-2 and RFEPC-3, respectively. The detailed formulas were shown in Table 2-1. Test specimens were prepared by cutting and machining the composites to the standard size for the characterization of tensile and flexural properties (strength and modulus), flame retardancy, etc.

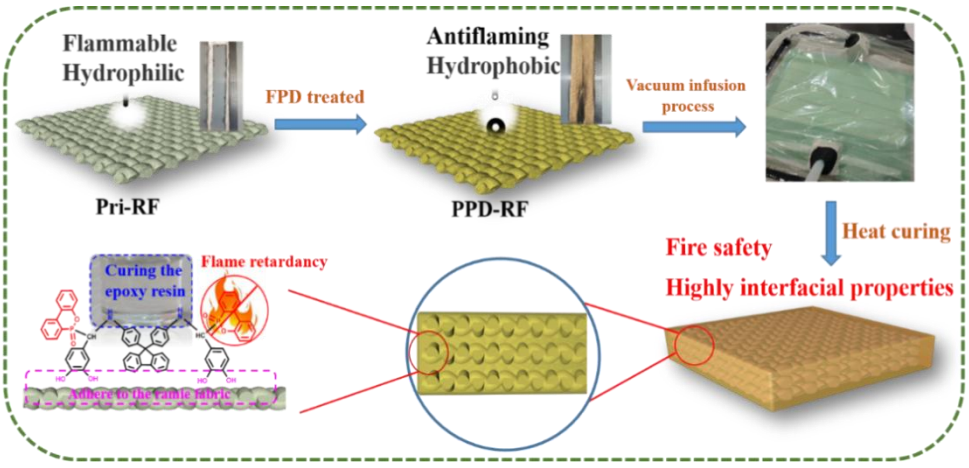

Figure 2-3. The schematic diagram of the preparation process of composite materials.

Table 2-1. Formulations of different samples.

Samples	Ramie fiber (g)	DER-331 (g)	DDM (g)	FPD (g)	Content of P (wt.%)
RFEPC-0	120	120	30.3	0	0
RFEPC-1	120	120	29.6	12	1.70
RFEPC-2	120	120	28.9	24	3.38
RFEPC-3	120	120	28.2	36	5.04

2.2.5 Characterization

^{1}H, ^{13}C, and ^{31}P nuclear magnetic resonance (NMR) spectra were collected on a 400 MHz Bruker AVANCE III spectrometer (Bruker, Switzerland) at 25 °C with DMSO-d_6 as solvent and tetramethyl silane as internal standard reagent. The attenuated total reflection-Fourier transform infrared (ATR-FTIR) spectrum was recorded on an infrared spectrometer (Cary660 + 620, Agilent, La Jolla, California, USA) from 4000 to 400 cm^{-1} with a resolution of 4 cm^{-1} at room temperature. The X-ray diffraction spectrometry (XRD) was conducted to research the crystallization of samples by a Bruker D8 advance diffractometer with Cu Ka radiation (1.54 Å) in the range of 5°-60°. The static water contact angle (WCA) in the air was performed using a contact angle-measuring instrument (OCA25, Dataphysics, German) with a 2 μL DI water droplet at room temperature. The results were taken from the average of the WCAs of five different parts of each sample. All the atomic force

microscope (AFM, Bruker, Germany) measurements were performed in PeakForce quantitative nanomechanical mapping (PF-QNM) mode at ambient conditions. The adhesive force measurements were performed with the spring constant (SNL-10, k = 0.35 N/m) of a standard silicon nitride AFM tip to quantitatively determine adhesion forces between the fibers and AFM tip according to the adhesion force–distance curves. Differential scanning calorimetric (DSC) measurements were conducted on a Mettler Toledo MET DSC (METTLER TOLEDO, Switzerland) at heating rates of 5, 10, 15, and 20 °C/min from 25 to 250 °C. Thermogravimetric analyses (TGA) were performed using a Mettler Toledo TGA/DSC1 (METTLER TOLEDO, Switzerland) with a 20 °C/min heating rate from 25 to 800 °C under a nitrogen atmosphere (flow rate: 25 mL/min). The limiting oxygen index (LOI) values of ramie fabric composites, with the size of 150 mm (length) × 6.5 mm (width), were acquired by a digital oxygen index apparatus (Jiangning Analytical Instrument Co. Ltd., China) according to the ASTM D2863-2008 standard. A vertical flame test was conducted on an automatic vertical burning tester (Jiangning Analytical Instrument Co. Ltd., China). Vertical flame tests of composites were performed according to ASTM D3801 standard with sample dimensions of 130 × 13 × 3 mm. The heat release of the composites was analyzed with a cone calorimeter test (CCT) (Fire

Testing Technology, the UK) for two samples, with sample dimensions of 100 mm × 100 mm were exposed to a heat flux of 35 kW/m^2 according ISO 5660-1. The surface morphologies of ramie samples before and after modification, fracture surfaces after tensile test, and char residues after CCT were observed using field-scanning electron microscopy (FE-SEM, EVO18, Zeiss) equipped with an energy-dispersive spectrometer. Thermogravimetric analysis–infrared spectrometry (TGIR) analysis was carried out on a TGA 8000 thermogravimetric analyzer coupled with a two-Clarus SQ8T spectrometer (PerkinElmer, Valencia, California, USA) from room temperature to 800 °C with a heating rate of 10 °C/min. The Raman spectra were collected from a Raman spectrometer via Reflex (Renishaw, Britain) to further characterize the char residues after CCT. The flexural and tensile properties were performed by universal material testing machine (5567, Instron, China) as per ASTM standard D-3039 method and ASTM D-2344, respectively, with a sample quantity of five for each test. The impact strength was carried out on a CEAST 9050 impact resistance device (Instron, Norwood, Massachusetts, USA), also using a sample quantity of five.

2.3 Results and discussion

2.3.1 Synthesis and characterization of FPD

The synthesis illustration and chemical structure of FPD were displayed in Figure 2-2. To confirm the success synthesis of FPD, the ^{1}H, ^{13}C and ^{31}P NMR, FTIR spectra were collected. Figure 2-4 and Figure 2-5 showed the ^{1}H NMR and ^{13}C NMR spectra of FPD, where the characteristic signals were the powerful evidence for the successful synthesis. As shown in Figure 2-4, the characteristic signals for -CH could be seen at 5.16 and 4.67 ppm, signals for Ph-H and -NH were at 8.3-6.4 and 6.05 ppm, and signals for -OH could also be observed at 9.2–8.5 ppm. To further confirm whether the -NH was in 8.3-6.4 ppm, the ^{1}H NMR with D_2O was conducted in Figure 2-6, the -OH in 9.2-8.5 ppm and -NH in 6.05 ppm were disappeared. Moreover, the integration of 8.3-6.4 ppm was decreased by 1, which proved that the -NH was in 8.3-6.4 ppm and the successful synthesis of FPD. In Figure 2-7, the peak in ^{31}P NMR spectrum showing at 28.9 and 31.2 ppm revealed that DOPO was successfully attached on the monomer.

FTIR was also taken for further structure identification. As can be seen in Figure 2-8, the absorption peaks at 3370 and 3068 cm^{-1} were assigned to the N-H bond and Ph-H bond, and a series of peaks located at 1198 cm^{-1} (P-O-C stretching) and absorption peaks at 1276 cm^{-1} (P=O bond) and 1610 cm^{-1} (P-Ph) stood for DOPO[166]. All these evidences proved that the FPD as the target product was successfully synthesized.

In the previous research, mussel-inspired improvement of the interfacial performance of fiber-reinforced composites was always a co-deposition of catechol onto fiber and subsequently prepared modified fiber reinforced composites[2]. The reported chemical compound DPDDM[156], containing the catechol structure agent, was utilized as a co-curing agent for epoxy resin and it was added to the epoxy resin directly. Additionally, DPDDM was insolube in any organic solvent except DMF due to the strong rigidity of the structure, which indicated that it cannot achieve the adhesion function of catechol and be used for the modification of composite materials. In this way, the FPD was designed to overcome the solubleness problem. To further explore its solubleness, FPD was placed in a common low-boiling-point solvent, such as alcohol, acetone, dichloromethane, trichloromethane, and tetrahydrofuran, and the results showed that the FPD could dissolve in tetrahydrofuran with a high solubility and the image of dissolution status was demonstrated in Figure 2-9.

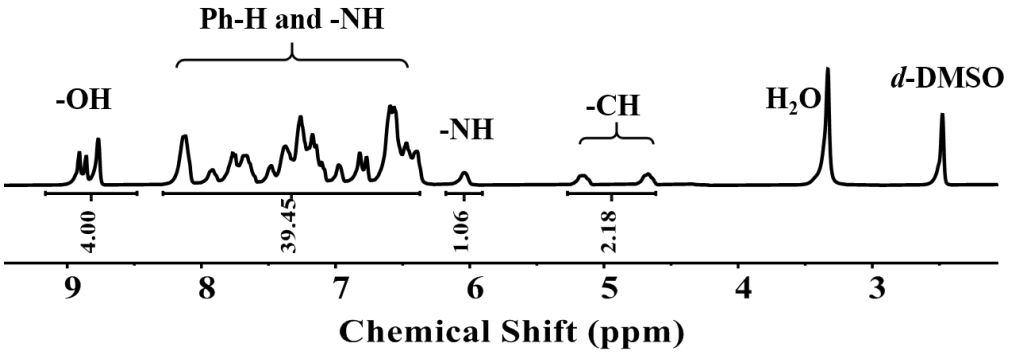

Figure 2-4. ^{1}H NMR spectrum of FPD.

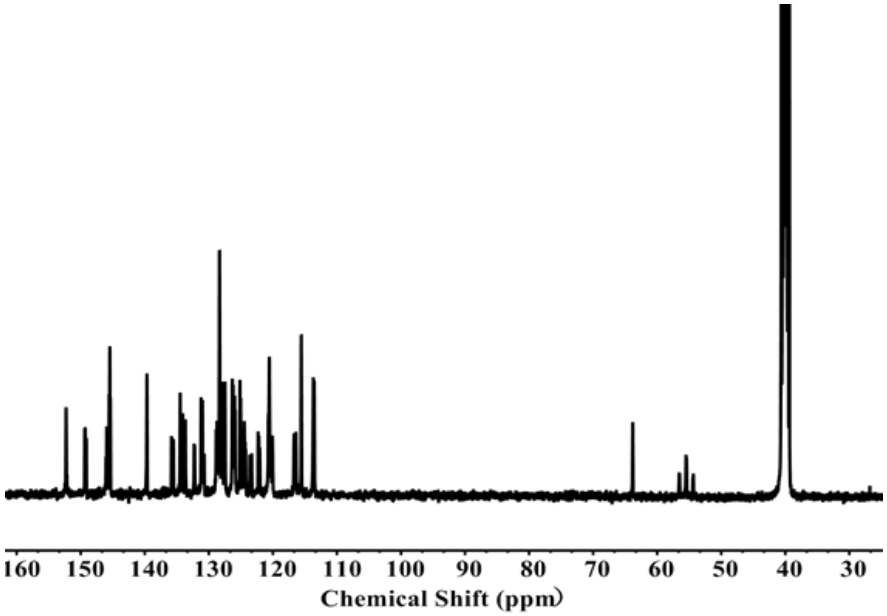

Figure 2-5. ^{13}C NMR spectrum of FPD.

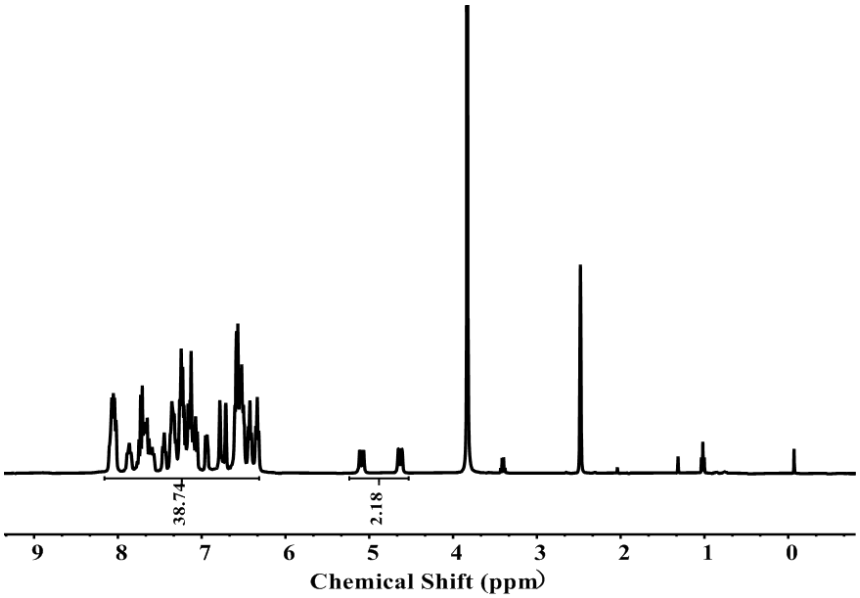

Figure 2-6. ^{1}H NMR spectrum with D_2O of FPD.

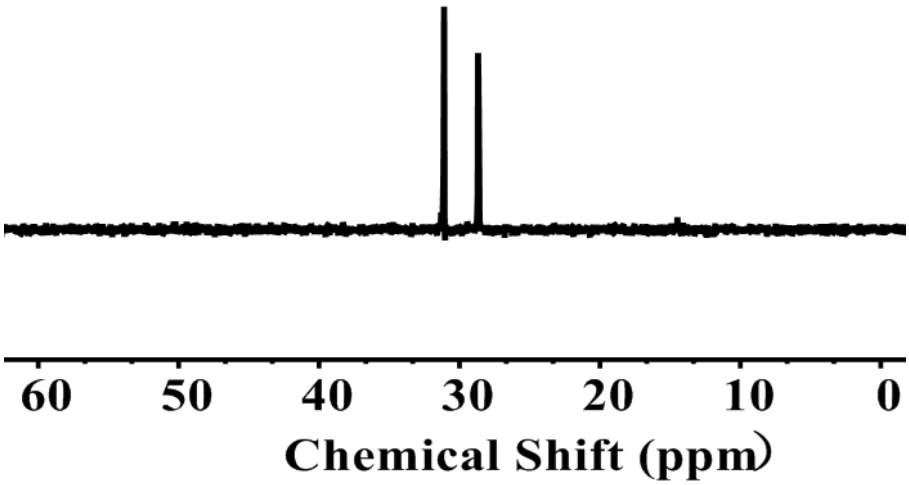

Figure 2-7. ^{31}P NMR spectrum of FPD.

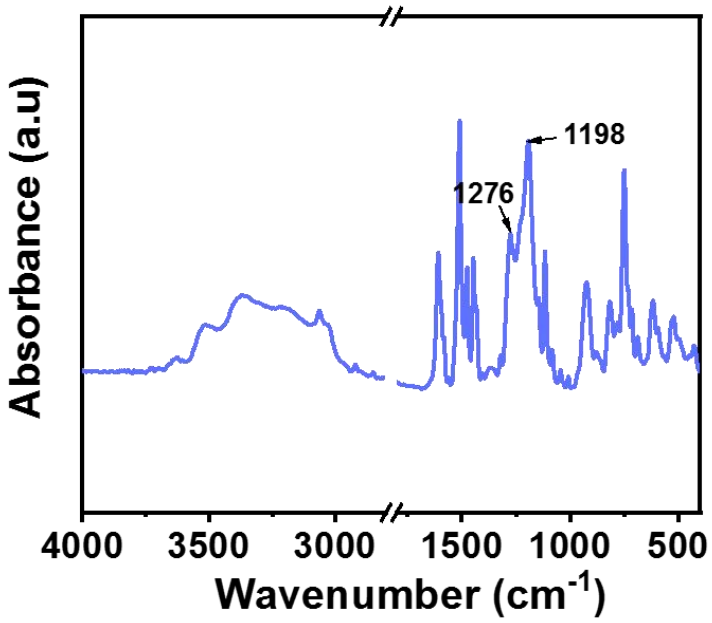

Figure 2-8. FTIR spectrum of FPD.

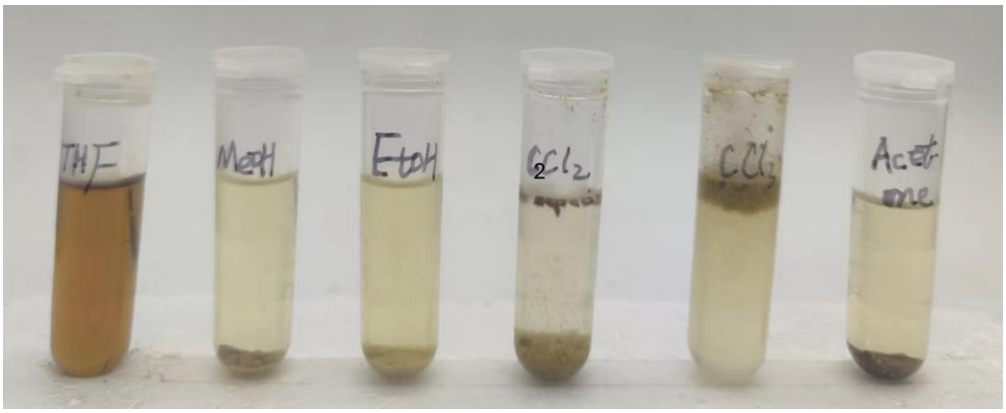

Figure 2-9. From left to right are the image of FPD dissolution status in alcohol, acetone, ethyl alcohol, dichloromethane, trichloromethane and tetrahydrofuran, respectively.

2.3.2 Characterization of mussel-inspired ramie fabric

To confirm whether the modification process was successful, SEM and EDS were characterized to analyze the uncoated (RF-0) and coated fabrics (RF-1, RF-2, and RF-3). Figure 2-10 presented the SEM pictures of the four kinds of fibers. The surface of the uncoated fabric was smooth and flat, as shown in Figure 2-10a. The SEM images in Figure 2-10b-d clearly showed that FPD particles were deposited on the surface of ramie fiber. EDS mapping was further used to investigate the element distribution of FPD-treated ramie fabric. In summary, the above results confirmed that FPD was successfully coated onto the ramie fiber.

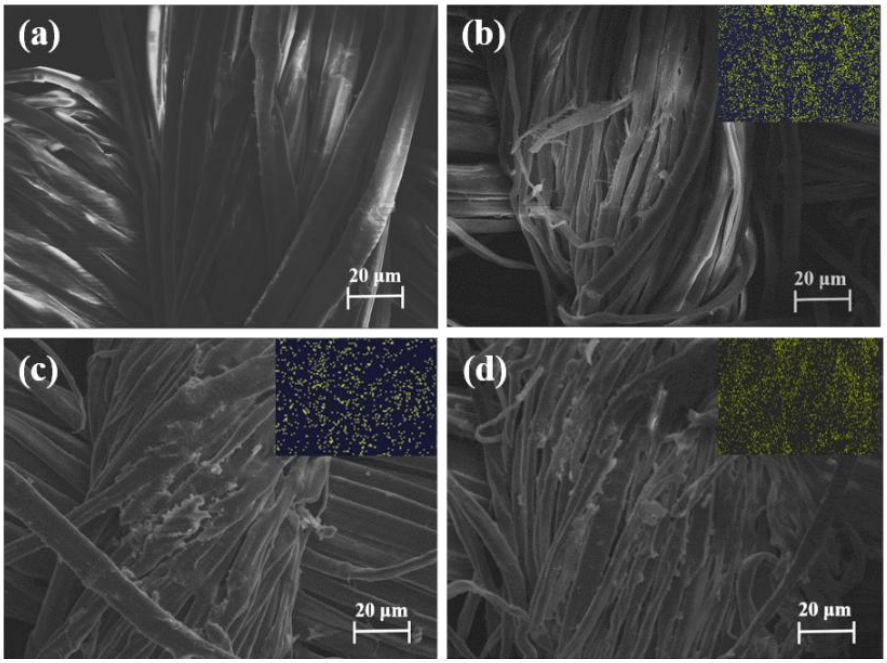

Figure 2-10. SEM micrographs and their corresponding elemental mappings of P element for RF-0 (a), RF-1 (b), RF-2 (c), and RF-3 (d).

2.3.3 Mechanical properties and compatibility

In this work, FPD acted with a role of linking the matrix and reinforcement of the composites, and it was expected that the FPD would confer the composites' better mechanical properties and interface performance. By comparing the mechanical behavior of composites in Figure 2-11 and Table 2-2, as can be seen from Figure 2-11a and b, the flexural strength, flexural modulus, tensile strength, and modulus of RFEPC-0, RFEPC-1, RFEPC-2, and RFEPC-3 increased in that order. Namely, the maximum flexural modulus and tensile modulus of 5570 MPa and 6779 MPa were observed for RFEPC-3, which was 19.3% and 60.9% higher than that of RFEPC-0 (4670 MPa and 4212 MPa), respectively. With regard to the flexural and tensile strength, it an enhancing trend from 107 MPa and 70 MPa for RFEPC-0 to 116.5 MPa and 96 MPa for RFEPC-3, respectively, was also demonstrated. The impact strength (Figure 2-11c) was also increased from 5.61 for RFEPC-0 to 7.22 $kJ \cdot m^{-2}$ for RFEPC-3. Moreover, the ILSS was also showed an increasing trend with the increase of FPD (Figure 2-11d). Hence, it can be concluded that the presence of the FPD did enhance the mechanical performance. Moreover, it is well known that the mechanical properties of fiber-reinforced composites are greatly influenced by the interfacial bond strength.

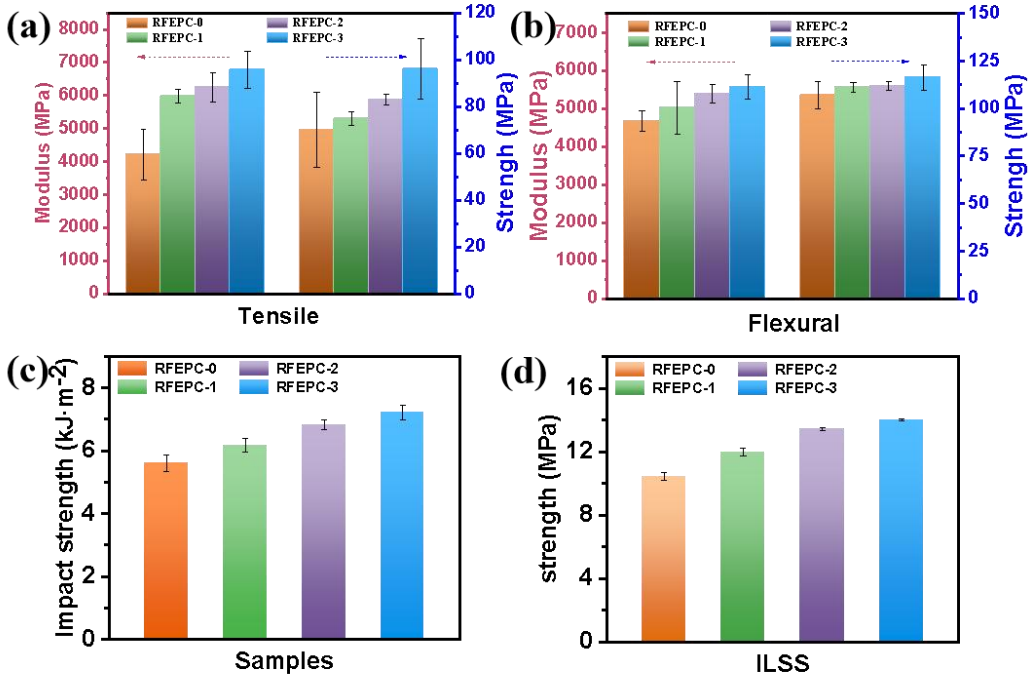

Figure 2-11. Mechanical properties for all composites: tensile strength and tensile modulus (a), flexural strength and flexural modulus (b), Impact strength (c) and ILSS (d).

Table 2-2. The mechanical properties of different samples.

Sample	Tensile		Flexural		Impact strength ($kJ·m^{-2}$)
	Strength (MPa)	Modulus (MPa)	Strength (MPa)	Modulus (MPa)	
RFEPC-0	70.0±16	4212±776	107±7	4670±276	5.61±0.27
RFEPC-1	74.8±3	5979±207	111±2	5020±688	6.17±0.21
RFEPC-2	83.0±2.4	6248±435	112±2.2	5390±252	6.83±0.15
RFEPC-3	96.0±13	6779±563	116±6.7	5570±322	7.22±0.24

To further acquaint the improvement of mechanical composites, the fractured surfaces of the composites after the tensile test were observed by SEM micrographs. As shown in Figure 2-12a, it was easy to identify

the ramie fiber with long and smooth surfaces were pulled out in clusters from the matrix, leaving some voids[167]. It can be observed that most of the fractured surfaces were fiber (indicated by yellow dotted circles) rather than epoxy resin, and it was hard to identify the interface between ramie fiber and resin, and some obvious voids (indicated by blue dotted circles) could be identified easily. This morphology basically indicated that there was little or no epoxy resin adhering on the surface of the pulled-out-ramie fabric, namely a very weak interfacial adhesion between fibers and the matrix. From Figure 2-12b, the ramie fiber seem to be trapped within the resin matrix since no obvious pulled-out fibers and voids were observed (indicated by red and white dotted circles), suggesting a much stronger interfacial interaction between the FPD-treated ramie fabric and the resin matrix, indicating that compatibility was strengthened, and thus the stress from matrix to reinforcements can be transferred efficiently, avoiding stress concentrations, which leads to higher tensile and flexural strengths, as evidenced by the mechanical test.

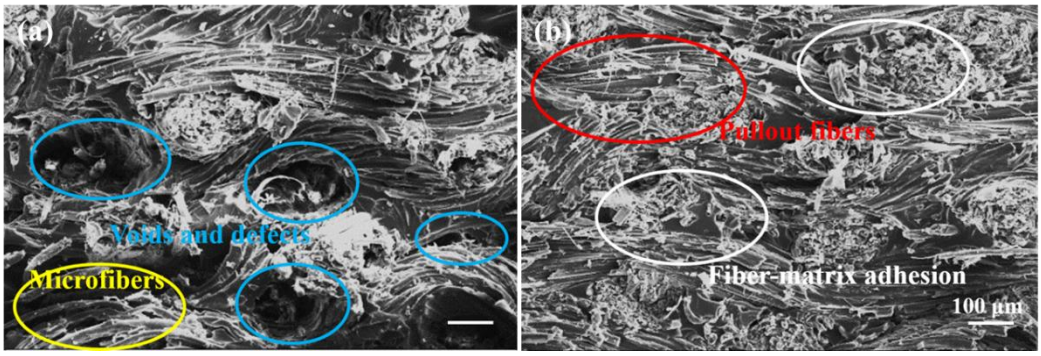

Figure 2-12. SEM images of fracture surfaces of composites after tensile test: RFEPC-0 (a) and RFEPC-3 (b).

Normally, when the cellulose is treated by organic solvent, the cellulose on the surface of ramie fiber may be damaged to a certain extent; for example, the cellulose Ⅰ in the crystalline region of ramie fiber gradually would change to the fiber Ⅱ in the amorphous region, which leads to the mechanical properties of ramie fiber being decreased due to the decrease in crystallinity, and further lowering the mechanical properties of ramie fabric/epoxy resin composite[8, 62]. The crystal structures of the three kinds of ramie fiber were analyzed by XRD, which was clearly shown in Figure 2-13a. The peak values of pristine ramie fiber were at 2θ = 14.64°, 16.47°, 22.75°, and 34.45° positions, corresponding to the crystal planes of cellulose (101), (110), (002), and (004), respectively[168-170]. The crystal structure and the intensity of the peak of the modified ramie fiber were basically consistent with that of the original one. These structures indicated that the two chemical

modifications did not change the crystal structure of ramie fiber, which means that the mechanical property of the ramie fiber was not damaged.

The poor compatibility between the polymer matrix and untreated ramie fiber is a very significant factor for the weak mechanical performance. The compatibility between the polymer matrix and ramie fiber would be facilitated via reducing the polarity difference between ramie fiber and epoxy resin. In this chapter, the compatibility between the two phases was increased by improving the hydrophobicity of ramie fiber. To verify whether the FPD could change the waterproof property of ramie fiber, the water contact angle and AFM were tested. It was a surprise to find that the water contact angle of the ramie fabric modified by FPD could reach 138.7° (Figure 2-13b); this may due to the fact that FPD was intrinsically structurally rigid and hydrophobic. Moreover, the adhesive forces between a standard silicon nitride AFM tip and fibers were quantitatively characterized by AFM of the PF-QNM mode. A clear adhesion force–distance curve among the different samples can be observed on Figure 2-13c. It was interesting to observe that there was a big gap for the mean adhesion force between pristine fiber and FPD-modified fabric, which was because the AFM tip was hydrophilic, leading the adhesion forces between the hydrophilic AFM tip and the hydrophobic FPD-modified fiber to decrease, which was highly echoed

with the water contact angle result. The enhanced hydrophobicity of ramie might be attributed to the FPD that was hydrophobic and it was successfully incorporated into the ramie fabric. In addition to the SEM analysis, ATR-FTIR was measured as well, and the result was shown in Figure 2-13d, the broad peak between 3000 and 3600 cm^{-1} was attributed to the O-H stretching vibration of the cellulose. Similarly, the peaks observed in the region of 800 to 1200 cm^{-1} were also attributed to cellulose[171]. Comparing the spectrum of the pure fiber with that of FPD-treated ramie, the new characteristic peaks appearing at 1276 and 1594 cm^{-1} for the FPD-treated fabric attributed to the DOPO absorption could be observed clearly, which also demonstrated that the FPD was successfully coated onto the ramie fabric.

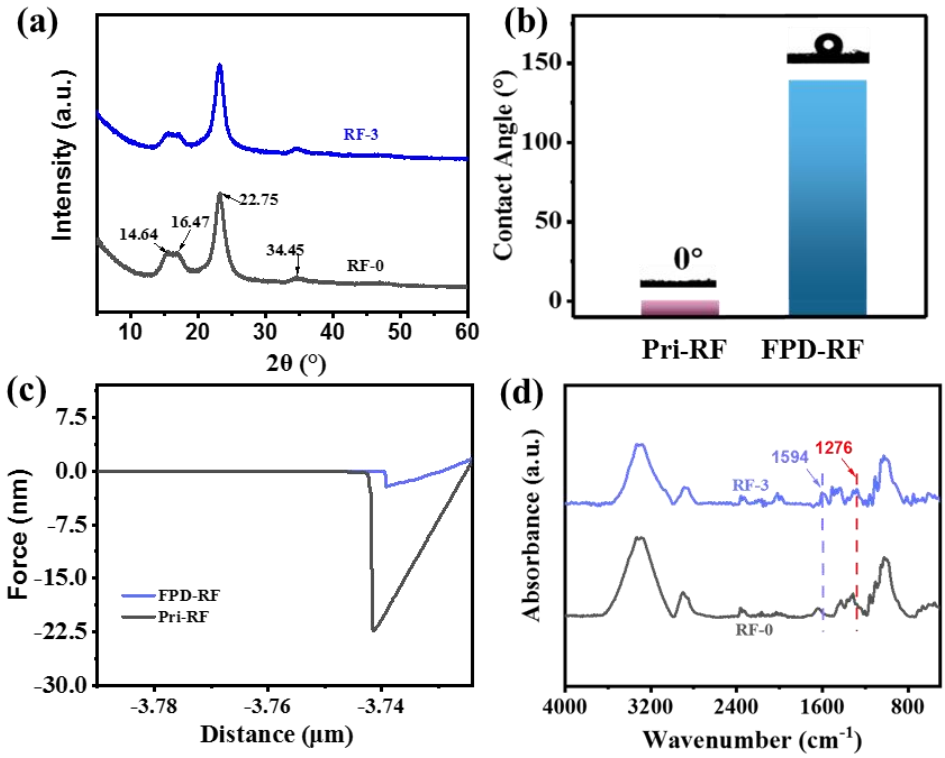

Figure 2-13. XRD spectra for RF-0 and RF-3 (a), water contact angle of RF-0 and RF-3 (b), adhesive force curves between RF-0, RF-3 and AFM tip (c), ATR-FTIR spectra for RF-0 and RF-3 (d).

In this chapter, FPD had a role of linking the matrix and reinforcement of the composites; in addition to the undamaged fiber and improved compatibility between fiber and matrix, FPD also could play the role of being a co-curing agent for the matrix, and to investigate whether the FPD could cure the epoxy resin, DSC was tested and the results were shown in Figure 2-14. Interestingly, there was only one exothermic peak when the PFD acted as the co-curing agent for epoxy resin. Additionally, the temperature of the opening ring was also decreased, which can

avoid the mechanical destroying of plant fiber when exposure high temperature for long time. What's more, the possible reaction mechanism of FPD and 4, 4'-diaminodiphenylmethane (DDM) with DER-331 was illustrated in Figure 2-15.

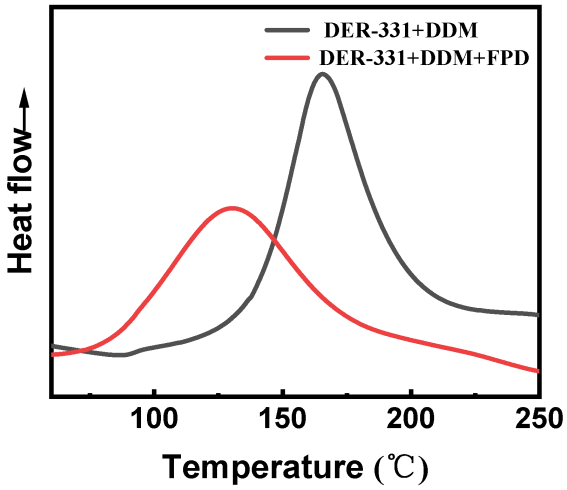

Figure 2-14. DSC curves for FPD as the co-curing agent.

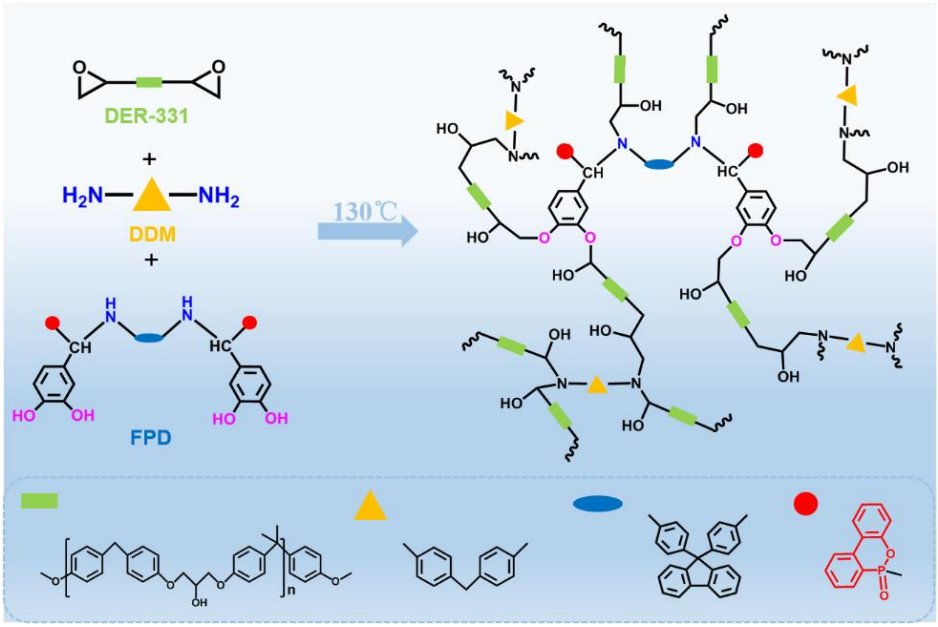

Figure 2-15. The possible reaction mechanism of FPD and 4, 4'-diaminodiphenylmethane (DDM) with DER-331.

2.3.4. Thermal stability of composites

The thermal degradation and stability of the material have important effects on the anti-flame performance. Hence, TGA was assessed to evaluate the thermal decomposition process under nitrogen atmosphere of all samples. As displayed in Figure 2-16 and Table 2-3, the thermal stability of the samples obviously showed an improvement with the addition of FPD. Accordingly, as shown in Figure 3-14a and b, the T_{d10} (the temperature of 10% mass loss) of the three cured composites were tiny and declined in the order of RFEPC-0, RFEPC-1, RFEPC-2, and RFEPC-3 (342.3, 329.3, and 318.3 *vs.* 272.3 °C), indicating that FPD led to the earlier decomposition. This was ascribed to FPD and began to decompose first at a lower temperature to form phosphoric acid or polyphosphate compound since the lower thermal stability of P-C and O=P-O bonds in FPD, compared with the C-C bond[172]. In addition, the carbon residue at 800 °C was increased in that order, the highest char residues value of 27.77% was obtained for RFEPC-3, which was higher than that of RFEPC-0, only 9.92%, and might indicate the improved thermal stability flame safety of composites after the FPD incorporation.

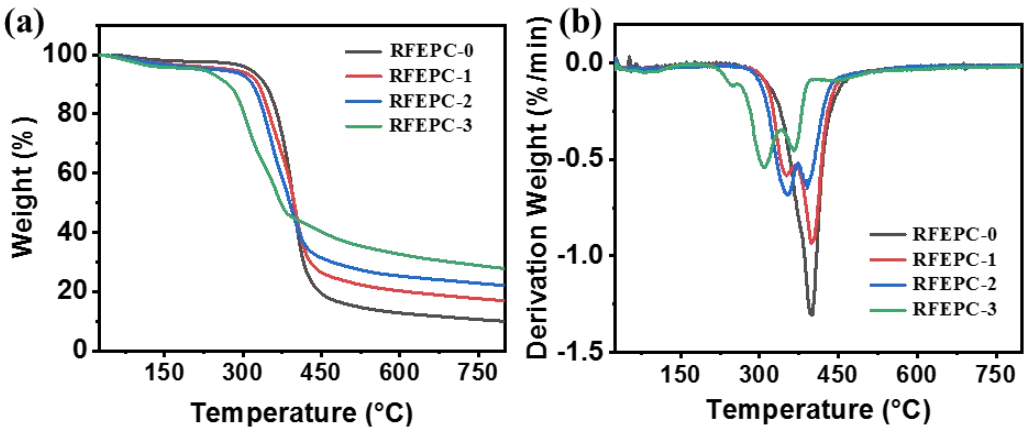

Figure 2-16. TGA (a) and DTG (b) curves for composites.

Table 2-3. Results of thermal stability of composites.

Samples	T_{d10} (°C)	Char yield at 800 °C (%)	R_{max} (°C)
RFEPC-0	342.3	9.92	398.7
RFEPC-1	329.3	16.84	399.0
RFEPC-2	318.3	22.05	353.0
RFEPC-3	272.3	27.77	309.0

2.3.5 Flame resistance performance of composites

The flammability of the composites was investigated by the limit oxygen index (LOI). Generally speaking, the value of the LOI of RFEPC-0 was only 23.4%. What's more, the LOI value increased to

34.6% rapidly after 30% FPD was modified, which demonstrated that the flame retardancy increased after adding FPD.

Further assessment of the flammability of the ramie/epoxy resin composites with different loading of FPD was conducted by vertical burning test. The obtained data and images are collected in Table 2-4 and Figure 2-17. Since ramie and epoxy resin are flammable materials, RFEPC-0 was completely consumed during the UL-94 tests, and no rating was obtained. Things changed better in the presence of 20% FPD, but it was still inhibited to some extent, and the flame retardancy was not enough to extinguish fire itself. It was noticed that RFEPC-3 self-extinguished within 10 s after the second fire was removed, rarely producing smoke during the combustion process, which indicated that FPD could impart to the composite high-flame retardancy property.

Table 2-4. Results of flame retardant measurements.

Samples	LOI	t_1/t_2 (s)	Dripping	UL-94
RFEPC-0	23.4	-[a]	No	No-rating
RFEPC-1	26.8	-[a]	No	No-rating
RFEPC-2	29.6	-[a]	No	No-rating
RFEPC-3	34.6	2.3/5.6	No	V-0

-[a]: Does not extinguish fire after ignition.

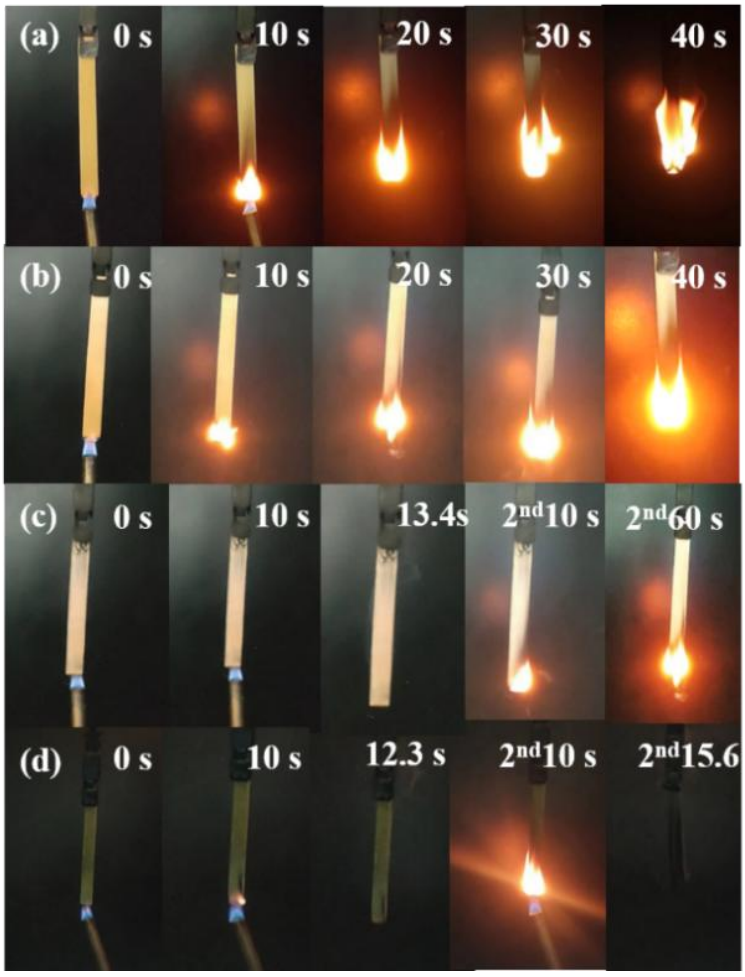

Figure 2-17. Digital photographs of RFEPC-0 (a), RFEPC-1 (b), RFEPC-2 (c), and RFEPC-3 (d) during the vertical test.

The cone calorimeter test is normally analyzed to evaluate the combustion performance of material in actual fire condition, and the heat release rate (HRR) and total heat release (THR) are two important indicators; the higher HRR or THR, the greater risk of fire for the material. The cone calorimeter test results for composites were exhibited in Figure 2-18. As shown in Figure 2-18a and b, both HRR and THR were

significantly decreased with the increasing loading of FPD. Accordingly, the HRR and THR declined from 513.8 W/m^2 and 85.13 W/m^2 for RFEPC-0 to 258.9 kW/m^2 and 64.23 kW/m^2 for RFEPC-3, respectively. This trend was similar to that observed for the flammability tests, and in agreement with the TGA results. In addition, Figure 2-18c and d revealed that FPD could slow down the smoke production rate (SPR) and the total smoke production (TSP) of composites, illustrating that FPD could efficiently suppress the smoke formation during burning, and thus improving the fire safety of composites. The smoke suppression might be relevant with the excellent char-forming efficient of FPD, which not only isolates and protects the materials inside from fire, but also restrains the diffusion of the produced flammable gases[173]. Interestingly, the CO production rate (COP) for the RFEPC-3 increased (Figure 2-18e), which may be attributed to the fact that the PO· and PO_2· free radicals released from DOPO can be effectively quenched and eliminated from the free radical chain reaction, resulting in incomplete combustion of the matrix. Moreover, the CO_2 production rate (CO_2P) for the RFEPC-3 also increased (Figure 2-18f), which could take away the heat as well as dilute the flammable gas and oxygen in the gas phase and indicates the presence of the gaseous-phase flame-retardant effect of FPD[143].

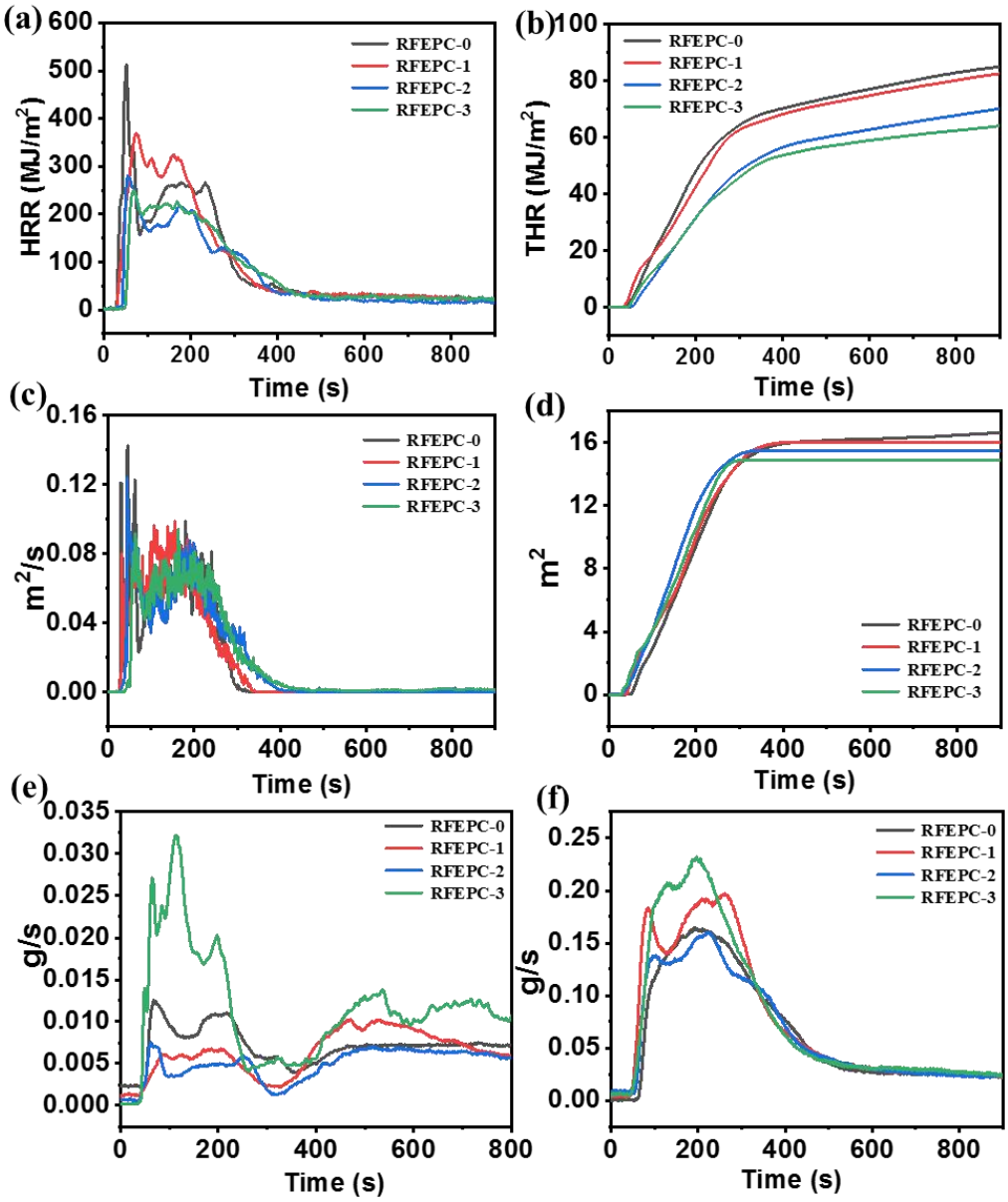

Figure 2-18. HRR (a), THR (b), SPR (c), TSP (d), COP (e), and CO_2P (f) curves for composites.

To sum up, through the analysis of thermal stability, LOI, UL-94, and CCT behavior, the flammability of the composites was investigated by the limit oxygen index (LOI). Generally speaking, the value of the LOI of

RFEPC-0 was only 23.4%. Moreover, the LOI value increased to 34.6% rapidly after 30% FPD was modified, which demonstrated that the flame retardancy increased after adding FPD.

Based on above results, it was concluded that the addition of FPD could not only significantly improve the thermal and flame retardancy of ramie fiber/epoxy resin composites, but also simultaneously increase its mechanical properties, including flexural, tensile, and impact. Compared with the previous work[62], ammonium polyphosphate (APP) was used as a flame-retardant modifier and the composite with 8.9% flame retardant could achieve a UL-94 V-0 rating. However, slight damage in flexural strength or modulus under different APP loading appeared with the composite without APP as the control, which indicated that FPD was more of an all-round modifier than APP.

2.3.6 Flame-retardant mechanism

The analysis of thermal degradation gaseous products

TG-FTIR was performed in order to analyze gaseous products of materials during the thermal decomposition process and further unveil the gaseous-phase action of flame retardants, as illustrated in Figure 2-19 and Figure 2-20. As depicted in Figure 2-19, the absorption positions of FTIR peaks in 3D images were quite similar, but the

absorption intensities of RFEPC-0 were stronger than that of RFEPC-3, which implied that the introduction of flame retardants would suppress the thermal degradation process rather than change it. As displayed in Figure 2-20a, with RFEPC-3, the P-O absorption peak appeared at 1060 cm^{-1}, indicating that the phosphorus in FPD played a fire-resistant role in the gaseous phase. Figure 2-20b was the absorption peak intensity of the main thermal degradation products that changed with time, the time of gas-phase degradation products of RFEPC-3 was earlier, and the gas release rate was lower, which mainly indicated the catalytic degradation effect of flame retardants on the composites, consistent with the results of TGA results. The release of carbonyl compounds was declined for RFEPC-3 when compared with RFEPC-0 (Figure 2-20c), which indicates that the free radical cracking reaction was effectively inhibited in the RFEPC-3 system. Meanwhile, the release of flammable gases such as hydrocarbons (Figure 2-20d), aromatic compounds (Figure 2-20e), and ethers (Figure 2-20f) was also restrained, while the production of nonflammable gases such as water (Figure 2-20g) and carbon dioxide (Figure 2-20h), can be promoted, which could take away the heat as well as dilute the flammable gas and oxygen in the gas phase. In a word, FPD could improve the flame retardancy through facilitating the release of non-flammable gases such as H_2O and CO_2, and restraining the

release of flammable gases including hydrocarbons, carbonyl, aromatic, and ethers compounds, etc. These CO_2 trend results are consistent with the CO_2P value in the CCT test.

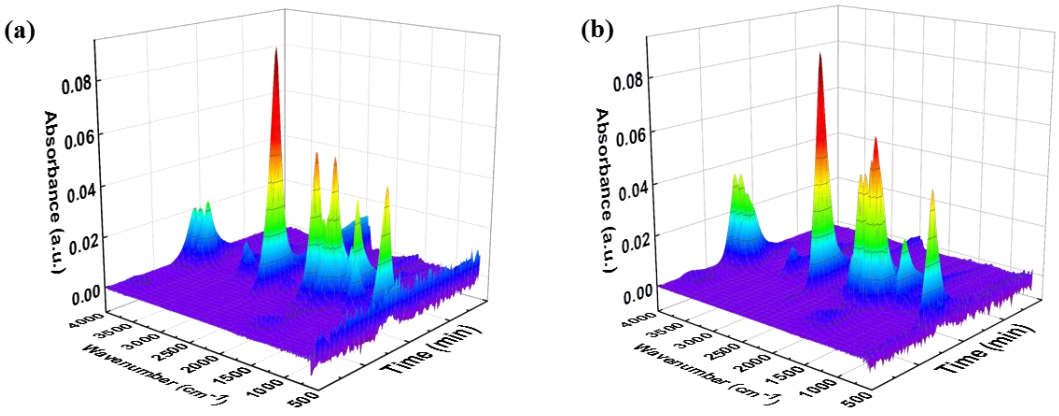

Figure 2-19. TG-FTIR 3D spectra for RFEPC-0 (a) and RFEPC-3 (b).

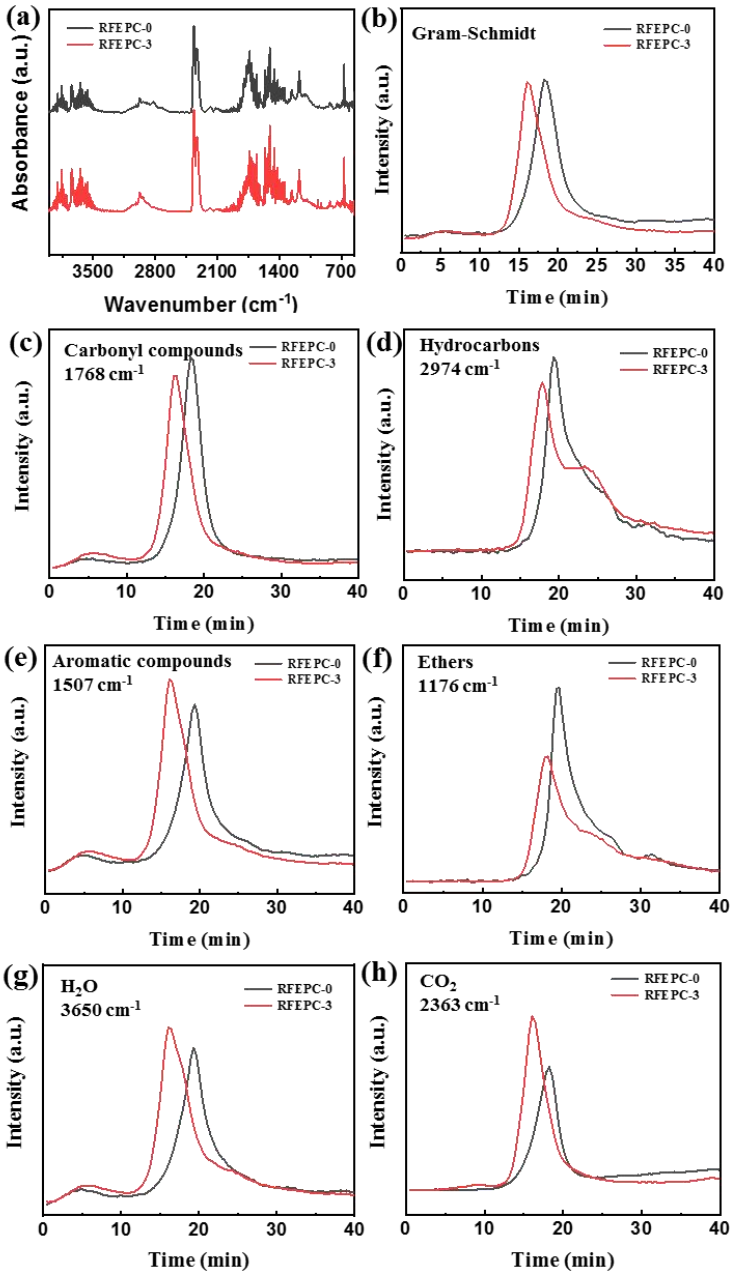

Figure 2-20. FTIR spectra of pyrolysis products for RFEPC-0 and RFEPC-3 at maximum decomposition rate (a); intensity of pyrolysis products (b), carbonyl compounds (c), hydrocarbons (d), aromatic compounds (e), ethers (f), H_2O (g), and CO_2 (h) versus time for RFEPC-0 and RFEPC-3.

The characteristic of the condensed phase

Normally, besides releasing non-flammable gases in the gaseous phase, the DOPO-containing flame retardants also can exert flame-retardant effects through promoting the formation of a dense char layer in the condensed phase. To further ascertain the flame-retardant mechanism, the condensed phases obtained after cone calorimeter tests for RFEPC-0 and RFEPC-3 were investigated. As shown in Figure 2-21a and c, some char residue was observed for RFEPC-0, and the char residue was broken and discontinuous. This was probably ascribed to the rapid decomposition of composites, which would break through the thin char layer. On the contrast, that the char layer became more compact, continuous, and intumescent could be observed since the addition of FPD leading the char residue increased and gentler degradation happened, as displayed in Figure 2-21b and d.

Further analyzing the morphology of char residue by SEM (Figure 2-22a and c), it was found that the char residue of RFEPC-0 exhibited the homogeneous and complete morphology of burned fiber structures, which may be attributed to the incomplete combustion of composites. Conversely, the incorporation of FPD, which was demonstrated in Figure 2-22b and d, made the char residue be denser and only a few fibers could be observed; the fiber would be protected by epoxy resin, which

also can indicate that the FPD did participate in the curing process of epoxy resin. Furthermore, the combination of a compact external char layer and hollow char fiber residue was capable of storing considerable pyrolysis gases with masses of phosphorous free radicals and nonflammable gases during combustion, which were instantly released to snuff out the flame when the gas pressure in the interior was sufficient to break through the char layer.

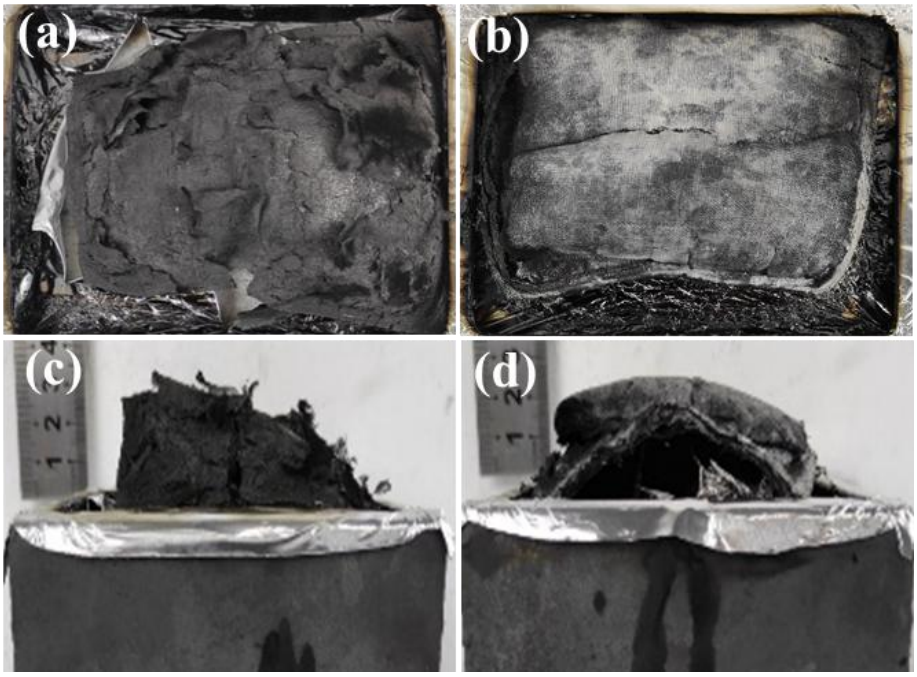

Figure 2-21. The vertical and the horizontal views of the char residue of RFEPC-0 (a and c) and RFEPC-3 (b and d) after the cone calorimeter test.

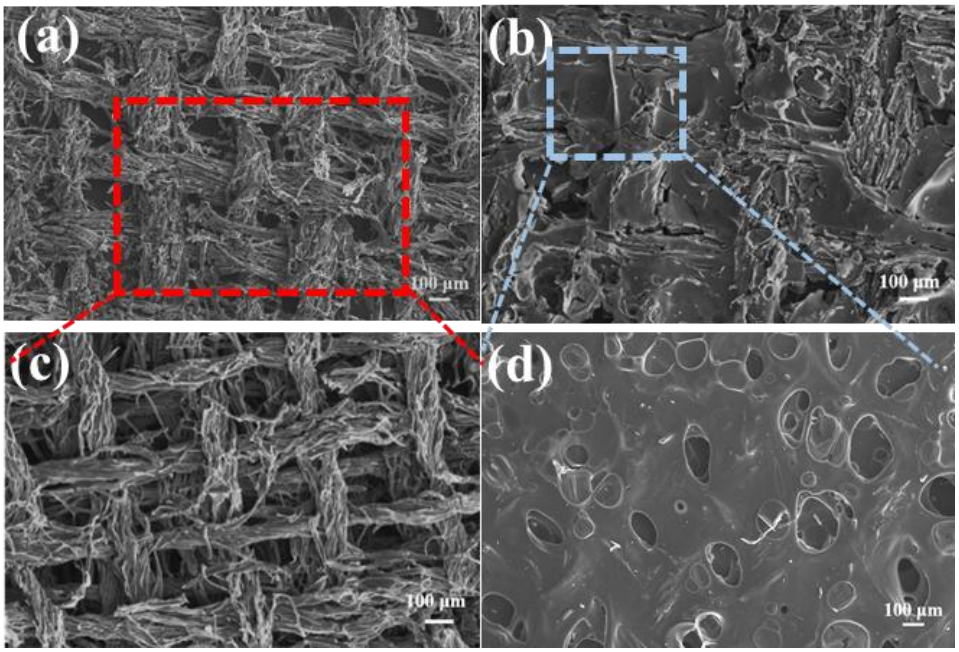

Figure 2-22. SEM micrographs of char residues of RFEPC-0 (a) and (c), and RFEPC-3 (b) and (d) under different magnificent.

The Raman spectra also demonstrated the former conclusion. As we know, the ratio of two peak areas (ID/IG) represents the graphitization degree, which is the ratio of disordered graphite (located at 1350 cm^{-1}) and ordered graphite (located at 1590 cm^{-1}), which means the lower ID/IG is, the more regular the char layer is[157]. Therefore, compared with RFEPC-0 (Figure 2-23a) and RFEPC-3 (Figure 2-23b), RFEPC-3 exhibited a lower ID/IG than that of RFEPC-0. Based on the above results, a supposed mechanism is presented for the enhanced flame retardancy. In a word, the integrated and continuous char layer was more conducive to prevent the heat transfer, O_2, and flammable volatiles,

revealing a strong barrier effect to improve the fire safety of the epoxy composites. Based on the above analysis, the schematic diagram of the possible flame retardant mechanism of ramie fiber/epoxy composites modified by FPD was demonstrated in Figure 2-24.

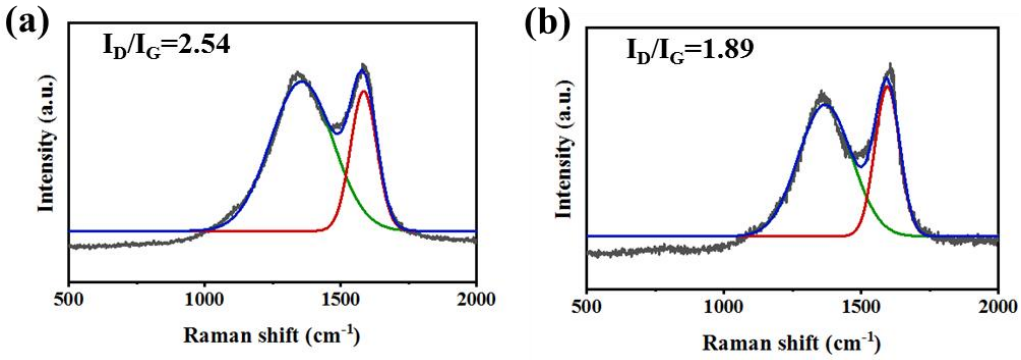

Figure 2-23. Raman spectra of char residuals for RFEPC-0 (a) and RFEPC-3 (b).

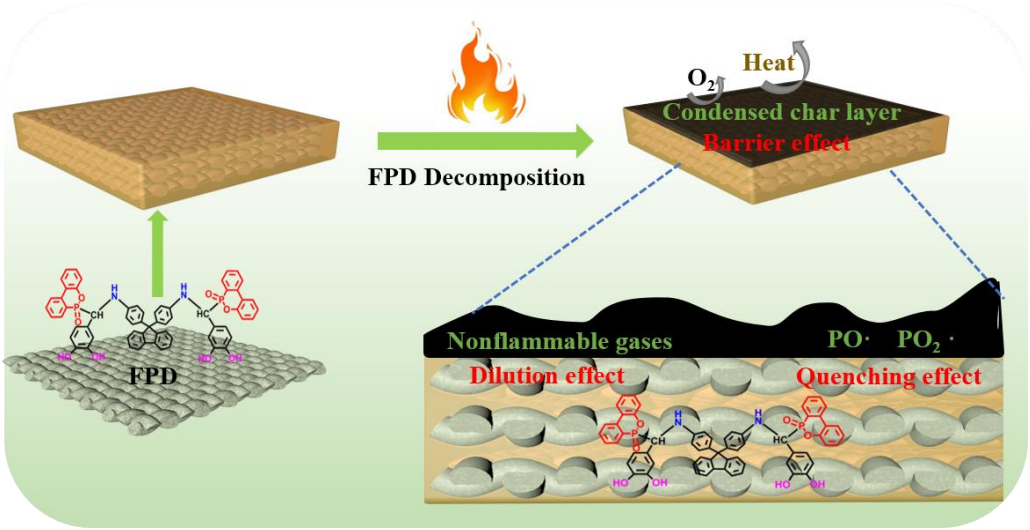

Figure 2-24. The schematic diagram of the possible flame-retardant mechanism of ramie fiber/epoxy composites modified by FPD.

2.4 Conclusion

In this chapter, inspired by mussel, a multi-functional modifier, which could improve the mechanical and thermal performance of ramie-reinforced epoxy resin composites, simultaneously was designed and synthesized successfully through just one step. It can be successfully introduced and firmly adhere to the ramie fabric, and the hydrophobic property and N-H were both integrated into ramie fabrics so the compatibility between fiber and epoxy resin could be facilitated; and thus, FPD can play a bridging role to enhance the interfacial properties of ramie epoxy composites. The flexural and tensile strength and modulus were all increased, from107 MPa, 70 MPa, 4670 MPa, and 4212 MPa for RFEPC-0 to 116.5 MPa, 96 MPa, 5570 MPa, and 6779 MPa for RFEPC-3. In addition, the fire safety of modified RFEPC was also improved by forming compact and continuous char layers and facilitating the release of non-flammable gases, which enabled RFEPC-3 to achieve a UL-94 V-0 rating. This work offers an effective approach to fabricate strong interfacial and flame-retardant ramie performance-reinforced epoxy composites, which may enable potential application prospects in the files of construction, trains, and automobiles with interior trim.

Chapter 3 Study on preparation of HGB as well as mechanical and flammability properties of HGB and PA coated Suncell fiber reinforced epoxy resin composite

3.1 Introduction

Benoxazine is a triazine nitrogen-containing heterocyclic organic compound. Due to its high nitrogen content, benoxazine usually has good flame retardant performance. It can be used as a nitrogen-based flame retardant and an air source of traditional expansive flame retardants, and phenolic and amine sources are required for synthesis. The benzoxazine synthesized from arbutin can be used as carbon source and air source at the same time, and can be used as a good char forming agent in the expansion flame retardant. At the same time, arbutin has a certain water solubility, and the water solubility can be soaked with fabric fibers. At the same time, participating in the curing of epoxy resin is conducive to improving the interface properties of ramie-epoxy resin composites.

Biobased phytic acid has the advantages of non-toxic, renewable and biodegradable. Because of its high phosphorus content and reactivity, it can be used as an acid source in intumescent flame retardants, which has attracted wide attention in textile finishing, especially in the field of

flame retardant finishing. Therefore, phytic acid and benzoxazine can be combined to form a new type of bio-based expansive flame retardant, which can be regarded as a green and ecological sustainable finishing technology for the flame retardant modification of textiles.

Inspired by intumescent flame retardants which contain an acid source, a carbon source (the charring agent), and a gas source (the blowing agent)[174 175-177], an arbutin-based benzoxazine (HGB) and PA as combination modifier were selected for the following reasons: Ⅰ) The renewable sources conform to the requirements for sustainable preparation of green composites, while their water-solubility and hydrogen bonds-forming ability contribute to mild processing and easy adhesion to the fiber surface; Ⅱ) HGB with high char yield play a role of char forming agent which can also react with epoxy resin upon curing; Ⅲ) PA with high phosphorus content (28 wt.%) act as an acid source to induce char formation by releasing carboxylic or phosphoric. It can be expected that both compatibilizer and flame-retardant effects could be achieved by this combination.

In this chapter, water-soluble fiber modifier that simultaneously enhances interface adhesion and flame retardancy were proposed, consisting of arbutin-based benzoxazine (HGB) and phytic acid (PA). The mechanical property of ramie fabric was initially tested after treated

by this combination. However, significant degradation in mechanical properties was observed, likely due to the strong acidity of phytic acid reacting with the hemicellulose in ramie. To mitigate this issue, Suncell fabric, a 100% artificial cellulose fiber was switched to using in this chapter. This change was made to reduce the destructive interaction of phytic acid with the reinforcement material, thereby improving the system's overall performance. This combination modifier can directly be coated on the surface of the regenerated cellulose fiber fabrics (trademark: Suncell) through impregnation in the aqueous phase, which concurrently improves surface polarity fire resistance. The modified fabrics were further composited with an intrinsic flame-retardant epoxy resin (DGEBDB) to obtain composite materials. Benefiting from the intumescent flame retardants (IFR)-like behavior of the combination modifier and the fireproof effect of the epoxy matrix, the developed composite exhibited a V-0 rating in the UL-94 test and an excellent LOI value of 33.8%. The results provide a simple strategy for synergistically enhancing interfacial compatibility and flame retardancy of plant fiber-reinforced composite under mild conditions, and offer novel solutions for achieving advanced development of green composite materials.

3.2 Material and methods

3.2.1 Materials and chemical used

Suncell Fiber was provided by Zhengzhou Zhongyuan Spandex Machine Co., Ltd, and the areal density is approximately 232 g/m^2. Arbutin (99%) was obtained from Xi'an Lishi Biotechnology Co., Ltd. (Xi'an, China). 4, 4′- Diamino diphenylmethane (DDM), 1,3-propane diamine (99%), Phytic acid (PA, biochemical reagent, 70.0% aqueous solution) and 1,4-dioxane (99%) were purchased from Aladdin Chemistry Co., Ltd. (China). Diglycidyl ether of bisphenol A (abbreviated as DGEBA, trade name DER-331) with an epoxy value around 0.51-0.53 mol/100 g was purchased from Dow Chemical Company. Self-retardant epoxy resin (DGEDBD, epoxy value: 0.47) was prepared in our lab according to the previously reported method the specific information can be found in relevant work[150]. Distilled water was supplied by our lab. All other chemical agents were commercially available and used as received.

3.2.2 Synthesis of HGB

The HGB was synthesized via the Mannich condensation reaction of arbutin, propane diamine, and paraformaldehyde, as shown in Figure 3-1. The synthesis of HGB followed the following procedure: under an N_2 atmosphere, 60.06 g of 1,3-propane diamine (0.5 mol, 37.1 g) and 60.06

g of paraformaldehyde (2 mol) together with 150 mL of 1,4-dioxane were mixed and poured into a 250 mL three-neck flask, after the mixture was stirred at room temperature for 30 min, arbutin (1 mol, 27.2 g) was added. Then the mixture was stirred vigorously at 90 °C for 12 h. The crude products were filtered and washed with ethyl alcohol several times to remove impurities. Finally, the product was dried under a vacuum at 80 °C for 12 hours. After the residual solvent was removed in the vacuum oven (-0.1 MPa) at 80 °C, the target product HGB was obtained (yield: 56%).

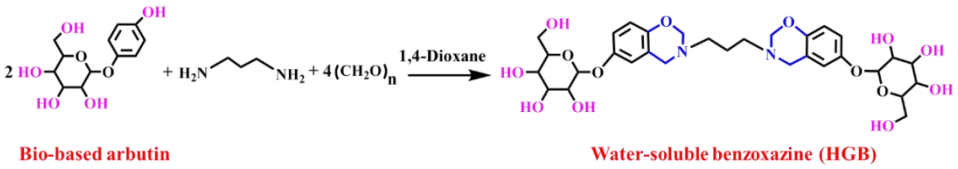

Figure 3-1. Synthesis illustration and chemical structure of HGB.

3.2.3 The flame-retardant modification for ramie fabric

The HGB- and PA-modified ramie fiber was prepared by the dip-coating method. The HGB and PA were dissolved in deionized water, and the concentration of HGB and PA were 1, 1.5, and 2 mg/mL, respectively. The ramie fabric was immersed into the solution, and after the padding and drying process (70 °C for 30 min), it was designated sequentially as PAHG-RF-1, PAHG-RF-1.5 and PAHG-RF-2 and the

breaking strength them were tested and the result were demonstrated in Figure 3-9.

3.2.4 The flame-retardant modification for Suncell fabric and F-EP

The HGB- and PA-modified Suncell fiber (F-SF) was prepared by the dip-coating method. The HGB and PA were dissolved in deionized water, and the concentration of HGB and PA were 1, 1.5, and 2 mg/mL, respectively. The Suncell fabric was immersed into the solution, and after the padding and drying process (70 °C for 30 min), it was designated sequentially as SF-1, SF-1.5 and SF-2. To optimize the best concentration, the breaking strength and flammability regime of them were tested and the result were listed in Table 3-2. The result revealed that SF-2 could self-extinguish while maintaining the mechanical properties to the maximum extent, which was renamed F-SF and chosen for fabricating composites. According to the formula:

$$\mathrm{w} = \left(m_{SF-x} - m_{SF}\right) / m_{SF} * 100\% \quad (3\text{-}1)$$

where w is the weight gain of fabric after the FR dip-coating process, m_{SF-x} is the average weight of SF after FR modification, and m_{SF} is the original average weight of RF. The areal density of SF was 232 g/m^2. after FR treatment, the areal densities of SF-1, SF-1.5, SF-2 were

increased to 241, 251, and 259 g/m^2, so the weight gains of HGB and PA on SF was 3.9%, 8.2% and 11.6%, respectively.

The F-EP matrix was mixed using DER-331 and DGEBDB by the ratio of 7:3, which was the best ratio according to the report[150].

3.2.5 Fabrication of resin/fabric prepregs

To prepare the resin/fabric prepregs, the epoxy resin (EP) (or) epoxy resin (F-EP) and DDM (0.5 times the amount of the epoxy group) were dissolved in acetone, then blended well until transparent, and then the mixed solution was painted onto the Suncell fabrics (SF) or flame-retardant Suncell fabrics (F-SF) (300 mm * 300 mm) by hairbrush. The ratio of the resin/acetone solution to fabric was 4:1 by weight. The painted fabric was then placed into the vacuum oven at 60 °C for 1 h to dry. By combining SF or F-SF with EP or F-EP, four types of resin/fabric prepregs labeled as SF/EP, F-SF/EP, SF/F-EP, and F-SF/F-EP were fabricated and the detailed formulas were shown in Table 3-1.

Table 3-1. Formulations of different samples.

Samples	Suncell fiber (g)	DER-331 (g)	PA (mg·mL)	HGB (mg·mL)	DGEBDB (g)	DDM (g)
SF/EP	233	250	0	0	0	62.5
F-SF/EP	233	250	2	2	0	62.5
SF/F-EP	233	175	0	0	75	62.5
F-SF/F-EP	233	175	2	2	75	62.5

3.2.6 Manufacturing of Suncell-epoxy resin composites

For the fabrication of four kinds of composites, 10 layers of 300*300 mm^2 prepregs were stacked on two steel molds. The molds were pre-coated with a release agent for better demolding. Several metal dams with 3 mm thickness were placed between two molds to control the final thickness of the composite sample. Then the samples were fabricated using the vacuum bag-assisted compression molding method. Release films were used on the top and bottom of the prepregs to ensure the separation of the sample from the mold. A breather ply was positioned on the mold to absorb resin squeezed out during compression molding. The vacuum bag with sealing tape and a vacuum outlet connected to the vacuum pump was prepared to provide an even pressure during the melting of resin in the pre-curing process (90 °C for 30 min). After pre-curing, the post-curing reaction was conducted at 90 °C for 2 h, 110 °C for 2 h, and 130 °C for 2 h, while the pressure was increased to 10 MPa using a hydraulic compression machine. Finally, when it was cooled and stayed unused for one day, the composite laminate was obtained. The schematic diagram of the preparation process of composite materials is shown in Figure 3-2.

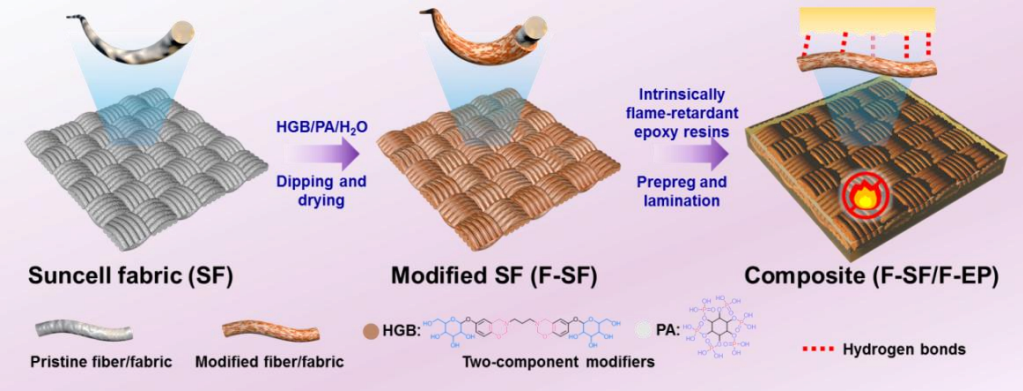

Figure 3-2. The schematic diagram of the preparation process of composite materials.

3.2.7 Characterizations

^{1}H, ^{13}C, and nuclear magnetic resonance (NMR) spectra were collected on a 400 MHz Bruker AVANCE III spectrometer (Bruker, Switzerland) at 25 °C with D_2O as solvent. Thermogravimetric analyses (TGA) were performed using a Mettler-Toledo TGA/DSC1 (METTLER TOLEDO, Switzerland) with a 20 °C/min heating rate from 25 °C to 800 °C under a nitrogen atmosphere (flow rate: 25 mL/min). The flame retardancy behavior of fabrics was performed by a Micro combustion calorimeter (MCC). About 5 mg sample was heated to 700 °C at a heating rate of 1 °C/s under a nitrogen stream. The limiting oxygen index (LOI) values of Suncell fabric composites with 5 samples were acquired by a digital oxygen index apparatus (Jiangning Analytical Instrument Co. Ltd., China) according to the ASTM D2863-2008 standard. The size is 150 mm (length) × 6.5 mm (width). Vertical flame tests of composites

were performed according to ASTM D3801 standard with sample dimensions of 130 × 13 × 3 mm. The tensile properties were performed by a universal material testing machine (5567, Instron, China) with 5 samples as per ASTM standard D-3039 method and ASTM D-2344 respectively. The impact strength was carried out on a CEAST 9050 impact resistance device (Instron, Norwood, MA, USA) with 5 samples. The heat release of the composites with 2 samples were analyzed with a cone calorimeter test (CCT) (Vouch Testing Technology, East Grinstead, UK). Sample dimensions of 100 mm × 100 × 3 mm were exposed to a heat flux of 35 kW/m^2 according to ISO 5660-1. The surface morphologies of Suncell samples before and after modification, fracture surfaces after tensile test, and char residues after CCT were observed using field-scanning electron microscopy (FE-SEM, EVO18, Zeiss, Jena, Germany) equipped with an energy-dispersive spectrometer. Thermogravimetric analysis–infrared spectrometry (TG-IR) analysis was obtained on a TGA 8000 thermogravimetric analyzer, coupled with a two-Clarus SQ8T spectrometer (PerkinElmer, Valencia, CA, USA) from room temperature to 800 °C with a heating rate of 20 °C/min. The Raman spectra were collected from a Raman spectrometer via Reflex (Renishaw, Britain) to further characterize the char residues after CCT.

X-ray photoelectron spectra (XPS) were carried out on a Kratos Axis Ultra DLD (Kratos, Japan), and the excitation source was Mg Kα.

3.3 Results and discussion

3.3.1 Synthesis and structure characterization of HGB

HGB was synthesized through a typical Mannich condensation reaction using arbutin, propylenediamine, and paraformaldehyde, as displayed in Figure 3-2. To confirm the success of synthesis and high purity of HGB, the ^{1}H, ^{13}C, and FTIR spectra were collected in Figure 3-3 and Figure 3-4. Figure 3-3 showed the ^{1}H NMR spectrum of HGB, a series of characteristic signals in the ^{1}H NMR spectrum located at 5.02-4.96 and 3.92 ppm were assigned to protons of the methylene units in N-CH_2-O and N-CH_2-ph in the oxazine ring, respectively. At the same time, the integral ratio of the different characteristic peaks was also close to the theoretical value, especially the methylene in the amine part (2.88-2.73 ppm) and the methylene in the monosaccharides (4.81-4.44 ppm). The ^{13}C NMR spectrum was obtained for further structure identification (Figure 3-4), where the characteristic peaks at 77.66, 77.06, 50.26, and 49.37 ppm respectively corresponding to the N-CH_2-O and N-CH_2-ph provided powerful evidence for the successful synthesis.

In order to make a further structural confirmation, Figure 3-5 represents the FTIR results of HGB. Compared with the raw material propylenediamine and arbutin (figure 3-6), the disappearance of NH_2 at 1582 $cm^{-1}$and the phenol hydroxyl group at 3289 cm^{-1} demonstrated the formation of the oxazine ring. The absorbance bands for the asymmetric and symmetric stretching of C-O-C in the oxazine ring were found at 1043 and 1207 cm^{-1}, while the characteristic signal standing for benzoxazine emerged at 939 cm^{-1}, the wide peaks at 1492 cm^{-1} and 3303 cm^{-1} represented the -OH of arbutin. This evidence confirmed the target structure and acceptable purity. In addition, both the transparent solution of HGB in water (inserted picture in Figure 3-7) and the ^1H NMR result based on D_2O as a deuterium reagent (Figure 3-7) further demonstrated its good water solubility. The water solubility and hydrogen-bonds-forming ability contribute to mild processing and easy adhesion to the fiber surface. Interestingly, HGB facilitates a co-curing reaction with epoxy resin, as evidenced by a lower curing temperature observed in the DSC result (Figure 3-8).

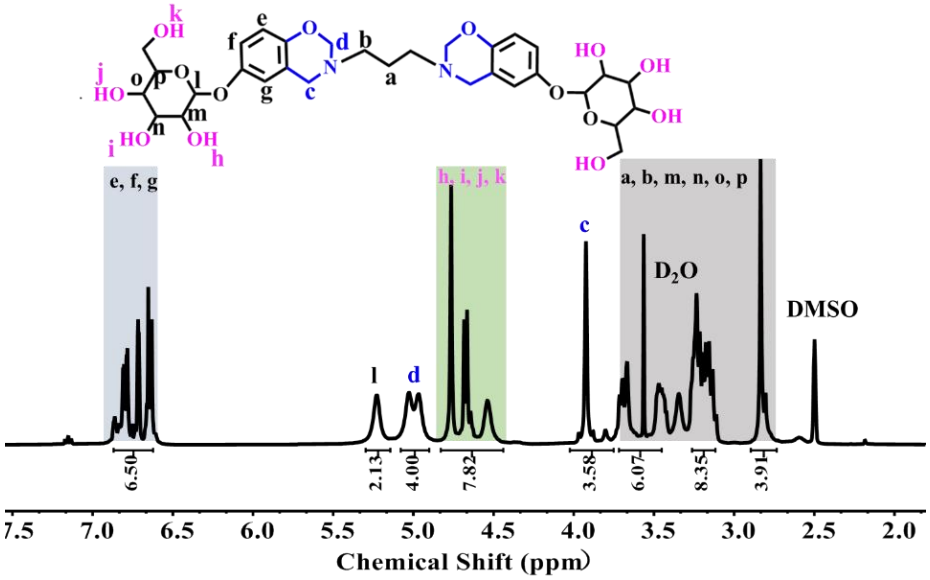

Figure 3-3. ^{1}H NMR spectrum of HGB.

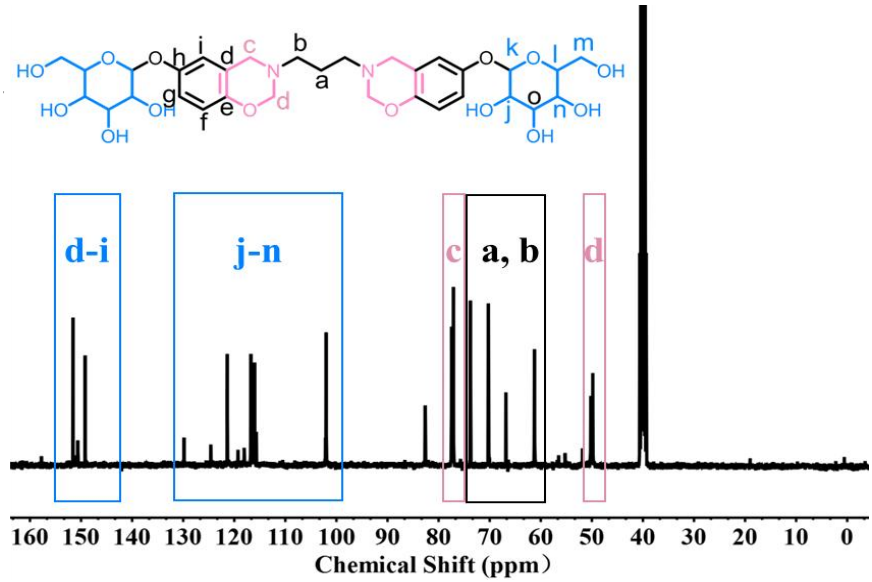

Figure 3-4. ^{13}C NMR spectrum of HGB.

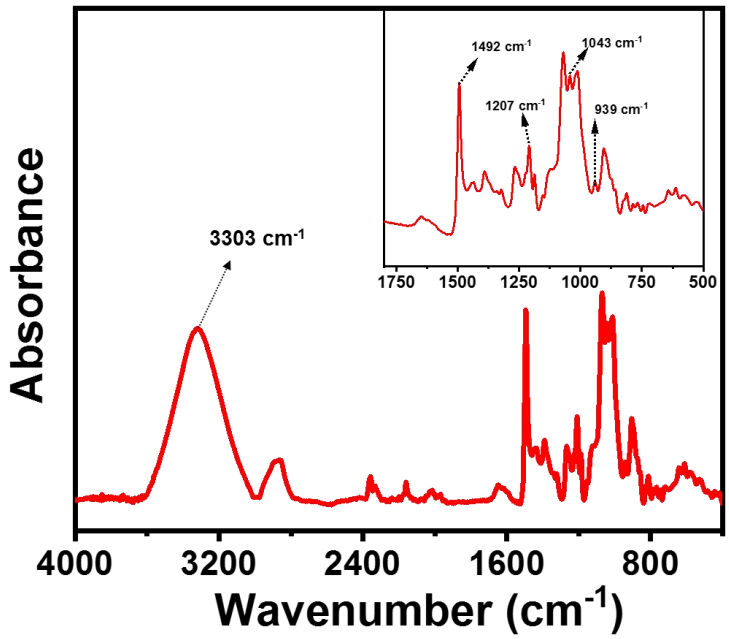

Figure 3-5. FTIR spectrum of HGB.

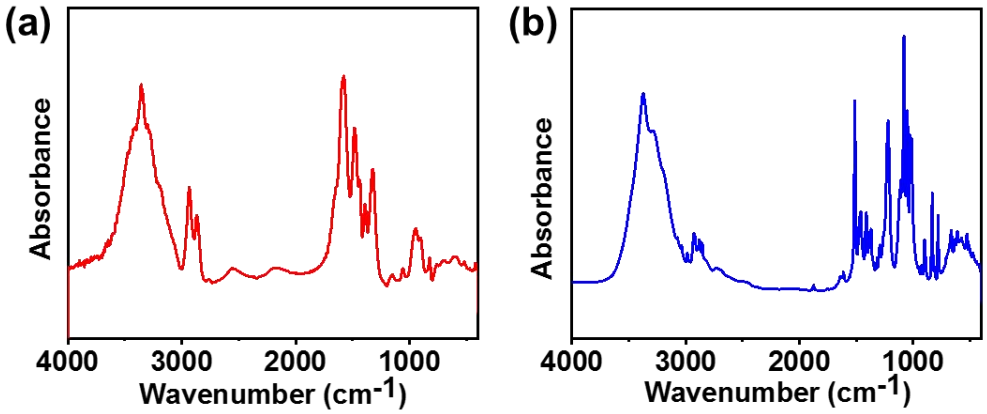

Figure 3-6. FTIR spectra of 1,3-propane diamine (a) and arbutin (b).

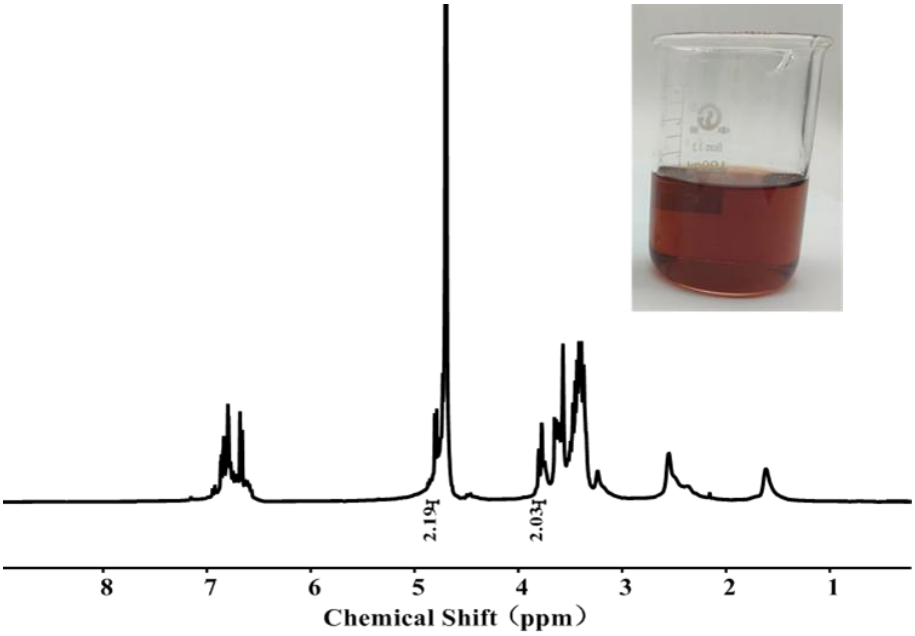

Figure 3-7. ^{1}H NMR result based on D_2O as deuterium reagent of HGB; Insert picture: transparent solution of HGB in water.

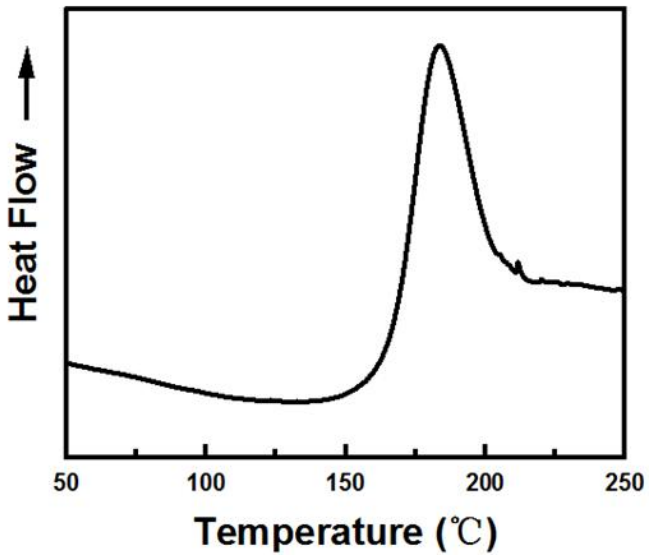

Figure 3-8. The DSC curve of HGB and epoxy resin.

3.3.2 Breaking strength test of modified ramie fabric

As shown in Figure 3-9, the breaking strength of ramie fiber under different concentration of PA and HGB was deteriorate seriously. This may attribute to the high hemicellulose of ramie could react with phytic acid and further destroy the breaking strength of ramie fiber. Due to the decrease of mechanical properties, the treated ramie fiber can't be used as the reinforcement of composite materials. In this way, Suncell Fiber, a regenerated cellulose fiber (cellulose content:100%) was selected to be an enhancement in this chapter.

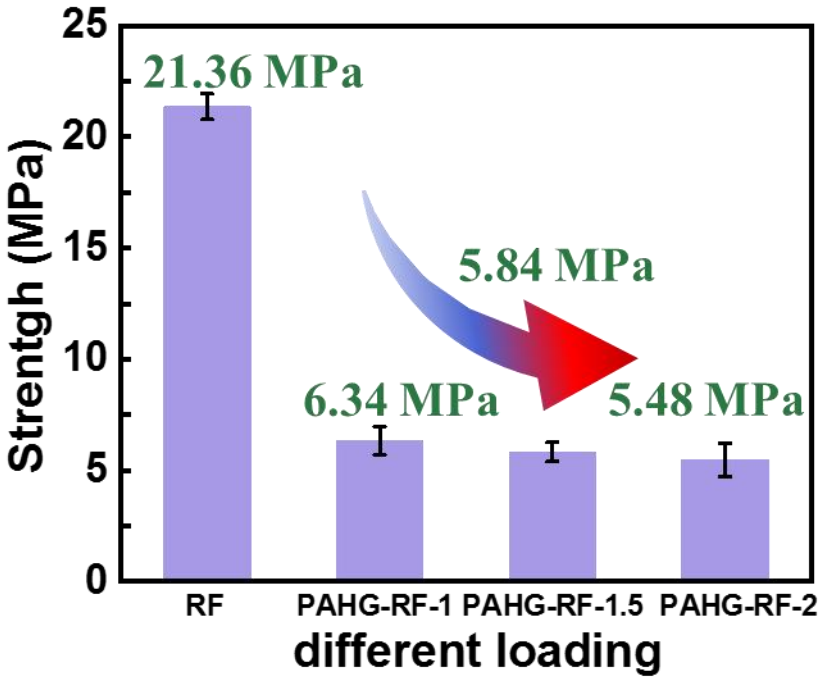

Figure 3-9. The breaking strength of ramie fiber under different concentration of PA and HGB.

3.3.3 Morphological structural characterization, burning performance and breaking strength test of modified Suncell fabric

In contrast to the typical synthetic fibers such as carbon fiber, glass fiber, and Kevlar fiber, natural fibers exhibit a notably high variability in their mechanical properties due to factors such as plant age, meteorological and geographic growing circumstances, harvesting techniques, and purifying technology[178]. However, as a special case, the regenerated cellulose fibers exhibit lower performance variability while possessing comparable strength to glass fibers. Accordingly, Suncell fabric composed of regenerated cellulose fiber was selected as the reinforcement phase. After immersing the Suncell fabric in the aqueous solution containing HGB and PA, the surface morphology and composition were detected by Scanning electron microscope (SEM) and energy dispersive spectrometer (EDS). As illustrated in Figure 3-10a, the raw Suncell fabric obviously exhibited a smooth and flat surface. After being coated with HGB and PA, the modified fabric maintained its original morphology well (Figure 3-10b, c and d), which was attributed to the mild processing condition based on the water phase. EDS mapping was further used to investigate the element distribution of the treated Suncell fabric. It can be clearly observed that P elements were dispersed uniformly on the surface of modified samples, which demonstrated the

successful adsorption of HGB and PA chemicals on its surface. Technically, PA with high phosphorus content (28 wt.%) acts as an acid source to induce char formation by releasing carboxylic or phosphoric acids. In addition, HGB with high char yield plays the role of a char forming agent and blowing agent since its nitrogen-contained molecule.

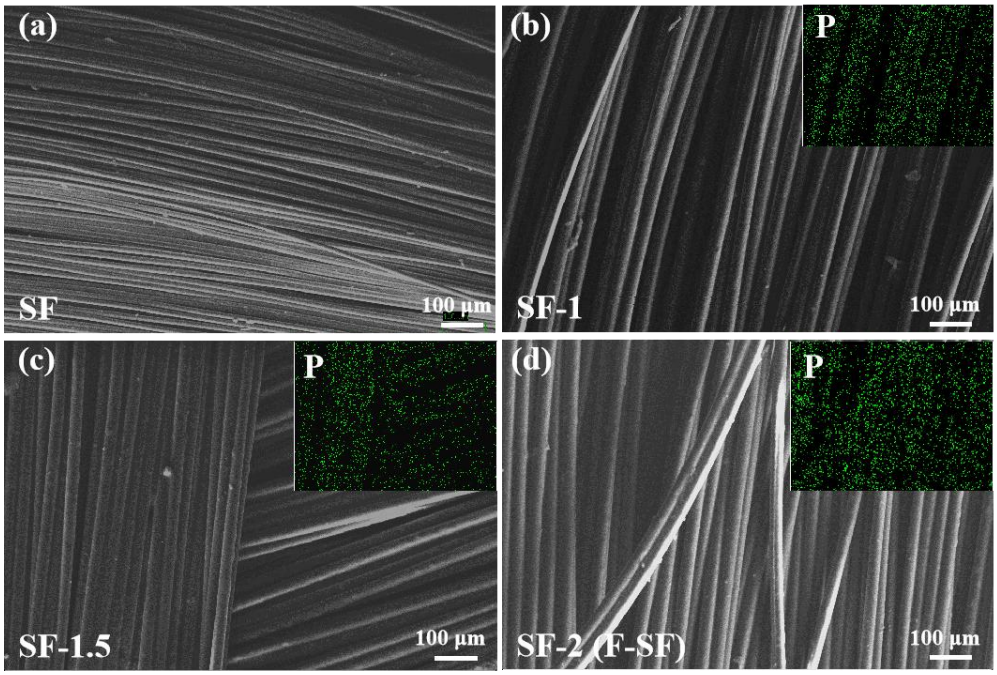

Figure 3-10. SEM images and EDS spectra of the fabrics: SF (a), SF-1 (b), SF-1.5 (c) and SF-2 (F-SF) (d).

The attachment of HGB and PA to fabric offers the first layer of protective barrier for fire hazards, which is reflected in its fire-proof ability. To determine the flame-retardant performance of the fabric before and after coating the samples were burned under the same conditions. The digital photos of the combustion test were recorded in Figure 3-11, where

the pristine Suncell fabric was easy to ignite and could not self-extinguish, resulting in a complete combustion due to its poor flame-retardant performance (Figure 3-11a). Meanwhile, the surface of the burnt modified fabric displayed a clear char layer and maintained its structural integrity well, which will be discussed in detail in the next section (Figure 3-11b).

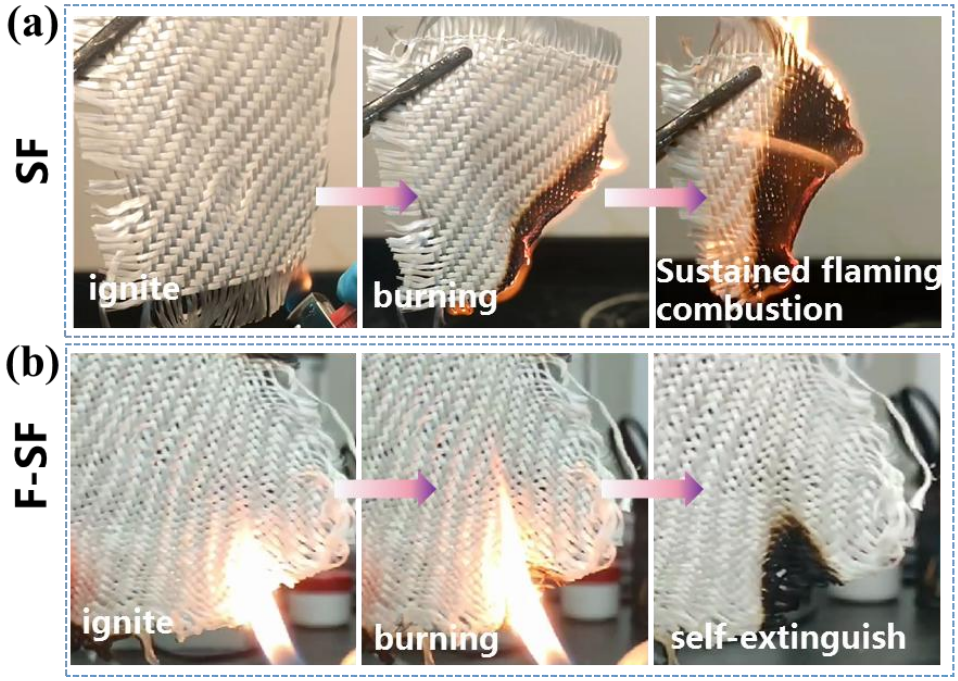

Figure 3-11. Digital photographs during the burning test of SF (a) and F-SF (b).

Microscale combustion calorimetry (MCC) based on the chemical heat value was carried out to quantitatively predict the fire risk of materials. Generally speaking, the typical parameters including the heat release rate (HRR), and total heat release (THR) are positively related to the combustion intensity of the sample. The results were depicted as

temperature-dependent curves. As shown in Figure 3-12a, the diagram of the heat release rate demonstrated that the peak heat release rate of F-SF modified with PA and HGB was significantly reduced by 54.3% compared to the original Suncell fabric, while the corresponding temperature shifted from 369.6 °C to 291.4 °C. The earlier heat release of the pre-treated fabric was mainly ascribed to the low-temperature thermal degradation of the phosphorus-based flame retardant that contributed to a phosphoric acid-containing protect layer and it is in agreement with the TGA result (Figure 3-13). Meanwhile, the THR of the F-SF also exhibited a remarkable decrease (Figure 3-12b), which was beneficial to prevent intense combustion. Besides, the TGA curves also demonstrated that both the char yield and anti-hygroscopicity of the fabric were enhanced after modification.

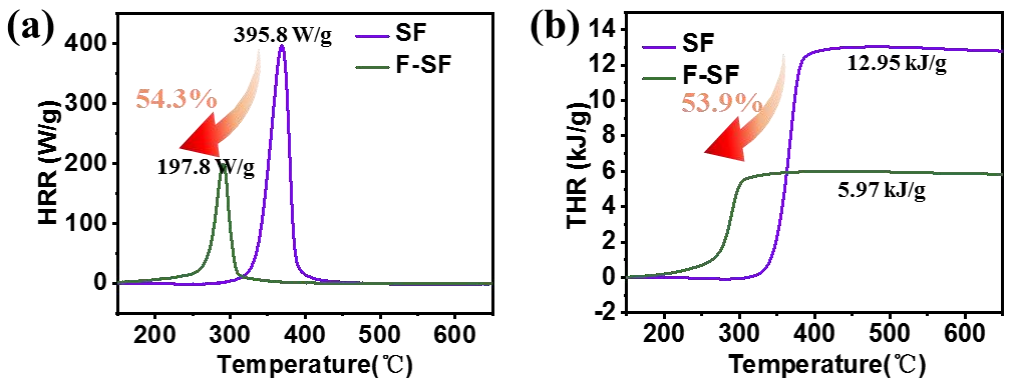

Figure 3-12. Heat release rate curves (a) Total heat release curves of SF and F-SF (b).

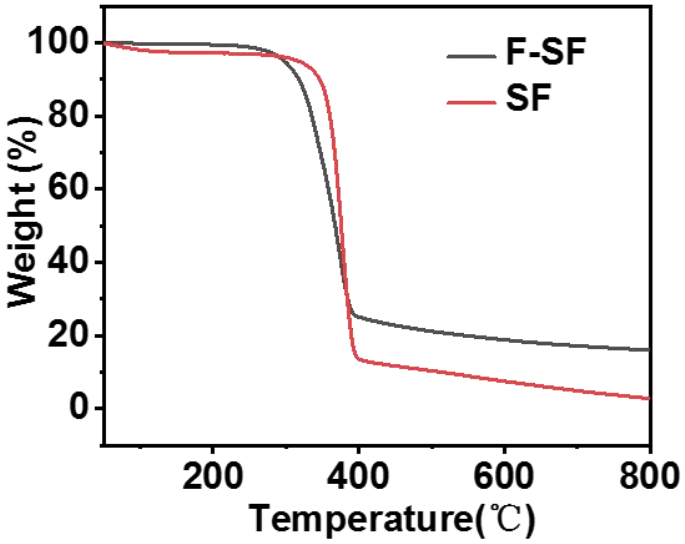

Figure 3-13. The TGA curves of SF and F-SF.

Although the aqueous process can minimize the negative impact of pre-treatment, the use of acidic PA can also cause slight damage to the fabric, which was consistent with the results reported in the literature[179]. As a result, there was a slight but acceptable decrease in the breaking strength of the yarn from 67.1 N to 57.6 N (Table 3-2) before and after modification.

Table 3-2. The breaking strength and flammability regime of Suncell fiber under different concentration of PA and HGB.

Samples	PA (mg/mL)	BOZ (mg/mL)	Breaking strength (N)	Self-extinguish (Yes or No)
SF	0	0	67.1±2.5	No
SF-1	1	1	59.4±6.3	No
SF-1.5	1.5	1.5	61.3±0.5	No
SF-2 (F-SF)	2	2	57.6±0.7	Yes

3.3.4 Mechanical properties

As discussed before, the HGB/PA modifier can optimize the surface polarity. Interestingly, this modifier also enables a co-curing reaction with epoxy resin, which was reflected in a lower curing temperature in the DSC result (Figure 3-8). Both of them are beneficial to the improvement of the composite interface, and thus promote the stress transfer from the polymer phase to the fiber under the force field, leading to enhanced mechanical properties. The mechanical properties of EP and four composites were determined by tensile, impact, and ILSS tests and the data were collected in Figure 3-14 and Table 3-3. As shown in Figure 3-14 a and b, compared with the tensile strength and modulus of EP (71.5 MPa and 5.50 GPa) and F-EP (91 MPa and 2.85 GPa), respectively, it is evident that all the composites exhibited significantly higher tensile strength and modulus due to the efficient reinforcement effect of the fabric. Unfortunately, compared with SF/EP, the tensile strength demonstrated a slight decrease for F-SF/EP, SF/F-EP, and F-SF/F-EP, which might be ascribed to both the low crosslink density of F-EP[150] and the strong acidity of PA. In addition, F-SF/EP and F-SF/F-EP exhibited a slight increase in tensile modulus compared with SF/EP and SF/F-EP (10.82 and 11.29 GPa *vs.* 9.82 and 10.03 GPa). Moreover, the tensile strength of F-SF/F-EP was also higher than that of SF/F-EP. Meanwhile, the composites with the modified fabric also showed improved impact strength. The cross-comparison between the SF-based composites and F-SF-based composites demonstrates that the modifier endows the composite with better deformation resistance and stress transfer efficiency, which well reflects its improved interface properties. Specifically, in Figure 3-14c, the impact strength of

F-SF/F-EP was enhanced from 6.58 to 7.21 kJ·m^{-2} compared with the untreated SF/EP composite, showing an improvement of approximately 9.57%. As a technical indicator related to interface compatibility, ILSS reflects the adhesion property between two phases. As expected, F-SF/F-EP exhibited an extraordinary ILSS of 13.89 MPa, outperforming those of SF/EP, F-SF/EP, and SF/F-EP, which were 11.41, 12.42, and 12.77 MPa, respectively (Figure 3-14d). Notably, by comparing the samples with the same matrix resin, the treated fabric significantly leads led to significantly higher ILSS, which strongly supported the interfacial compatibilization role of the devised modifier. Compared with the reported methods based on fabric flame-retardant modification, the present method had less damage to the mechanical properties of composite materials[62, 180]. Simultaneously, the enhanced efficiency of ILSS was also outperform that of the composites derived from surface treatment in the literature[181-182].

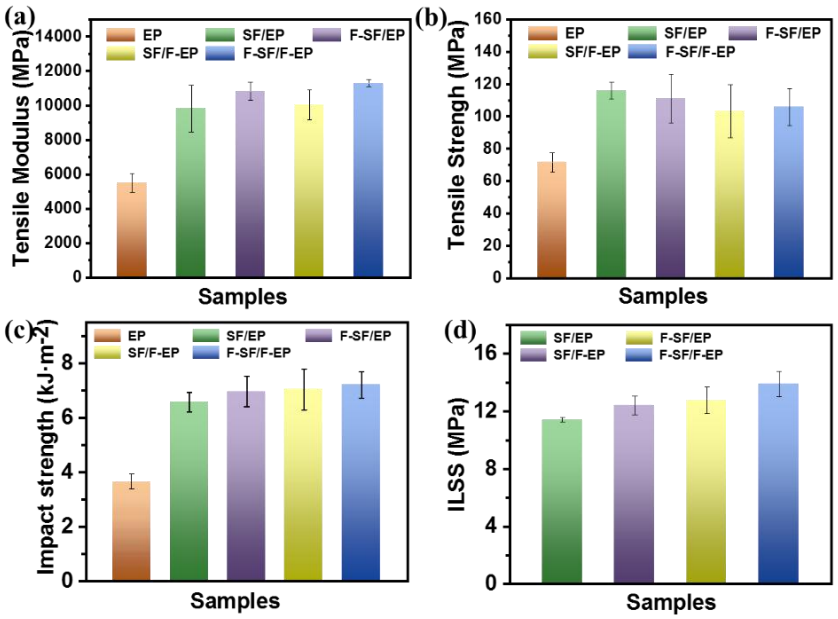

Figure 3-14. Mechanical performance of different materials: tensile strength (a), tensile modulus (b), impact strength (c) and ILSS (d).

Table 3-3. The mechanical properties of different samples.

Samples	Tensile modulus (GPa)	Tensile strength (MPa)	Impact strength ($kJ \cdot m^{-2}$)	ILSS (MPa)
EP	5.50±0.54	71.5±5.9	3.65±0.27	-
SF/EP	9.82±1.36	116.0±5.2	6.58±0.36	11.41±0.15
F-SF/EP	10.82±0.54	111.0±14.9	6.97±0.56	12.42±0.65
SF/F-EP	10.03±0.87	103.0±16.5	7.05±0.75	12.77±0.92
F-SF/F-EP	11.29±0.21	105.9±11.4	7.21±0.48	13.89±0.89

The fractured surfaces after the tensile test of SF/EP and F-SF/F-EP were determined with SEM measurement (Figure 3-15). For SF/EP, obvious voids between EP and SF were observed in Figure 3-15a and b, indicating weak interactions between the two phases. For F-SF/F-EP composites, the interphases between F-EP and F-SF became unclear with few cracks (Figure 3-15c and d), suggesting the improved compatibility in the presence of the HGB and PA surface modification of SF. The optimized interfacial adhesion facilitates energy transfer and dissipation and results in higher mechanical performance of F-SF/F-EP.

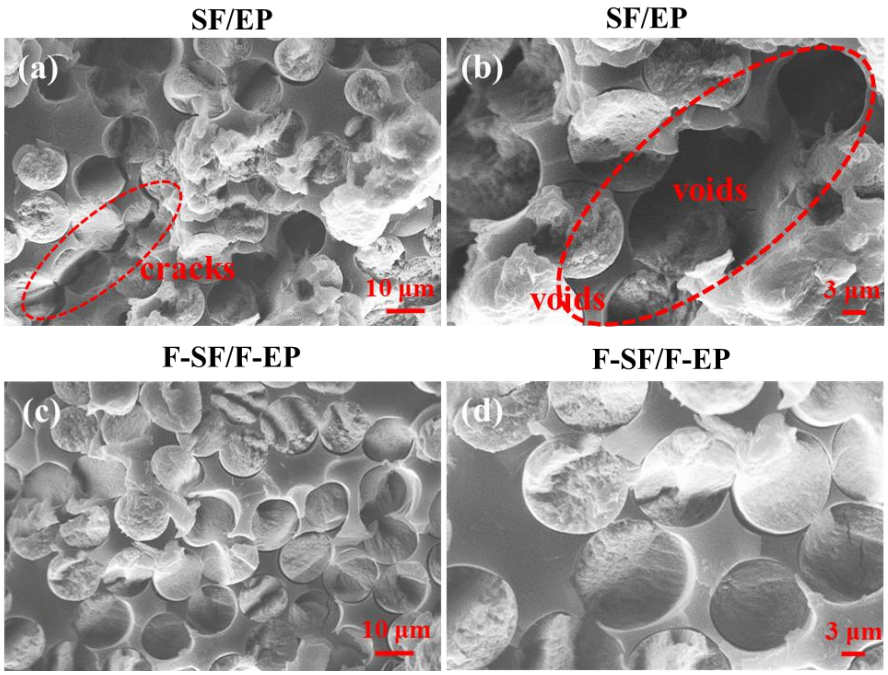

Figure 3-15. The SEM images under different magnificent of fracture surfaces of composites after tensile test: SF/EP (a and b) and F-SF/F-EP (c and d).

The hydrogen-bonds-forming ability of the modifier will contribute to better interfacial adhesion. As demonstrated in FTIR spectra for SF/F-EP and F-SF/F-EP (Figure 3-16), the redshift phenomenon across the absorption bands of the hydrogen-bonding donator (mainly O-H and N-H) in F-SF/F-EP corresponds to a stronger hydrogen-bonding system than that of SF/F-EP.

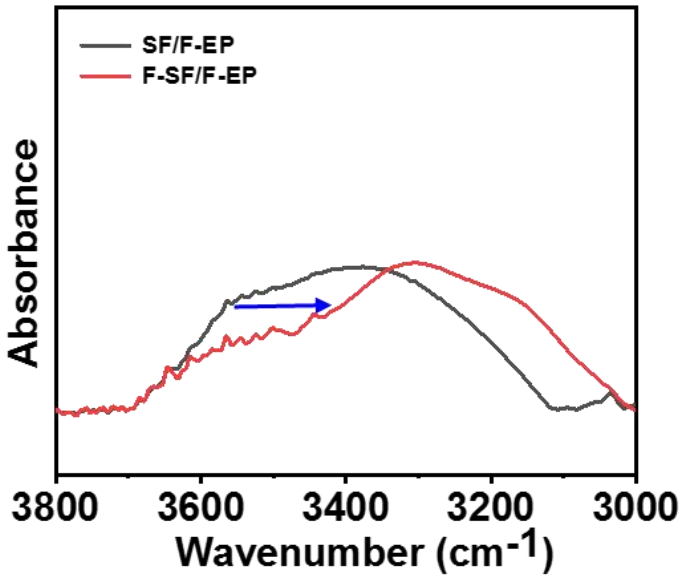

Figure 3-16. The FTIR spectra for SF/F-EP and F-SF/F-EP.

3.3.5 Thermal stability of composites

Both SF and F-SF were further integrated with epoxy resin to yield the composites, in which an intrinsic epoxy resin (DGEBDB, labeled as F-EP) reported in our previous work[150] was employed to achieve dual flame-retardant protection, and a commercial Bisphenol-A epoxy resin (DGEBA, labeled as EP) was also used for comparison, yielding four composites named SF/EP, F-SF/EP, SF/F-EP, and F-SF/F-EP. The thermal stability of the as-prepared composites under an N_2 atmosphere was first estimated by TGA measurement, as illustrated in Figure 3-17a and b, and the related values including T_{d10} (10% weight loss

temperature), T_{max} (maximum weight loss temperature), and R_{800} (char yield at 800 °C) were collected in Table 3-4. Obviously, all composites displayed similar trends; however, the degradation processes were different. Specifically, SF/EP possesses a T_{d10} of 330.3 °C, which was slightly higher than F-SF/EP with 328.7 °C, probably owing to the presence of PA. When DGEBDB was used as the polymer matrix, a slight decrement in the T_{d10} value of the composite was noticed, from 330.3 °C for SF/EP to 319.7 °C for SF/F-EP, which was consistent with the previous result[183]. It can be predicted that the F-SF/F-EP composite showed the lowest T_{d10} value of 315.7 °C, which was related to its highest phosphorus content. The difference in T_{d10} can be ascribed to the early decomposition of PA and DOPO with unstable P-O-P, P-C, and P=O weak bonds, reducing the initial degradation temperature of the composite as a whole[172]. In addition, the lower T_{max} temperature in DTG results (Figure 3-17b) further confirms their earlier thermal decomposition behavior. There was an increase in the T_{max} of F-SF/EP composites and the possible reason for this phenomenon can be attributed to the good interface interaction leads to effective interfacial bonding between the SF and the epoxy matrix, which can reduce the occurrence of early thermal degradation. As for R_{800} values, SF/EP, F-SF/EP, SF/F-EP, and F-SF/F-EP respectively exhibit 12.2%, 14.2%,

18.9%, and 27.5%. Theoretically, the formation of phosphoric acid and its derivatives during the thermal-degradation process helps to yield a high-quality char residue[184]. In the present work, both PA and DGEBDB play the role of carbonization promotor, and HGB, with its inherently high char yield further enhances the char formation ability, which is favorable for enhancing flame retardancy especially in the condensed phase.

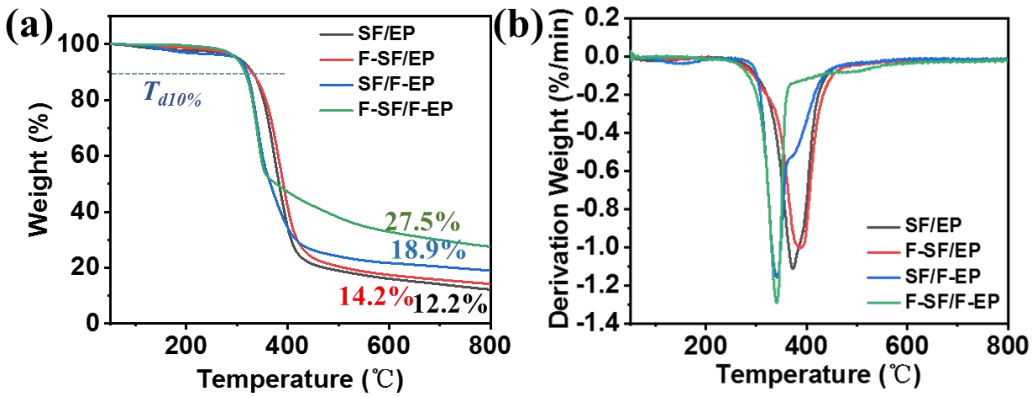

Figure 3-17. TGA (a) and DTG (b) curves for composites.

Table 3-4. Results of thermal stability of composites.

Samples	T_{d10} (°C)	Char yield at 800 °C (%)	T_{max} (°C)
SF/EP	330.3	12.2	374.3
F-SF/EP	328.7	14.2	385.0
SF/F-EP	319.7	18.9	344.7
F-SF/F-EP	315.7	27.5	339.7

3.3.6 Flammability analysis of composites

To evaluate the fire safety of these composites in detail, limit oxygen index (LOI) measurement, vertical burning test, and cone calorimetry test (CCT) were conducted. As shown in Table 3-5 and Figure 3-18, without modifier and flame-retardant epoxy matrix, the LOI value of SF/EP was only 23.6% and its UL-94 rating was NR (no rating, fully burned), indicating a high combustibility. For comparison, the LOI value of F-SF/EP and SF/F-EP increased to 27.8% and 28.7%, respectively, implying that either the modifier combination or DGEBDB could contribute to better flame retardancy of the composites. However, the insufficient fire-proof ability still resulted in NR classification. When both F-SF and F-EP were employed, the as-prepared composite presented an extraordinary LOI of 33.8%, along with a V-0 grade in the UL-94 test, hinting that this combination could achieve a satisfactory flame retardancy to cope with fire hazards. The LOI values for EP, F-EP, SF, and F-SF were 24.2%, 33.4%, 21.3%, and 26.7%, respectively. Notably, the excellent LOI of F-SF/F-EP is related to the high LOI values of F-EP and F-SF.

Table 3-5. Results of flame retardant measurements of composites.

Samples	LOI (%)	t_1/t_2 (s)	Dripping	UL-94
SF/EP	23.6	-[a]	No	No-rating
F-SF/EP	27.8	-[a]	No	No-rating
SF/F-EP	28.7	-[a]	No	No-rating
F-SF/F-EP	33.8	1.2/2.3	No	V-0

-[a]: Does not extinguish fire after ignition.

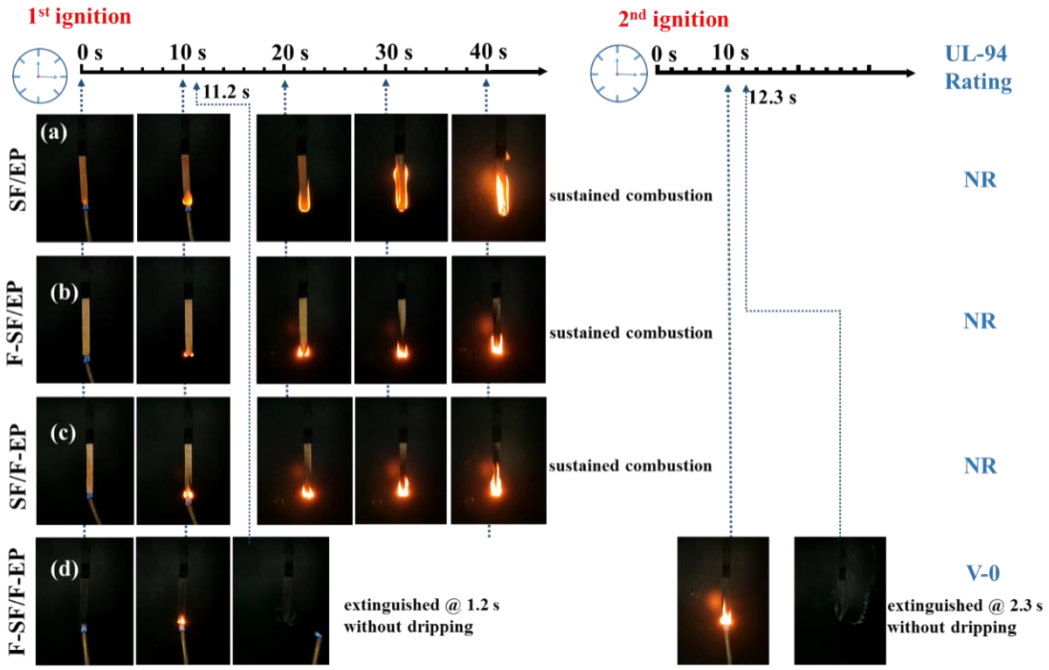

Figure 3-18. Digital photographs of SF/EP (a), F-SF/EP (b), SF/F-EP (c), and F-SF/F-EP (d) during the vertical burning test.

The cone calorimeter test (CCT) results of SF/EP and F-SF/F-EP were exhibited in Figure 3-19, in which F-SF/F-EP exhibited much lower heat release rate (HRR) and total heat release (THR) compared with those of SF/EP. Specifically, the peak value of HRR of F-SF/F-EP was reduced from 834.9 to 494.1 kW/m^2 by 40.8%, and the corresponding time was delayed from 115 to 165 s. Both the lower heat release and delayed maximum heat release time contribute to the lower combustion intensity. The delayed time to ignition and time to PHRR were related to the material's ability to resist ignition and its flammability once ignited. Fire retardant treatments typically promote the formation of char on the material's surface during heating. This char layer acted as a barrier, insulating the underlying material from heat and oxygen, which can delay ignition and reduce the PHRR. The discrepancy between the lower thermal stability and improved fire resistance properties can be attributed to the fire retardant's mode of action. While it might promote an earlier onset of thermal decomposition, it also enhances the material's ability to resist ignition and slow down the combustion process once ignited.

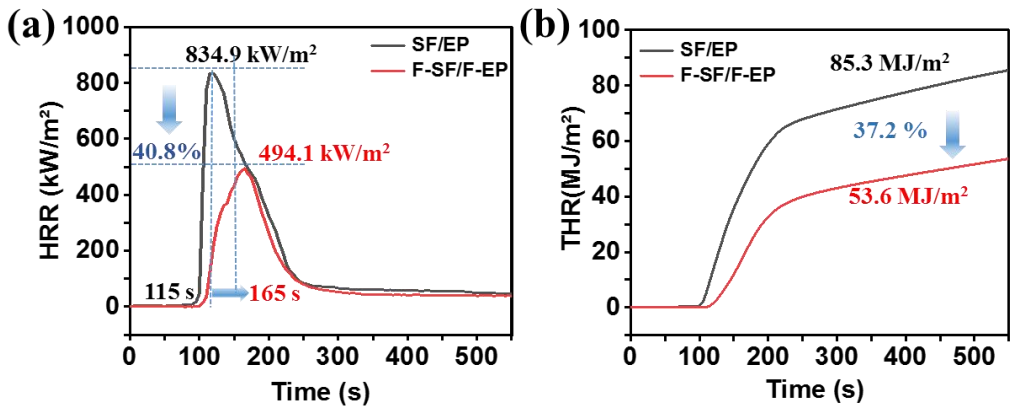

Figure 3-19. HRR (a) and THR (b) curves for for SF/EP and F-SF/F-EP..

3.3.7 Flame-retardant mechanism

The analysis of thermal degradation gaseous products

To reveal the considerable non-flammability mechanism behind F-SF/F-EP, TG-FTIR, SEM, XPS, and Raman tests were performed. In general, the fire-proof effect is the co-action of gaseous and condensed phases. Accordingly, TG-FTIR was first carried out to analyze gas behavior during combustion, as illustrated in Figure 3-20. The composite consisting of the pristine fabric and commercial epoxy resin (Figure 3-20a) showed a clearly lower onset decomposition temperature than F-SF/F-EP (Figure 3-20b), which was in agreement with the TGA results and was mainly due to the fact that PA and DOPO in DGEBDB expedited the thermal decomposition of the matrix and reinforcement, facilitated the formation of continuous carbon layer at a relatively lower temperature accordingly as well. In the meantime, as shown in Figure

3-21, the FTIR spectra of the degradation products of the two composites at different temperatures (300, 450, 520, and 600 °C) mainly consisted of H_2O (3745 cm^{-1}), hydrocarbon compounds (2978 cm^{-1}), CO_2 (2364 cm^{-1}), aromatic compounds (1508 and 1616 cm^{-1}), NH_3 (1600-1700 cm^{-1}) and ether compounds (1751, 1261, and 1178 cm^{-1}), corresponding to the similar compositions[172]. The decomposition products are the same but with different intensities (Figure 3-21a and c). Specifically, taking the curve of 300 °C as an example, the intensities of H_2O, CO_2, and NH_3 for F-SF/F-EP was stronger than those of SF/EP obviously, which could take away the heat and dilute the oxygen and flammable gas in the gas phase[185]. In theory, the N element in benzoxazine could produce the non-flammable gas NH_3 during the combustion process, but since DDM was used as a curing agent in this study and contains the N element, NH_3 was also produced in SF/EP. Notably, compared with SF/EP (Figure 3-21b), F-SF/F-EP displayed P-O absorption bands at 1060 cm^{-1} (Figure 3-21d), indicating that the phosphorus-containing chemicals in DGEBDB had a fire-resistance function in the gaseous phase. As we know, DOPO and its derivatives generally act in the gas phase by reducing the free radical[186], which was evidenced by the release intensity of carbonyl compounds[172]. As shown in Figure 3-22, the release of carbonyl compounds was decreased for

F-SF/F-EP when compared with SF/EP, revealing the effective inhibition of the free-radical cracking process in the F-SF/F-EP system. It is easy to conclude that DGEBDB not only released phosphorus-based free radicals to capture the active free radicals and interrupt the combustion reaction, thereby decreasing the release of flammable gases in the gaseous phase but also facilitated the release of non-flammable gases such as H_2O, CO_2, and NH_3 during the combustion process[172].

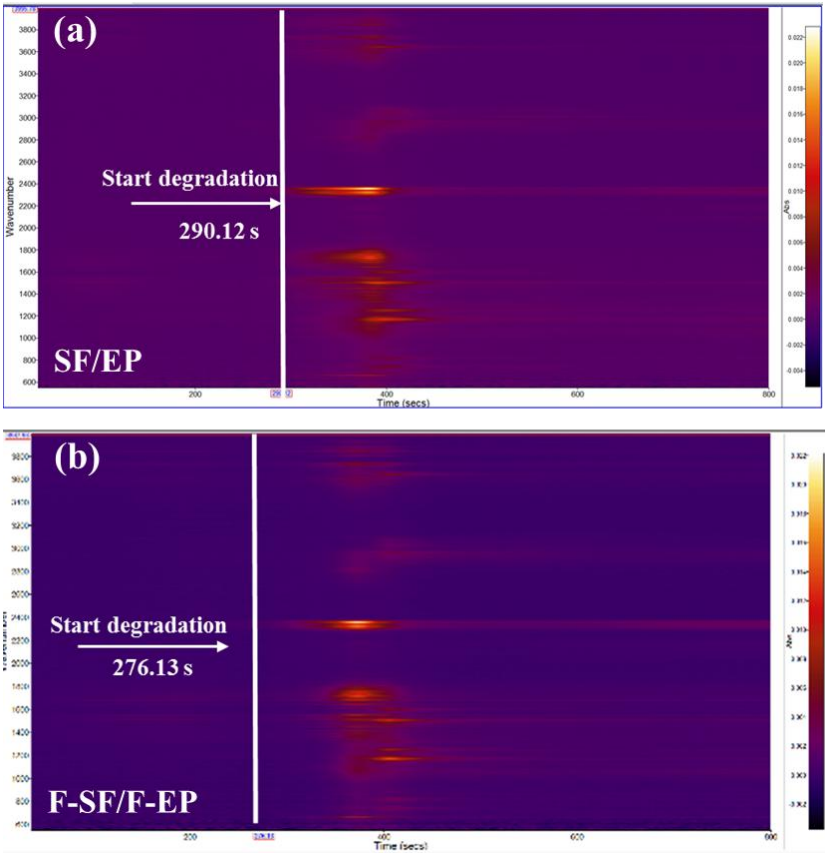

Figure 3-20. Images of TG-FTIR signal intensity over time for SF/EP (a) and F-SF/F-EP (b).

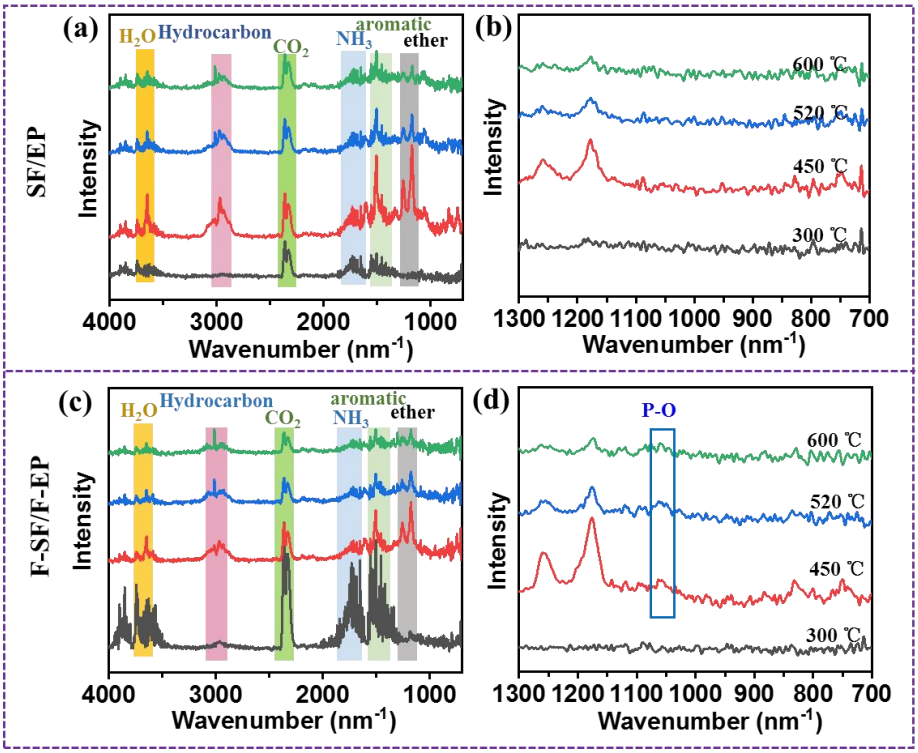

Figure 3-21. TG-FTIR degradation curves for SF/EP (a, b) and F-SF/F-EP (c, d) at different temperatures.

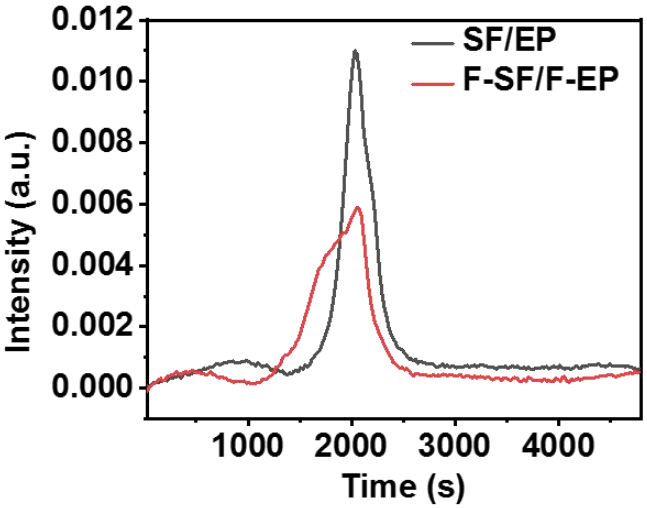

Figure 3-22. The release curves of carbonyl compounds for SF/EP and F-SF/F-EP.

The characteristics of the char residues

SEM, XPS, and Raman tests were further performed to investigate the condensed phases of two composites after CCT. As recorded in Figure 3-23, the digital photos of the char residues revealed that the char layer of SF/EP was loose and puffy (Figure 3-23a and b) since its high flammability, leading to a weak barrier and protective effect. In contrast, the carbon layer shown in F-SF/F-EP exhibited a denser and more compact morphology (Figure 3-23c and d), which was consistent with its high char yield in the TGA result. Upon further observation of the micro-morphologies of char residues by SEM, according to the preliminary observation on the morphology of char residues, it was found that the char residue of SF/EP (Figure 3-24a) presented the exposed fibers with a damaged structure due to the nearly complete combustion of the resin matrix and unprotected fibers. Conversely, the char residue of F-SF/F-EP was thicker and denser which well secured the inner fabric, as shown in Figure 3-24d. When further observing the higher resolution pictures of the char residue of burnt SF and epoxy resin, it was seen that the char residue of burnt fiber was fractured and the epoxy resin was loose and porous (Figure 3-24b and c). The incomplete and fragmented char layer provided pathways that allowed flammable gases, heat, and oxygen to reach the underlying matrix, resulting in flame retardant

failure[51]. In contrast, a continuous fiber shape and flatter carbon layer were formed on the surface of the burnt composites (Figure 3-24e and f), which could effectively prevent the transfer of heat, O_2, and flammable volatiles, revealing a strong barrier effect[150].

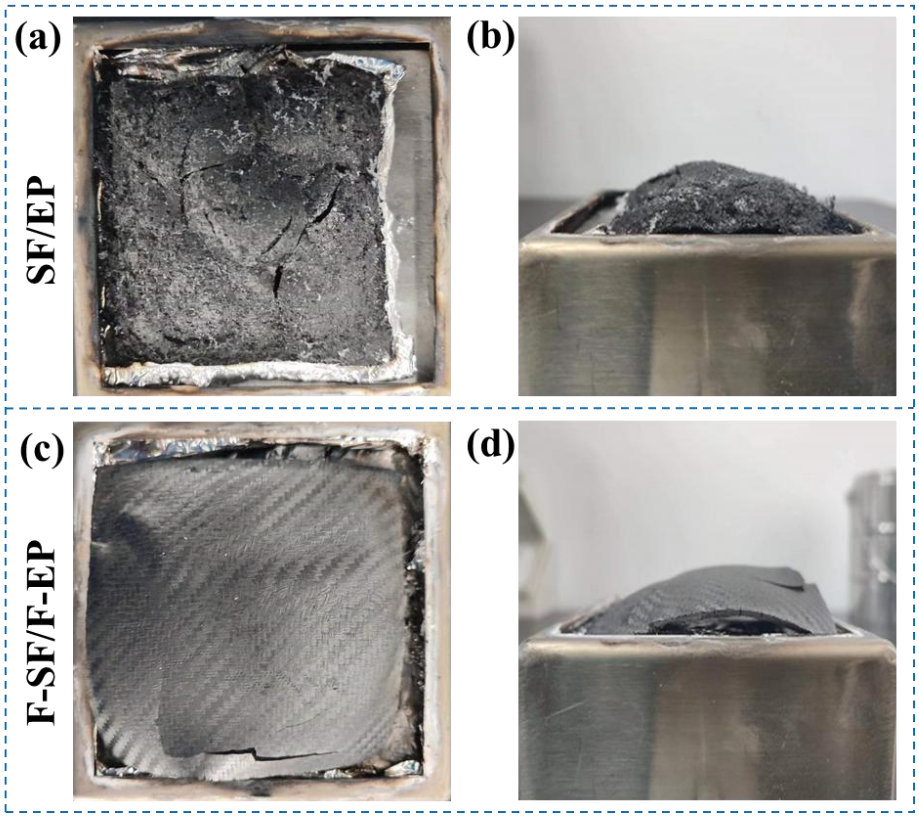

Figure 3-23. The vertical and the horizontal views of the char residue of SF/EP (a) and (b); F-SF/F-EP (c) and (d) after the cone calorimeter test.

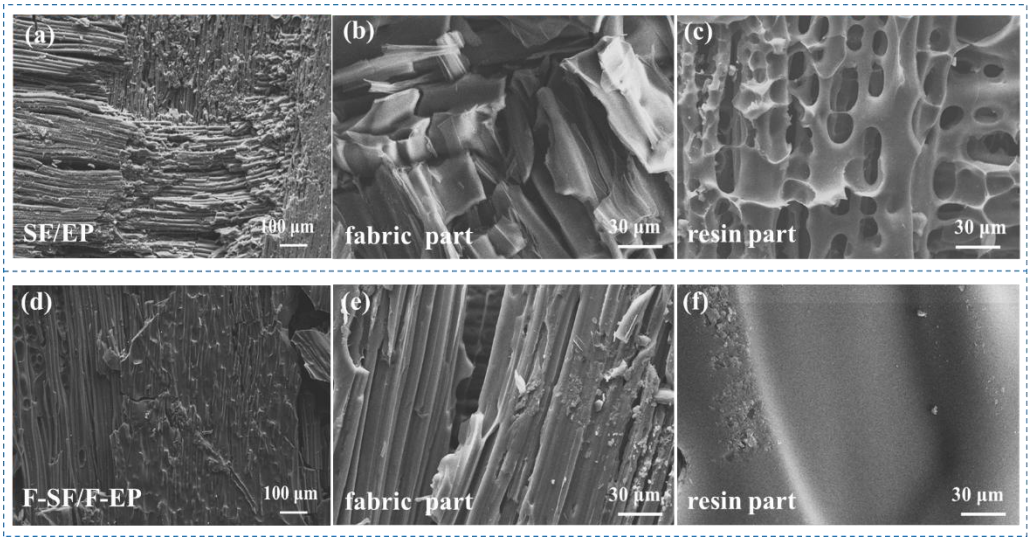

Figure 3-24. SEM micrographs of char residue of SF/EP (a, b and c), and F-SF/F-EP (d, e and f) under different magnificent.

Raman measurement was further used to examine the quality of the char residue samples. As shown in Figure 3-25a and b, two peaks located at 1350 and 1590 cm^{-1}, representing disordered graphite (D band) and ordered carbon (G band) could be observed, respectively. The quality of the carbon layer was closely related to the integral ratio of these two peaks (I_D/I_G), which also represents the graphitization degree[51, 157]. The I_D/I_G value of the char sample of F-SF/F-EP was calculated to be 2.88, which was significantly lower than that of SF/EP with 3.41, illustrating the higher graphitization degree of the former. In a word, the high yield and high quality of the condensed char was beneficial for flame inhibition effects[51], which could prevent the transfer of heat and

combustible fragments as well as keep oxygen away from the unburned composite as a physical barrier[187-188].

To explain the formation process of the char layer with physical barrier function, the chemical composition of char residue was analyzed by FTIR. As demonstrated in Figure 3-25c, the carbon residue of F-SF/F-EP had an apparent band at 1068 cm^{-1}, which was identified as the stretching vibrations of P-O-C_{Ar}, while this peak vanished in the FTIR spectra for SF/EP. Consequently, the phosphoric and polyphosphoric acids that were produced during the degradation of DGEBDB and PA should be responsible for the dense char layer of epoxy composites. These acids underwent esterification and dehydration reactions with the degraded composite, forming fused-ring aromatic compounds connected by P-O-C and enhancing the carbonaceous char[189]. Besides, the chemical compositions of the char residues were further identified by XPS, as shown in Figure 3-25d-i. Except for C, N, and O elements, two additional peaks at 133.8 eV and 191.2 eV attributing to P_{2s} and P_{2p} were detected in the char residue for F-SF/F-EP (Figure 3-25d and e), which explain the important role of P elements in the condensed phase[62, 150]. Meanwhile, in the fine spectrum of F-SF/F-EP, the split peaks at 285.9 eV in C_{1s} (Figure 3-25f), 532.4 eV in O_{1s} (Figure 3-25h), and 133.6 eV in P_{2p} (Figure 3-25i) indicate the presence of P-O-C, and the signals at

288.8 eV in C_{1s} and 399.6 eV in N_{1s} (Figure 3-25g) were assigned to the formation of C=N, contributing to the yield of high-quality a char layer[190], revealing the important role of PA, HGB, and DGEBDB in promoting condensed phase.

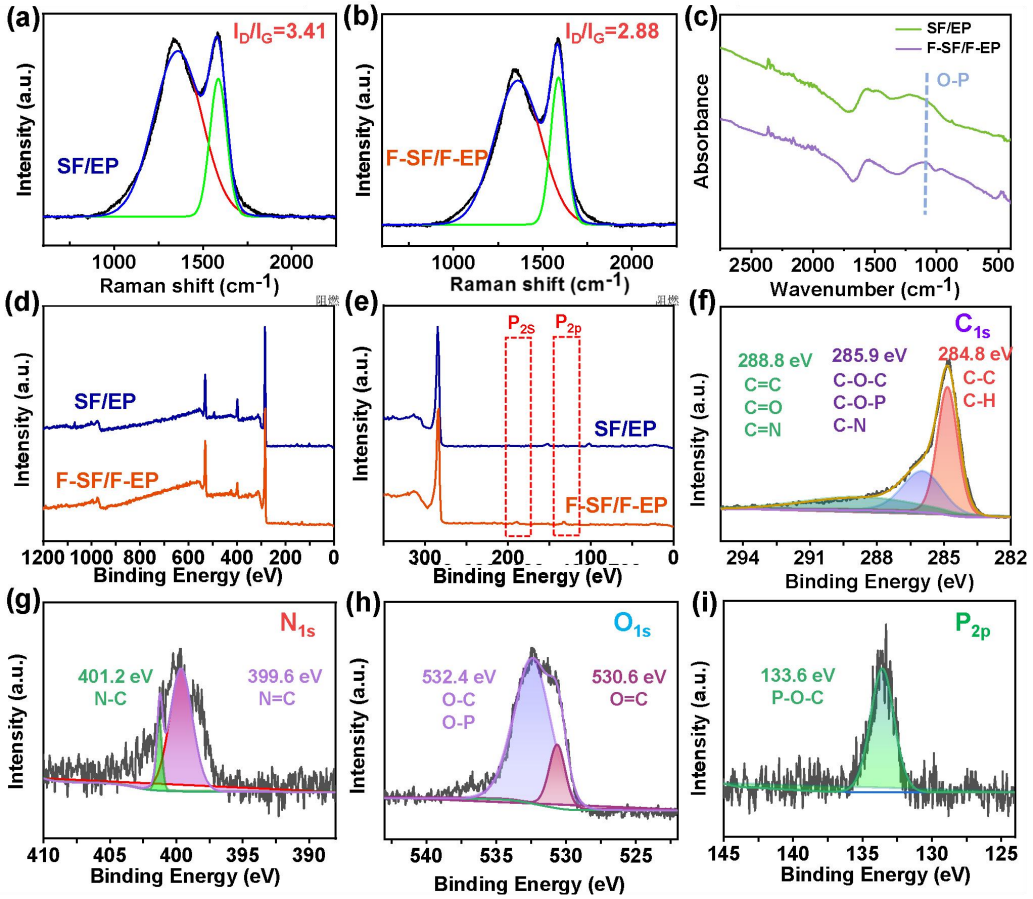

Figure 3-25. Raman spectra of residual chars for SF/EP (a) and F-SF/F-EP (b), FTIR spectra of the char layer for SF/EP and F-SF/F-EP after cone calorimeter tests (c), XPS spectra for the surface of residual char layers of burnt SF/EP and F-SF/F-EP: overall spectra (d), enlarged picture containing peaks for P_{2s} and P_{2p} (e); peak splitting for C_{1s} (f), N_{1s} (g), O_{1s} (h), and P_{2p} (i) for char residues obtained from F-SF/F-EP.

Based on the above results, the outstanding fire safety of the F-SF/F-EP composite can be ascribed to a synergistic flame-retardant mechanism of both the gaseous phase and condensed phase, which is proposed as follows:

a) During the combustion, the DOPO group in DGEBDB releases phosphorus-based free radicals, such as the PO• and PO_2• radicals, which can capture the active free radicals and interrupt the combustion reaction, decreasing the release of flammable components in the gaseous phase. Simultaneously, the nonflammable gases such as NH_3 produced by HGB could dilute the flammable gases and combustion-supporting gases, and consequently, the combustion process was restrained in the gaseous phase;

b) The formation of pyrophosphoric acid, metaphosphoric acid, and phosphorous acid as a result of the early decomposition of PA and DOPO groups could pose dehydration and carbonization effects, promoting char formation and leading to a char residue with compact morphology, continuous surface, and a high graphitization degree. The integrated and continuous char layer acted as a physical barrier to protect the underlying polymeric substrate by preventing the transfer of heat, O_2, and flammable volatiles, revealing a strong barrier effect that

improves fire safety and oxygen transfer, which was consistent with the previous conclusion.

3.4 Conclusion

In conclusion, a water-soluble combined modifier composed of bio-based benzoxazine (HGB) and PA was successfully applied in the simultaneous improvement of interfacial adhesion and fire safety of the regenerated cellulose fabric/epoxy composite. Specifically, HGB was facilely synthesized through one step with confirmed structure and excellent purity. Then it was combined with PA to modify the regenerated cellulose fabric in the water solution phase via simple impregnation, which exhibited a self-extinguishing behavior after ignition. The modified fabric was further used to reinforce DGEBDB composites through prepreg preparation and a vacuum bag-assisted compression molding process. Results indicated that F-SF/F-EP well balanced its mechanical modulus and roughness due to the optimized interface, as reflected in the 14.9% and 9.6% improvements compared with SF/EP, respectively. Meanwhile, owing to the higher interface stress transfer efficiency, F-SF/F-EP possessed an ILSS of 13.89 MPa, outperforming that of SF/EP, F-SF/EP, and SF/F-EP with 11.41, 12.42, and 12.77 MPa, respectively. Besides, both the flame-retardant modified fabric and intrinsically fire-resistant epoxy matrix contributed to a V-0 classification

in the UL-94 test and to a 33.8% of the LOI value for the F-SF/F-EP composite, which was mainly achieved by avoiding the wick effect in the fabric phase, creating a barrier effect in the gaseous phase, and exerting an inhibition effect in the condensed phase. This work not only provides an advanced method for the efficient and integrated modification of plant fiber-reinforced composites, but also paves the way for the wider and safer application of green composite materials.

Chapter 4 Study on preparation of PAIM as well as mechanical and flammability properties of HGB and PAIM coated Suncell fiber reinforced epoxy resin composites

4.1 Introduction

In Chapter 3, a water-soluble combined modifier composed of bio-based benzoxazine (HGB) and PA was successfully applied in the simultaneous improvement of interfacial adhesion and fire safety of the regenerated cellulose fabric/epoxy composite. HGB was and used as a 'green' char forming agent, coupled with phytic acid (PA) to construct a new kind of bio-based intumescent flame retardant system (IFR). Fabrics can self-extinguish, and the mechanical properties and combustion properties of composite materials were also improved. Results indicated that this combination can well balance composites' interface property and flame-retardant behavior.

However, phosphoric acid may have a considerable vegetative effect on Suncell fiber and even nature fibers since it's strong acidity will destroy the strength of cellulose and natural fibers have high hemicellulose content which are not acid resistant[179]. In order to solve this problem, a new compound named PAIM simply synthesized by PA and imidazole (IM) in this chapter. The chemical structure of PAIM was

characterized by ^{1}HNMR and FTIR. The PAIM was water-soluble and the aqueous solution was neutral, which could prevent the damage to plant fibers. At the same time, it retained the characteristics of high P content of phytic acid, which ensure to achieve good flame retardant effect. Furthermore, PAIM is a kind of curing accelerator for epoxy resin, which can participate in epoxy curing process and further improve the interface properties of composite materials.

Then it was combined with HGB to modify the regenerated cellulose fabric in the water solution phase via simple impregnation. The flame retardant coating formed on Suncell together with HGB can make the fabric self-extinguish behavior after ignition. The modified fabric was further used to reinforce DGEBDB composites through prepreg preparation and a vacuum bag-assisted compression molding process. The overall properties of the composites including mechanical strength, interlayer properties, combustion performance was evaluated.

4.2 Materials and methods

4.2.1 Materials and chemical used

Suncell Fiber was provided by Zhengzhou Zhongyuan Spandex Machine Co., Ltd and the areal density is approximately 232 g/m^2. 4,4′-Diamino diphenylmethane (DDM), 1,3-propane diamine (99%),

Arbutin (99%) were obtained from Xi'an Lishi Biotechnology Co., LTD. (Xi'an, China). Phytic acid (PA, biochemical reagent, 70.0% aqueous solution), imidazole (IM, Standard for AR, 99.0%) and 1,4-dioxane (99%) were purchased from Aladdin Chemistry Co. (China). Diglycidyl ether of bisphenol A (abbreviated as DGEBA, trade name DER-331) with an epoxy value around 0.51-0.53 mol/100 g was purchased from Dow Chemical Company. Self-retardant epoxy resin (DGEDBD) was prepared in our lab according to the previously reported method. The specific information can be found in relevant work[150]. Distilled water was supplied by our lab. All other chemicals were commercially available and used without further purification.

4.2.2 Synthesis of HGB and PAIM

The synthesis method of HGB is the same as above 3.2.2.

The synthesis of PAIM was carried out according to the following procedure: 3.30 g (0.005 mol) of PA and 4.08 g (0.06 mol) of IM were separately dissolved in 20 mL acetone. The obtained PA solution was dropped into the IM solution and stirred at room temperature for 30 min. After the reaction was completed, the liquid was poured out, and ethanol was added to continue stirring for 1 h. After that, the liquid remained at 0 °C for 1 h. Ethanol was used to clean the product of any remaining raw

materials for 2-3 times. Finally, system was steamed at 50 °C for 1 h to remove residual ethanol and less water from the system. The 4.22 g of target purple liquid product (PAIM) was obtained (57.2% yield). The synthesis route is illustrated in Figure 4-1.

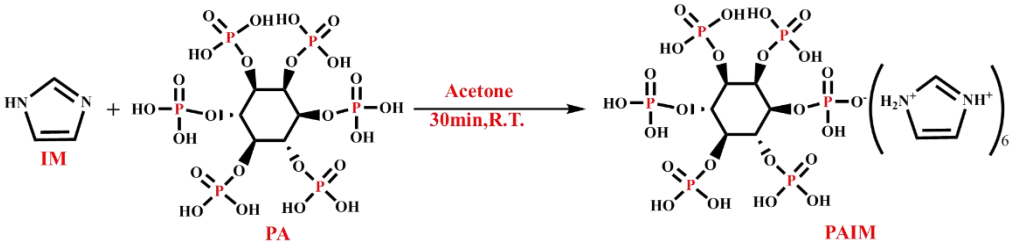

Figure 4-1. Synthesis illustration and chemical structure of PAIM.

4.2.3 The flame-retardant modification for Suncell fabric and F-EP

The HGB- and PAIM-modified Suncell fiber (F-SF) was prepared by the dip-coating method. The HGB and PAIM were dissolved in deionized water, and the concentration of HGB and PAIM were 1, 1.5, 2 mg/mL, respectively. The Suncell fabric was immersed in the solution, and after the padding and drying process (70 °C for 30 min), designated sequentially as SF-1, SF-1.5 and SF-2. To optimize the best concentration, the breaking strength and flammability regime of them were tested and the result were listed in Table 4-2. The result revealed SF-2 could self-extinguish while maintain the mechanical properties to

the maximum extent, which was renamed F-SF and chosen for fabricating composites.

The F-EP matrix, composed of DER-331 and DGEBDB in a 7:3 ratio, was determined to be the optimal ratio according to report[150]. Specifically, two epoxy resins with specified weights were dissolved in acetone. After stirring, the solvent was removed by vacuum, and the resulting homogeneous viscous liquid was collected as flame-retardant epoxy blend.

4.2.4 Fabrication of resin/fabric prepregs for composite applications

Here was a simplified step-by-step overview of the process. Epoxy resin (EP) or flame-retardant epoxy resin (F-EP) was dissolved in acetone with diaminodiphenylmethane (DDM), serving as the hardener. The ratio of DDM to the epoxy groups was maintained at 0.5. The components were mixed until the solution became transparent, ensuring the complete dissolution of the resin and hardener in the solvent. The solution was uniformly applied to a 300 mm * 300 mm piece of either Suncell fabric (SF) or flame-retardant Suncell fabric (F-SF) using a hairbrush. The mixture was coated on the fabric maintaining a weight ratio of resin/acetone solution to fabric of 4:1. The impregnated fabrics

were placed in a vacuum oven at 60 °C for 1 hour to ensure through impregnation of the fabric with the resin system and complete removal of the solvent, which were critical parameters for achieving high-quality composite parts. By implementing the described process, four types of resin/fabric prepregs were fabricated, namely SF/EP (Suncell fabric with epoxy resin), F-SF/EP (flame Suncell fabric with epoxy resin), SF/F-EP (Suncell fabric with flame-retardant epoxy resin), and F-SF/F-EP (flame Suncell fabric with flame-retardant epoxy resin). The prepregs were observed to have a consistent resin distribution and were adequately dried, as required for effective molding into composite structures. The detailed formulations and weight ratios were documented in Table 4-1.

Both SF and F-SF were further integrated with epoxy resin to yield the composites, in which an intrinsic epoxy resin (DGEBDB, labeled as F-EP) reported in our previous work[150] was employed to achieve dual flame-retardant protection, and a commercial Bisphenol-A epoxy resin (DGEBA, labeled as EP) was also used for comparison, yielding four composites named SF/EP, F-SF/EP, SF/F-EP, and F-SF/F-EP.

4.2.5 Manufacturing of Suncell-epoxy resin composites

For the synthesis of four distinct composite materials, a series of prepregs, each with dimensions of 300 x 300 mm² and comprising ten

layers, were methodically layered between a pair of steel molds. Prior to the assembly, the mold surfaces were treated with a release agent to facilitate the subsequent separation of the cured composites. To establish and maintain the desired thickness of the composite specimens, metallic spacers with a uniform thickness of 3 mm were strategically placed around the perimeter between the two molds. The composites were then subjected to a consolidation process utilizing vacuum bag-assisted compression molding. Release films were strategically placed above and beneath the prepreg stack to ensure that the resulting composite could be easily disengaged from the mold. Additionally, a breather ply was positioned atop the entire assembly to absorb any excess resin that might be extruded during the compression molding phase. A vacuum bag was meticulously sealed using sealing tape, incorporating a vacuum outlet that was connected to a vacuum pump to exert uniform pressure throughout the pre-curing phase, which was carried out at a temperature of 90 °C for a duration of 30 minutes. Subsequent to the pre-curing stage, a post-curing regimen was implemented, involving a temperature profile that increased sequentially: 2 hours at 90 °C, followed by 2 hours at 110 °C, and concluding with 2 hours at 130 °C. Concurrently, a hydraulic compression machine was employed to elevate the pressure to 10 MPa. Upon completion of the

curing cycle, the assembly was allowed to cool and was left undisturbed for a period of one day to ensure proper material stabilization. Thereafter, a composite laminate of the desired quality was obtained. The detailed formulas were shown in Table 4-1.

Table 4-1. Formulations of different samples.

Samples	Suncell fiber (g)	DER-331 (g)	PAIM (mg·mL)	HGB (mg·mL)	DGEBDB (g)	DDM (g)
SF/EP	233	250	0	0	0	62.5
F-SF/EP	233	250	2	2	0	62.5
SF/F-EP	233	175	0	0	75	62.5
F-SF/F-EP	233	175	2	2	75	62.5

4.2.6 Characterizations

^{1}H, ^{13}C, and nuclear magnetic resonance (NMR) spectra were collected on a 400 MHz Bruker AVANCE III spectrometer (Bruker, Switzerland) at 25 °C with D_2O as solvent. Thermogravimetric analyses (TGA) were performed using a Mettler-Toledo TGA/DSC1 (METTLER TOLEDO, Switzerland) with a 20 °C/min heating rate from 25 °C to 800 °C under a nitrogen atmosphere (flow rate: 25 mL/min). The flame retardancy behavior of fabrics was performed by a Micro combustion calorimeter (MCC). About 5 mg sample was heated to 700 °C at a heating rate of 1 °C/s under a nitrogen stream. The limiting oxygen index (LOI) values of Suncell fabric composites, with the size of 150 mm

(length) × 6.5 mm (width), were acquired from five test specimens using a digital oxygen index apparatus (Jiangning Analytical Instrument Co. Ltd., China) according to the ASTM D2863-2008 standard. Vertical flame tests of composites were performed according to ASTM D3801 standard with sample dimensions of 130 × 13 × 3 mm. The tensile properties were performed by a universal material testing machine (5567, Instron, China) as per ASTM standard D-3039 method and ASTM D-2344 respectively, with a sample quantity of five for each test. The impact strength was carried out on a CEAST 9050 impact resistance device (Instron, Norwood, MA, USA) with five samples. The heat release of the composites was analyzed with a cone calorimeter test (CCT) (Vouch Testing Technology, East Grinstead, UK). Two samples, with dimensions of 100 mm × 100 mm, were exposed to a heat flux of 35 kW/m^2 according to ISO 5660-1. The surface morphologies of Suncell samples before and after modification, fracture surfaces after tensile test, and char residues after CCT were observed using field-scanning electron microscopy (FE-SEM, EVO18, Zeiss, Jena, Germany) equipped with an energy-dispersive spectrometer. Thermogravimetric analysis–infrared spectrometry (TG-IR) analysis was obtained on a TGA 8000 thermogravimetric analyzer, coupled with a two-Clarus SQ8T spectrometer (PerkinElmer, Valencia, CA, USA) from room temperature

to 800 °C with a heating rate of 20 °C/min. The Raman spectra were collected from a Raman spectrometer via Reflex (Renishaw, Britain) to further characterize the char residues after CCT. X-ray photoelectron spectra (XPS) were carried out on a Kratos Axis Ultra DLD (Kratos, Japan), and the excitation source was Mg Kα.

4.3 Results and discussion

4.3.1 Synthesis, characterization of PAIM

PAIM was synthesized by a simple method of acid-base neutralization of phytic acid and imidazole. The chemical structure of PAIM was characterized by ^{1}H NMR and FTIR, as shown in Figure 4-2 and Figure 4-3.

In Figure 4-2, peaks at 8.46 and 7.19 ppm were attributed to the hydrogen of imidazole in PAIM, and peaks at 4.35-3.76 ppm was assigned to the hydrogen on the cyclohexane ring of phytic acid in PAIM. The integral area ratio of H_7, H_8 and $H_{1\text{-}6}$ is 1:2:1, which indicated that 6 mol imidazole reacted with 1 mol phytic acid to obtain PAIM.

Figure 4-3 showed the FTIR spectrum of PAIM. The absorption peak at 1595 cm^{-1} and 3148 cm^{-1} was assigned to NH_2^+ appeared[191], while the absorption peak at 2350 cm^{-1} was attributed to O–H bonds for PA[192,193], which disappeared according to the previous literture[191].

The above analyses showed that the experimental results matched well with the structural information of PAIM, indicating that PAIM was synthesized successfully. Moreover, the PAIM also can be dissolved in water, as shown in Figure 4-4. At the same time, HGB with hydroxyl groups and PAIM with imidazole can participate in and promote the curing process of epoxy resin, which provides the possibility to improve the interfacial properties of plant fiber reinforced epoxy resin composites, as reflected in the reduced curing temperature in DSC result (Figure 4-5).

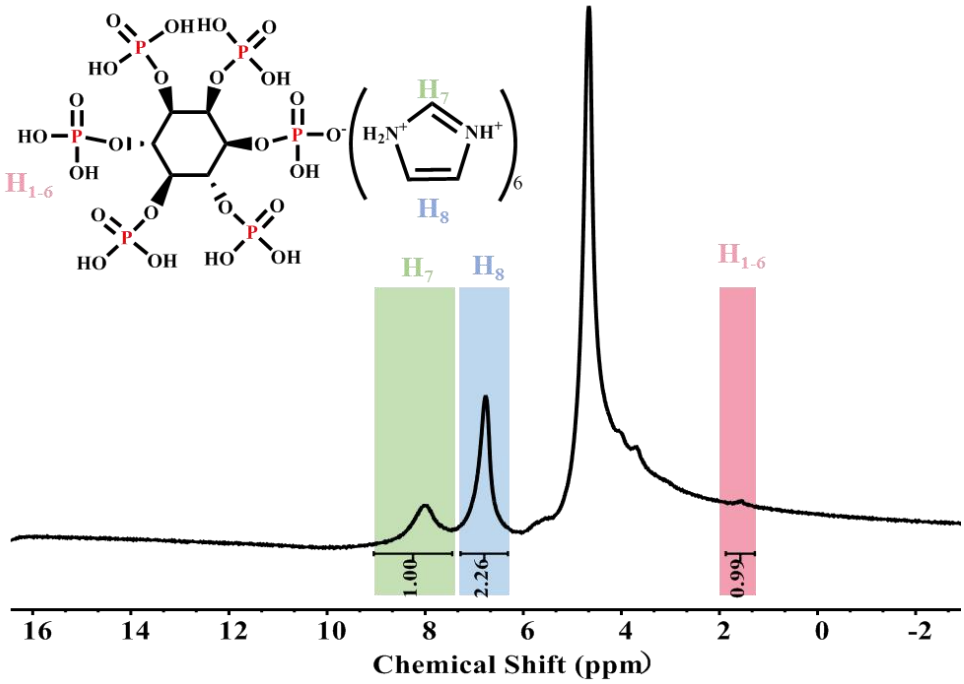

Figure 4-2. ^{1}H NMR spectrum of PAIM.

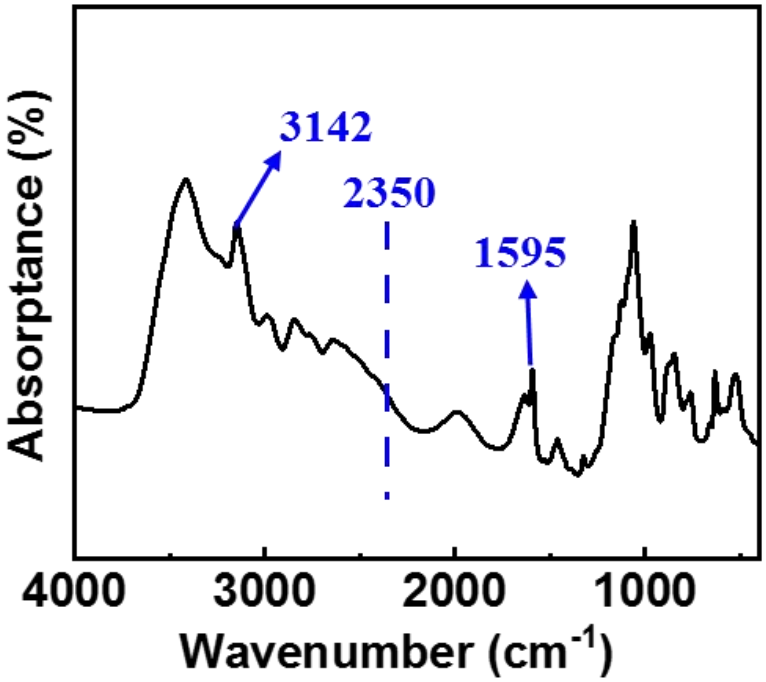

Figure 4-3. FTIR spectrum of PAIM.

Figure 4-4. Transparent solution of PAIM in water.

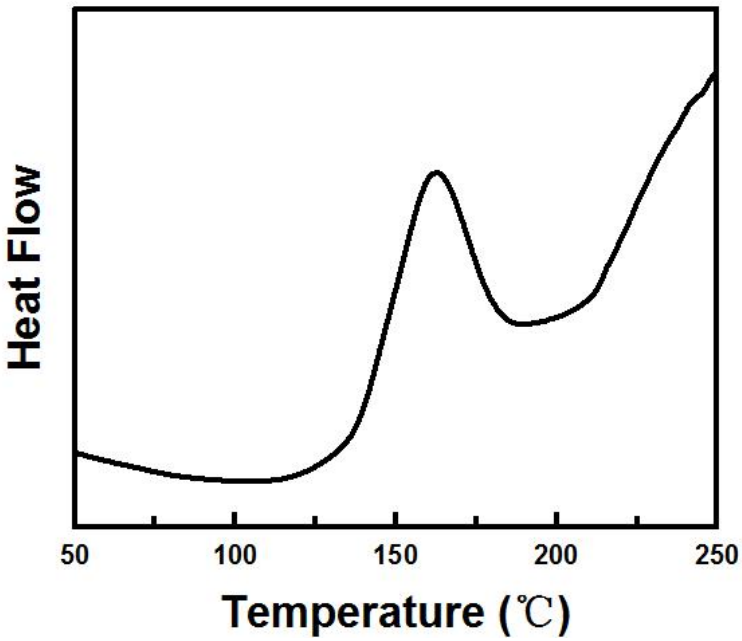

Figure 4-5. The DSC curve of PAIM and epoxy resin.

4.3.2 Morphological structural characterization, burning performance and breaking strength test of modified Suncell fabric

The surface morphology and composition of Suncell fabric after immersing into the aqueous solution containing HGB and PAIM were detected by Scanning electron microscope (SEM) and energy dispersive spectrometer (EDS). As illustrated in Figure 4-6a, obviously, the raw Suncell fabric exhibited a smooth and flat surface. After being coated with HGB and PAIM, the modified fabric maintained its original morphology well (Figure 4-6b,c and d), which was attributed to the mild processing condition based on the water phase. Moreover, it can be clearly observed that both P element were dispersed uniformly on the

surface of modified samples from the EDS mapping, which demonstrated the successful adsorption of HGB and PAIM chemicals on its surface.

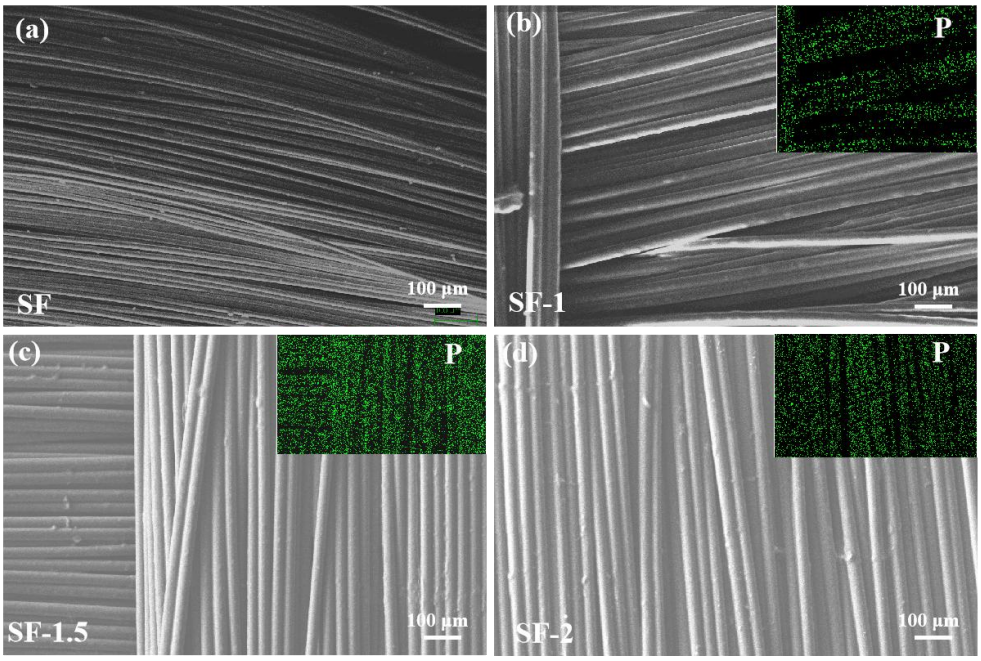

Figure 4-6. SEM images and EDS spectra of the fabrics: SF (a); SF-1 (b) SF-1.5 (c) SF-2 (d).

The attachment of HGB and PAIM to fabric offers the fire-proof ability for Suncell farbic. To determine the flame-retardant performance of the fabric before and after coated, the samples were burned under the same conditions. Figure 4-7 showed the digital photographs taken during the combustion test. The pure Suncell fabric performed poorly flame-retardant, making it simple to ignite and unable to self-extinguish, leading to a full combustion. On the other hand, the surface of the

burned modified fiber showed a distinct layer of char and retained its structural integrity.

The microscale combustion calorimetry (MCC) was carried out to quantitatively predict the fire risk of materials and the results were depicted as temperature-dependent curves in Figure 4-8. Generally speaking, the typical parameters including heat release rate (HRR), and total heat release (THR) are positively related to the combustion intensity of the sample. The Figure 4-8a indicated that the peak heat release rate of modified fabric was reduced by 64.4% compared with the original Suncell fabric. In the meantime, the THR of the F-SF also exhibited a noteworthy reduction (59.6%) in heat release (Figure 4-8b), which was helped to prevent violent combustion.

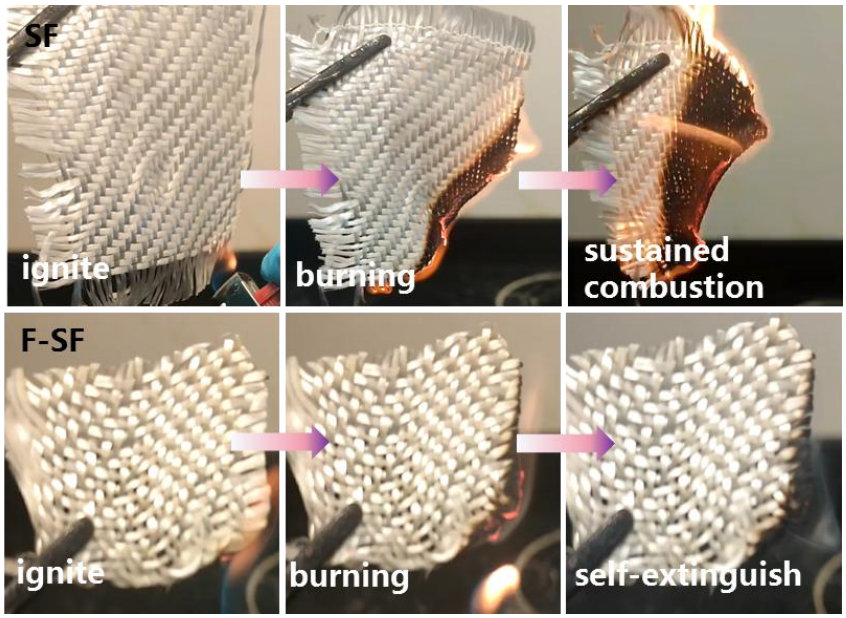

Figure 4-7. Digital photographs during the burning test of SF and F-SF.

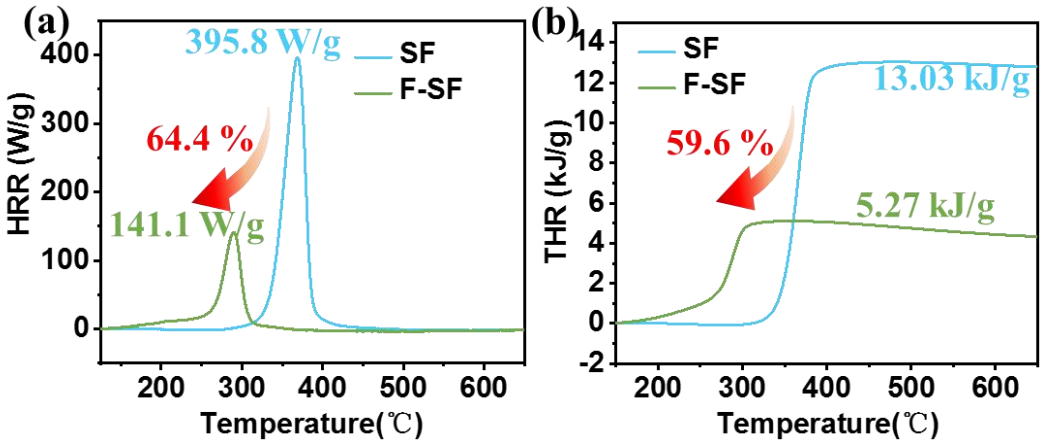

Figure 4-8. Heat release rate curves (a) total heat release curves of SF and F-SF (b).

In order to investigate whether the combination of PAIM and HGB could minimize the influence on the mechanical properties of the fabric, the breaking strength of yarn was tested. As a result, there was also a slight but acceptable decrease in the from 67.1 N to 66.8 N (Table 4-2) before and after modification. Compared with the breaking strength of fabric modified after PA and HGB (66.9 N), the use of neutral PAIM can effectively avoid the negative impact to the fabric.

Table 4-2. The breaking strength and flammability regime of Suncell fiber under different concentration of PAIM and HGB.

Samples	PAIM (mg/mL)	BOZ (mg/mL)	Breaking strength (N)	Self-extinguish (Yes or No)
SF	0	0	67.1 ± 2.5	No
SF-1	1	1	66.9 ± 0.4	No
SF-1.5	1.5	1.5	66.5 ± 1.0	No
SF-2 (F-SF)	2	2	66.9 ± 2.0	Yes

4.3.3 Mechanical properties

As discussed above, the modifier HGB/PAIM can optimize the surface polarity and also enables a co-curing reaction with epoxy resin, which was reflected in a lower curing temperature in the DSC results (Figure 4-5). In this way, the treat method would help to strengthen the composite interface and promote the transfer of stress from the polymer phase to the fiber in the force field, further improve the mechanical characteristics technically. The mechanical performance including tensile, impact, and ILSS tests of all samples were tested and the data were collected in Table 4-3 and Figure 4-9 .

As can be seen from Figure 4-9a and b, the effective reinforcement effect of the fabric gave all the composites a much greater modulus and tensile strength. Unfortunately, F-SF/EP and F-SF/F-EP exhibited a

slight increase in tensile modulus compared with SF/EP and SF/F-EP (11.08 and 11.33 GPa *vs.* 9.82 and 10.03 GPa). Meanwhile, in contrast to SF/EP, F-SF/EP, and SF/F-EP, F-SF/F-EP showed the highest tensile strength (116, 103.3 and 103.0 MPa vs. 121.6 MPa). This may be attributed to the strong acidity of PAIM as well as the low crosslink density of F-EP[150].

The composites containing the altered fabric also demonstrated increased impact strength. The comparison of SF-based and F-SF-based composites shows that the modifier improves the composite's deformation resistance and stress transfer efficiency, which accurately reflects the enhanced interface properties of the composite. To be more precise, Figure 4-9c showed that the impact strength of F-SF/F-EP increased from 6.58 to 7.26 $kJ \cdot m^{-2}$, which is an improvement of almost 10.3% over the untreated SF/EP composite. ILSS is a technical indicator that shows the adhesion characteristic between two phases in relation to interface compatibility. As predicted, F-SF/F-EP had an exceptional ILSS of 13.66 MPa, which was higher than SF/EP, F-SF/EP, and SF/F-EP's respective ILSS of 11.41, 12.84, and 12.77 MPa. Interestingly, when the samples with the identical matrix resin were compared, the treated fabric dramatically raises the ILSS, which strongly

supported the designed modifier's function in interfacial compatibilization.

Table 4-3. The mechanical properties of different samples.

Samples	Tensile modulus (GPa)	Tensile strength (MPa)	Impact strength ($kJ \cdot m^{-2}$)	ILSS (MPa)
EP	5.50±0.54	71.5±5.9	3.65±0.27	-
SF/EP	9.82±1.36	116.0±5.2	6.58±0.26	11.41±0.15
F-SF/EP	11.08±1.30	103.3±19.5	6.89±0.39	12.84±0.86
SF/F-EP	10.03±0.87	103.0±16.5	7.05±0.75	12.77±0.92
F-SF/F-EP	11.33±0.46	121.6±12.6	7.26±0.68	13.66±0.46

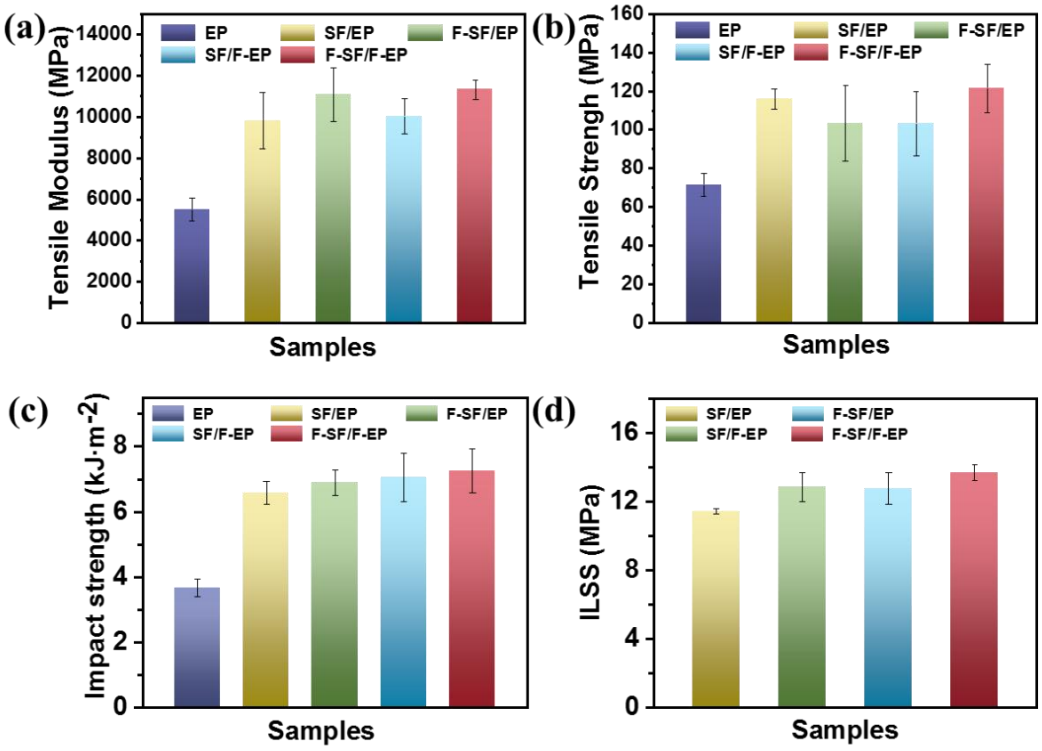

Figure 4-9. Mechanical performance of different materials: tensile strength (a); tensile modulus (b); impact strength (c) and ILSS (d).

In order to make a further confirmation of compatibility, the Scanning electron microscope (SEM) for the fracture surface after the tensile test of SF/EP and F-SF/F-EP was employed. As observed in Figure 4-10a and b, some big cracks and voids of the SF/EP composite suggested poor interfacial adhesion between the Suncell fiber and the epoxy resin, which impeding mechanical transfer and stress distribution. For F-SF/F-EP composites (Figure 4-10c and d), it was found out that no delamination or significant fracture occurred, and the mode of fracture were micro-cracks on the tension side of the samples. The fiber breakage could be detected in the image, the fibers were covered in the matrix and no indication of delamination was seen. These micrographs provided excellent justification for the composites mechanical properties findings.

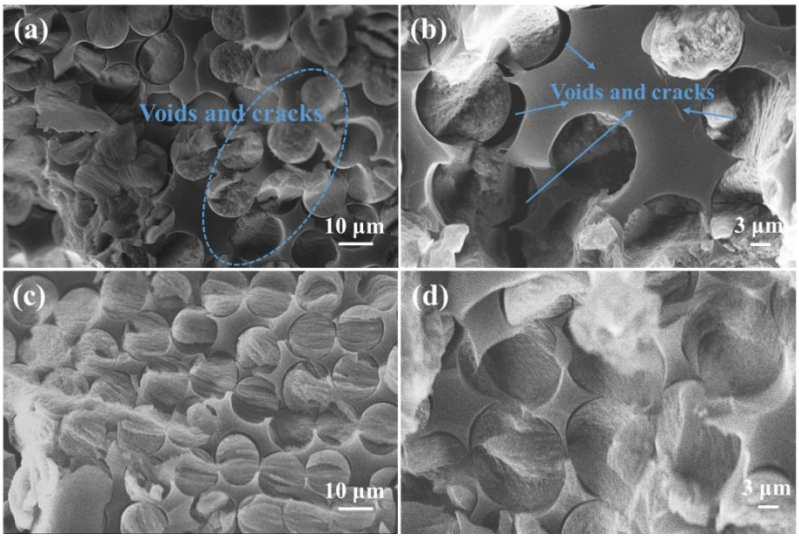

Figure 4-10. The SEM images under different magnificent of fracture surfaces of composites after tensile test: F-SF/F-EP (a and b) and F-SF/F-EP (c and d).

4.3.4 Thermal stability of composites

TGA measurement was used to determine the thermal stability of the prepared composites under N_2 atmosphere, as shown in Figure 4-11a and b. Table 4-4 contained the associated values, which included T_{d10} (10% weight loss temperature), T_{max} (maximum weight loss temperature), and R_{800} (char yield at 800 °C). Although the breakdown mechanisms differed, all of the composites displayed approximate tendencies. T_{d10} for SF/EP, in example, was 330.3 °C, which was somewhat higher than T_{d10} for F-SF/EP (332 °C). When DGEBDB was used as the polymer matrix, the T_{d10} value for the composite decreased somewhat, from 330.3 °C for SF/EP to 325.7 °C for SF/F-EP. This was in line with the previous outcome. With a $T_{10\%}$ value of 309.7 °C, the lowest of the three composites (F-SF/F-EP) was found, perhaps because of its higher phosphorus content. The early breakdown of P-O-P, P-C, and P=O weak bonds in PAIM and DOPO lowers the composite's initial degradation temperature, which accounted for the difference in T_{d10}. The lower temperature T_{max} in the DTG data (Figure 4-11b) further supported their earlier thermal breakdown tendency. In relation to R_{800} *value*, SF/EP, F-SF/EP, SF/F-EP, and F-SF/F-EP had comparable values of 12.2%, 18.7%, 22.7%, and 28.5% in that order. Theoretically, during the process of thermal degradation, phosphoric acid and its derivatives might yield a

high-quality char residue[184]. In the current work, PAIM and DGEBDB both enhance carbonization, which was advantageous to improving flame retardancy, especially in the condensed phase.

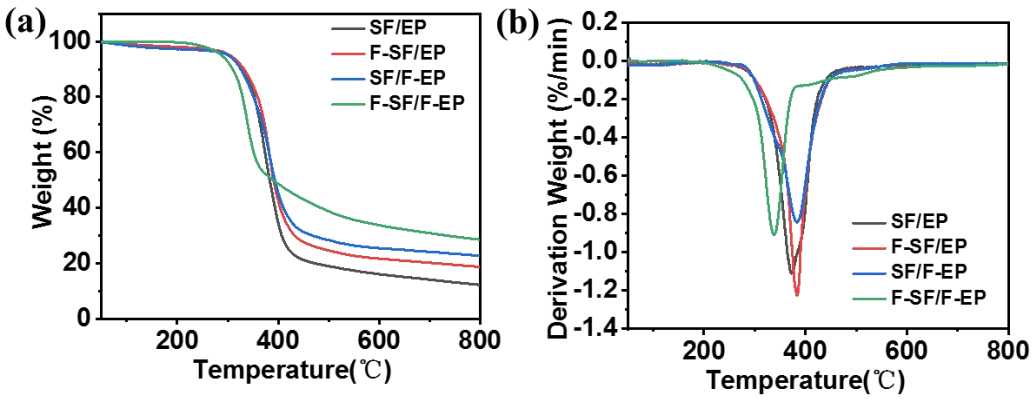

Figure 4-11. TGA (a) and DTG (b) curves for composites.

Table 4-4. Results of thermal stability of composites.

Samples	T_{d10} (°C)	Char yield at 800 °C (%)	T_{max} (°C)
SF/EP	330.3	12.2	374.3
F-SF/EP	332.0	18.7	385.0
SF/F-EP	325.7	22.7	344.7
F-SF/F-EP	309.7	28.5	339.7

4.3.5 Flammability analysis of composites

To evaluate the fire safety of these composites in detail, limit oxygen index measurements (LOI), vertical burning test, and cone calorimetry test (CCT) were conducted.

The limiting oxygen index method can be used to understand the difficulty of ignition and combustion of materials when they contact the flame in the air environment. It is often used to evaluate the combustion characteristics of materials. Moreover, vertical burning UL-94 test was performed to evaluate the flammability of the composites. The results were demonstrated in Table 4-5. As can be seen from the results of the limiting oxygen index, the LOI value of composite without a modifier and a flame-retardant epoxy matrix (SF/EP) was only 23.6%, and its UL-94 was no rating, suggesting a high combustibility. In contrast, the LOI values of SF/F-EP and F-SF/EP increased to 27.7% and 28.3%, respectively, suggesting that DGEBDB or the combination modifier may have a greater impact on the composite's ability to withstand flames. Unfortunately, the insufficient fire-proof ability of them still resulted in the NR classification. Furthermore, the as-prepared composite showed an exceptional LOI of 34.3% when both F-SF and F-EP were used. It also received a V-0 grade in the UL-94 test, which is the best classification of the vertical rating classification, suggesting that this combination may produce satisfactory flame retardancy (Figure 4-12).

Conical calorimetry test can reflect the combustion behavior of materials more comprehensively. The cone calorimeter test (CCT) results of representative composites, SF/EP and F-SF/F-EP, were

exhibited in Figure 4-13a and b, in which F-SF/F-EP exhibited much lower heat release rate (HRR) and total heat release (THR) as compared with that of SF/EP. Specifically, the peak value of HRR of F-EP/F-RF was reduced by 44.9%, from 834.9 to 459.9 kW/m^2, and the corresponding time was delayed from 120 to 190 s. Both the lower heat release and later maximum heat release benefited the lower combustion intensity.

Table 4-5. Results of flame retardant measurements of composites.

Samples	LOI (%)	t_1/t_2 (s)	Dripping	UL-94
SF/EP	23.6	-[a]	No	No-rating
F-SF/EP	27.7	-[a]	No	No-rating
SF/F-EP	28.3	-[a]	No	No-rating
F-SF/F-EP	34.3	1.6/2.4	No	V-0

-[a]: Does not extinguish fire after ignition.

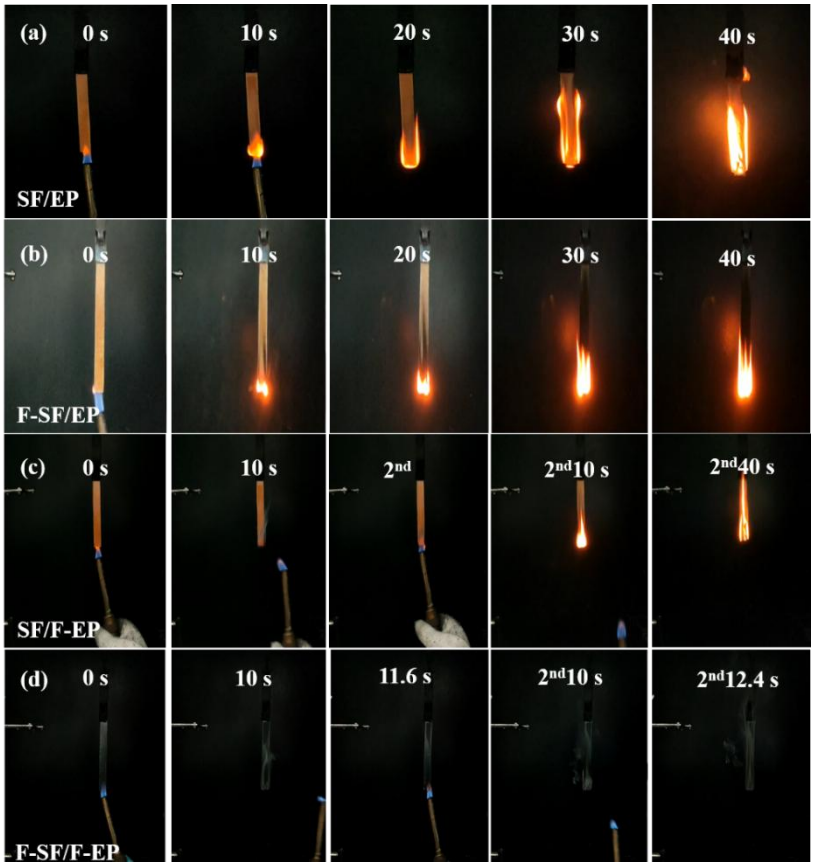

Figure 4-12. Digital photographs of SF/EP (a), F-SF/EP (b), SF/F-EP (c), and F-SF/F-EP (d) during the vertical burning test.

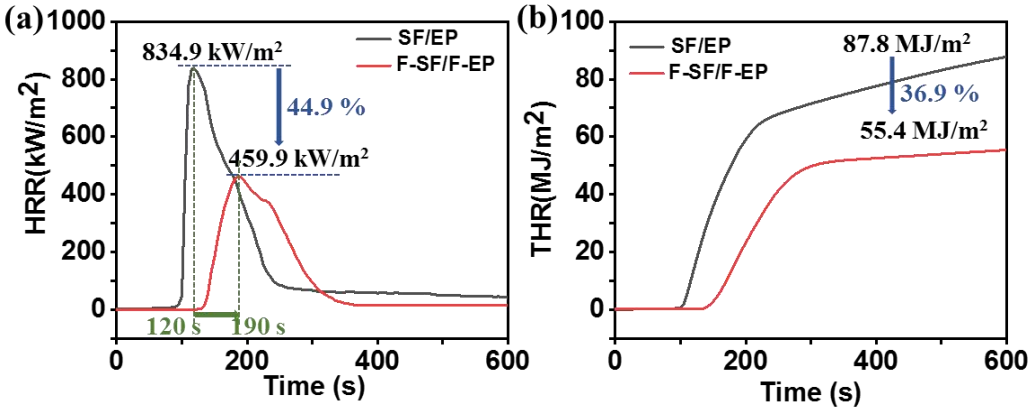

Figure 4-13. HRR (a) and THR (b) curves for composites.

4.3.6 Flame-retardant mechanism

The analysis of thermal degradation gaseous products

To reveal the considerable non-flammability mechanism behind F-SF/F-EP, TG-FTIR, SEM, XPS, and Raman tests were performed. In general, the fire-proof effect is the co-action of gaseous and condensed phases. Accordingly, TG-FTIR was first carried out to analyze gas behavior during combustion, as illustrated in Figure 4-14 and 4-15. The composite consisting of the pristine fabric and commercial epoxy resin (Figure 4-14a) showed a clearly lower onset decomposition temperature than F-SF/F-EP (Figure 4-14b), which was in agreement with the TGA results. Due to the fact that PAIM and DOPO in DGEBDB expedited the thermal decomposition of matrix and reinforcement, facilitated the formation of continuous carbon layer at relatively lower temperature accordingly as well. In the meantime, the FTIR spectra of the degradation products of two composites at different temperatures (300, 450, 520, and 600 °C) mainly consisted of H_2O (3745 cm^{-1}), hydrocarbon compounds (2978 cm^{-1}), CO_2 (2364 cm^{-1}), aromatic compounds (1508 and 1616 cm^{-1}), NH_3 (1600-1700 cm^{-1}) and ether compounds (1751, 1261, and 1178 cm^{-1}), corresponding to the similar compositions[172]. The decomposition products were the same but with different intensities

(Figure 4-15a and c). Specifically, taking the curve of 300 °C as an example, the intensity of H_2O, CO_2, and NH_3 for F-SF/F-EP was obviously stronger than that of SF/EP, which could dissipate heat and dilute oxygen and flammable gases in the gas phase[185]. The detected NH_3 signal may attributed to the nitrogen elements present in benzoxazine and the curing agent DDM.

Notably, compared with SF/EP (Figure 4-15b), F-SF/F-EP displayed P-O absorption bands at 1060 cm^{-1} (Figure 4-15d), indicating that the phosphorus-containing chemicals in PA and DGEBDB had a fire-resistance function in the gaseous phase. As we know, DOPO and its derivatives generally act in the gas phase by reducing the free radical[172, 186], which easy to conclude that DGEBAB also can release phosphorus-based free radicals to capture the active free radicals and interrupt the combustion reaction to decrease the release of flammable gases in the gaseous phase.

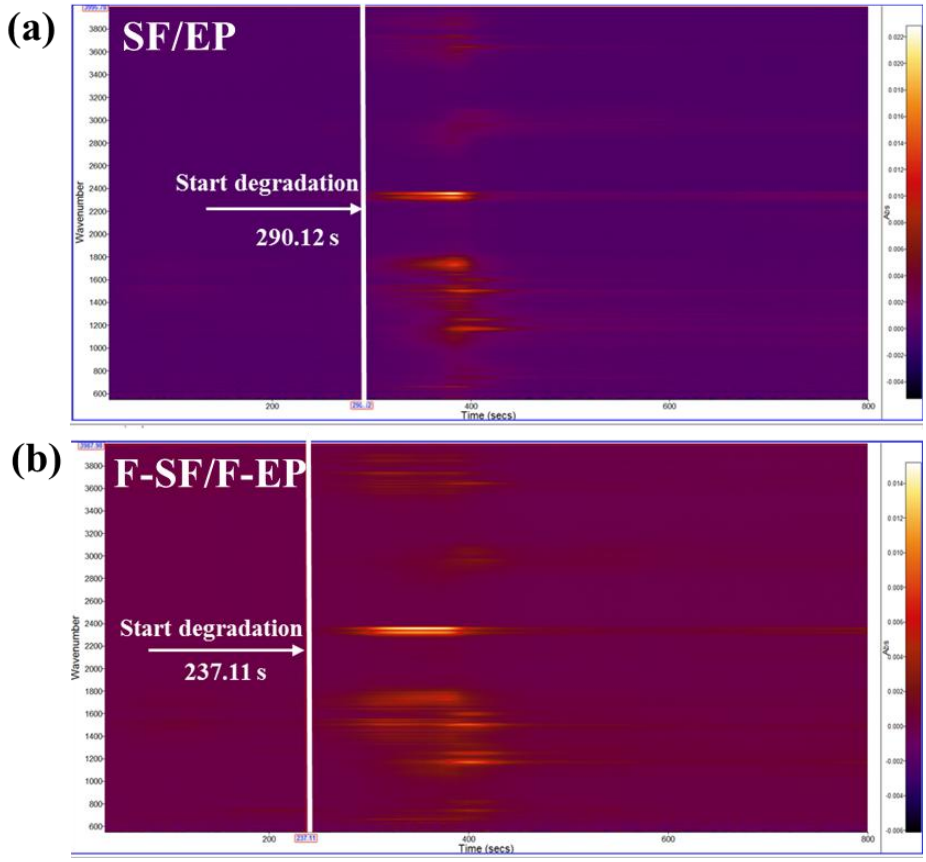

Figure 4-14. Images of TG-FTIR signal intensity over time for SF/EP (a) and F-SF/F-EP (b).

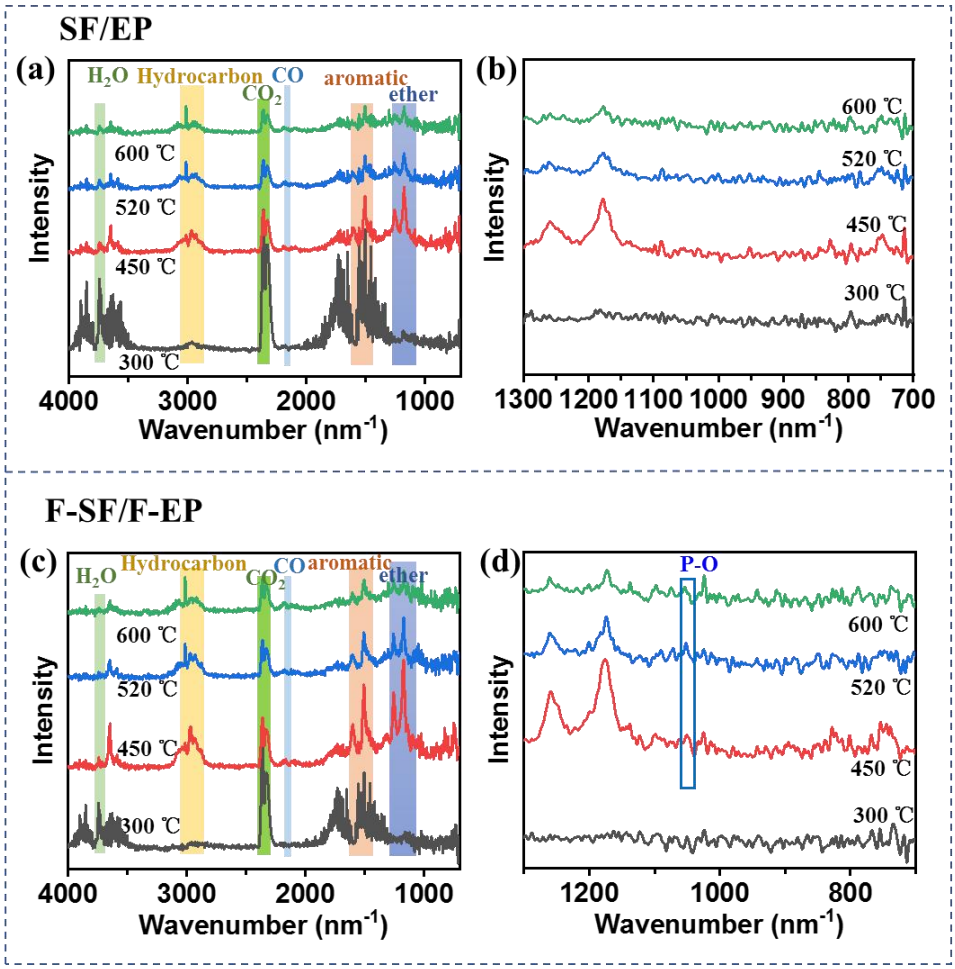

Figure 4-15. TG-FTIR degradation curves for SF/EP (a, b) and F-SF/F-EP (c, d) at different temperatures.

The characteristics of the char residues

The vertical views of the char of SF/EP and F-SF/F-EP in the top and bottom rows after the cone calorimeter test were presented. As recorded in Figure 4-16, the digital photos of the char residues revealed that the char layer of SF/EP without enhancement was loose and puffy (Figure 4-16a and b) since its high flammability, leading to a weak barrier and

protective effect. In contrast, the carbon layer shown in F-SF/F-EP exhibits denser and more compact morphology (Figure 4-16c and d), which was consistent with its high yield of char in the TGA result.

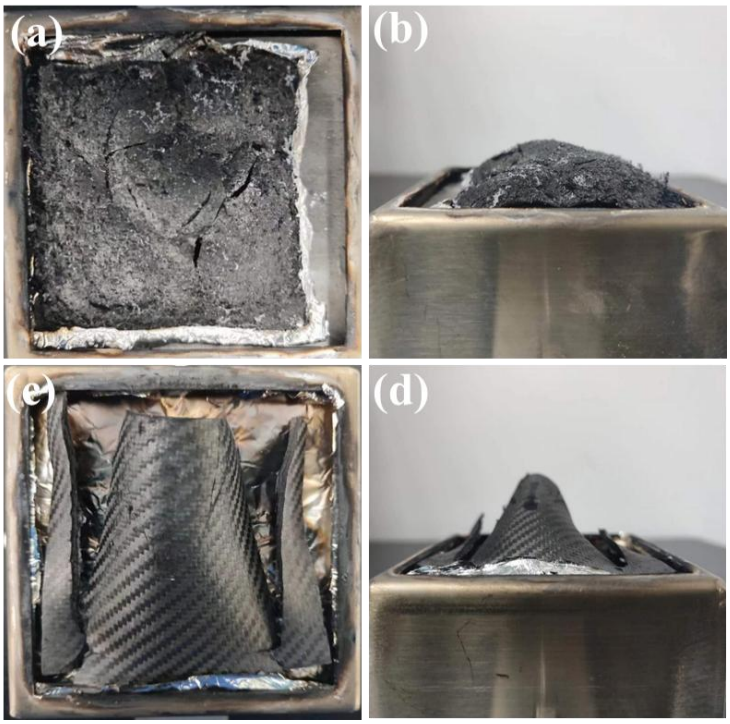

Figure 4-16. The vertical and the horizontal views of the char residues of SF/EP (a and b), F-SF/F-EP (c and d) after the cone calorimeter test.

Further detecting the micro-morphologies of char residue by SEM, according to the preliminary observation on the morphology of char residues, it was found that the char residue of SF/EP (Figure 4-17a) presents the exposed fibers with damaged structure due to the nearly complete combustion of the resin matrix and unprotected fibers. Conversely, the char residue of F-SF/F-EP was thicker and denser

which effectively secured the inner fabric, as shown in Figure 4-17d. When further observing the higher resolution pictures of the char residue of burnt SF and epoxy resin, it was seen that the char residue of burnt fiber was fractured and the epoxy resin was loose and porous (Figure 4-17b and c). The incomplete and fragmented charred layer provided pathways that allow flammable gas, heat, and oxygen to reach the underlying matrix, resulting in flame retardant failure[51]. In contrast, a continuous fiber shape and flatter carbon layer were formed on the surface of burnt composites (Figure 4-17e and f), which could effectively prevent the transfer of heat, O_2, and flammable volatiles, revealing a strong barrier effect[150].

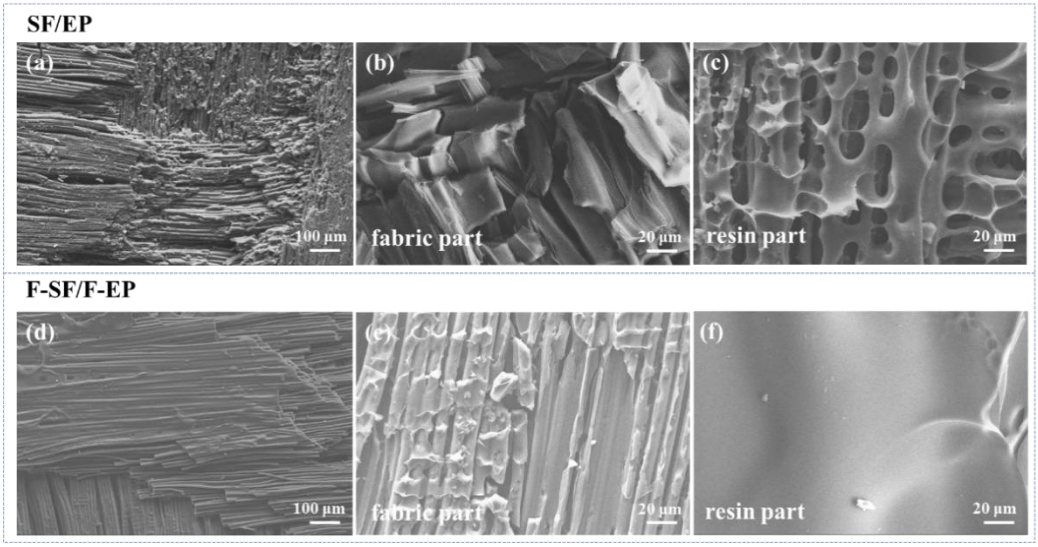

Figure 4-17. SEM micrographs of char residues of SF/EP (a, b and c), and F-SF/F-EP (d, e and f) under different magnificent.

Raman measurement was further used to examine the quality of the char residue samples. In Figure 4-18a and b, two peaks located at 1350 cm^{-1} and 1590 cm^{-1} stand for disordered graphite (D band) and ordered carbon (G band) could be observed, respectively. The quality of the carbon layer was closely related to the integral ratio of these two peaks (I_D/I_G), which also represents the graphitization degree[51, 157]. The I_D/I_G value of the char sample of F-SF/F-EP was calculated to be 2.69, which was significantly lower than that of SF/EP with 3.41, illustrating the higher graphitization degree of the former. In a word, the high yield and high quality of the condensed char was beneficial for flame inhibition effects[51], which could prevent heat and combustible fragments transfer as well as keep oxygen away from the unburned composite as a physical barrier[187-188].

Besides, the chemical compositions of the char residues were further identified by XPS, as shown in Figure 4-19. Except C, N, and O elements, two additional peaks at 133.8 eV and 191.2 eV attributing to P_{2s} and P_{2p} element was detected in the char residue for F-SF/F-EP (Figure 4-19a and b), which explain the important role of P elements in the condensed phase[62, 150]. Meanwhile, in the fine spectra of F-SF/F-EP, the splitting peaks at 285.6 eV in C_{1s} (Figure 4-19c), 532.2 eV in O_{1s} (Figure 4-19e), and 133.5 eV in P_{2p} (Figure 4-19f) indicated the presence

of P-O-C, and the signals of 288.4 eV in C_{1s} and 400.2 eV in N_{1s} (Figure 4-19d) were assigned to the formation of C-N, contributing to the yield of high-quality char layer[190].

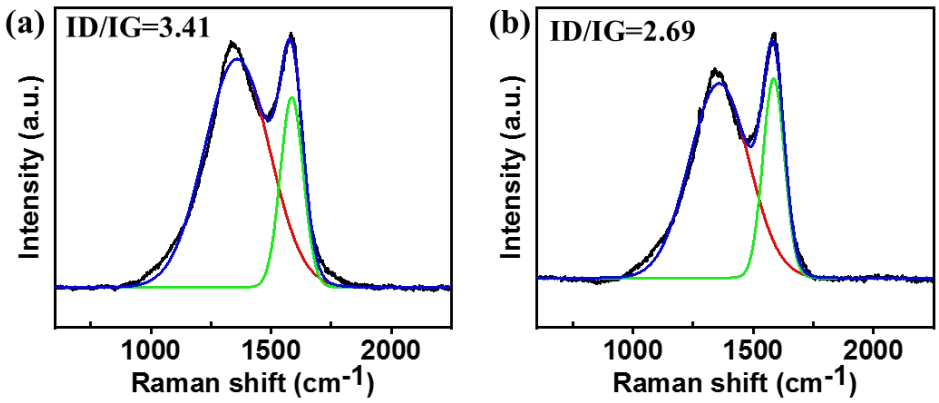

Figure 4-18. Raman spectra of char residuals for SF/EP (a) and F-SF/F-EP (b).

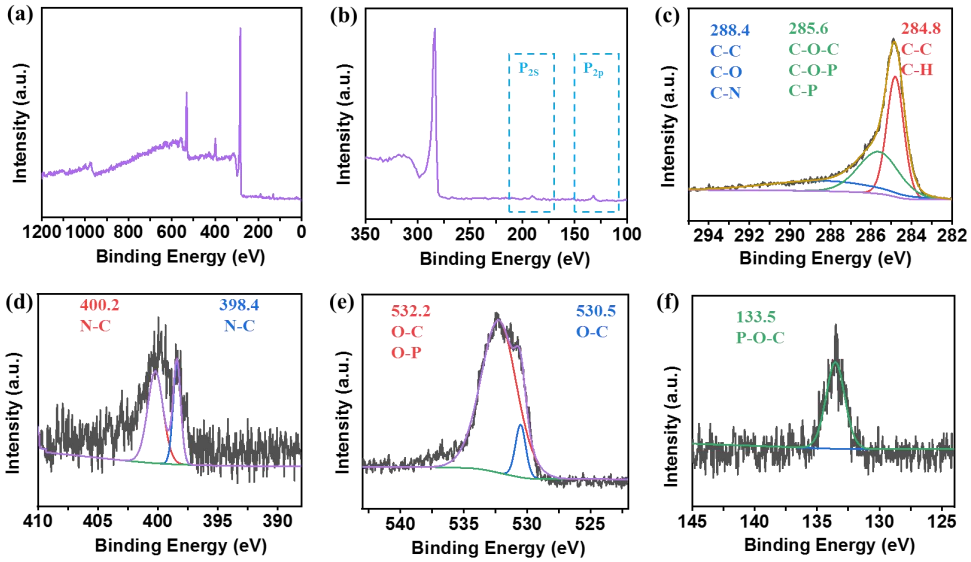

Figure 4-19. XPS spectra for the surface of residual char layers of burnt SF/EP and F-SF/F-EP: overall spectra (a); enlarged picture containing peaks for P_{2s} and P_{2p} (b); peak splitting for C_{1s} (c), N_{1s} (d), O_{1s} (e), and P_{2p} (f) for char residues obtained from F-SF/F-EP.

Based on the aforementioned findings, the F-SF/F-EP composite exhibited exceptional fire safety due to a synergistic flame-retardant mechanism that operated in both the gaseous and condensed phases. In particular, when combustion occurred, the release of phosphorus-based free radicals is capable of capturing active free radicals involved in combustion reaction, thereby reducing the release of flammable components in the gaseous phase. Meanwhile, the nitrogen-containing moieties including polybenzoxazine, DDM, and imidazole can produce N-containing nonflammable gases to dilute the gas atmosphere. Moreover, the yield of phosphorus acid derivatives during the early decomposition of PAIM and DOPO group could also promote the formation of a more compact and continuous char residue via inducing dehydration and carbonization, which would play a role in blocking heat, oxygen transfer, and flammable volatiles, further protect the underlying polymeric substrate

4.4 Conclusion

In this chapter, a water-soluble neutral epoxy curing accelerator (PAIM) was simply synthesized through one step. Then it was combined with bio-based benzoxazine (HGB) to modify the regenerated cellulose fabric in the water solution phase via simple impregnation, which exhibited a self-extinguishing behavior after ignition. The modified fabric

was further used to reinforce DGEBDB composites through prepreg preparation and a vacuum bag-assisted compression molding process, which could improve interfacial adhesion and fire safety of the regenerated cellulose fabric/epoxy composite in the simultaneous technically. Both HGB and PAIM partially participate in the curing of epoxy resin, improving the interface properties of the composite material, so the presence of flame retardants will not reduce the mechanical properties. The composites of F-SF/F-EP showed remarkably enhanced with the adding of PAIM and HGB due to the optimized interface, reflecting in the 14.9% and 9.6% improvement compared with SF/EP, respectively. Meanwhile, owing to the higher interface stress transfer efficiency, F-SF/F-EP possesses an ILSS of 13.89 MPa, outperforming that of SF/EP, F-SF/EP, and SF/F-EP with 11.41, 12.42, and 12.77 MPa, respectively. Besides, the composite constituted with both the flame-retardant modified fabric and intrinsically fire-resistant epoxy matrix exhibited super anti-flammability in terms of a high LOI value of 34.3% and UL-94 V-0 rating whereas the composite with no treated sample showed UL-94 V-1 and LOI value of 23.6%. In addition, cone calorimetry test showed that the cured F-SF/F-EP system exhibited a reduction of up to 44.9% and 36.9% for PHRR and THR, respectively, compared to the cured SF/EP system. The enhanced flame-retardant

property was attributed to the avoidance of the wick effect in the fabric phase, barrier effect in the gaseous phase, and inhibition effect in the condensed phase. This work not only provides an advanced method for the efficient and integrated modification of plant fiber-reinforced composites, but also paves the way for the wider and safer application of green composite materials.

Chapter 5 Overall summary of the thesis and future works based on research findings

5.1 Overall summary of the thesis

This thesis endeavors to tackle the issue that the majority of conventional techniques are constrained by their incapacity to enhance both mechanical and thermal characteristics. Thus, the goal of the current research is to generate fire-safe and high-performing materials by designing and synthesizing multifunctional modifiers that can satisfy the aforementioned specifications. This work offers three effective approaches to fabricate strong interfacial and flame-retardant plant fiber-reinforced epoxy composites that can develop fire-safe and high-performance materials. In Chapter 2, a multi-functional modifier (FPD) was designed and synthesized successfully through just one step. It can be successfully introduced and firmly adhere to the ramie fabric, and FPD can play a bridging role to enhance the interfacial properties of ramie epoxy composites, which could improve the mechanical and thermal performance of ramie-reinforced epoxy resin composites, simultaneously. In Chapter 3, a water-soluble combined modifier composed of bio-based benzoxazine (HGB) was facilely synthesized through one step with confirmed structure and excellent purity. Then it was combined with PA to modify the regenerated cellulose fabric in the

water solution phase via simple impregnation to simultaneous improvement of interfacial adhesion and fire safety of the regenerated cellulose fabric/epoxy composite. Results indicated that F-SF/F-EP well balanced its mechanical and fire-resistant performance. In Chapter 4, a curing accelerator (PAIM) has been successfully synthesized and the chemical structure was carefully characterized to reduce the effect of phytic acid on the mechanical properties of fiber. Here, polyphosphate (PAIM) and benzoxazine (HGB) was used to develop flame retardant coating on ramie fabrics to improve the interfacial behavior between Suncell fiber and epoxy resin matrix. The flame retardant Suncell fabric reinforced epoxy resin composites were prepared with PAIM/HGB treated ramie fabrics as reinforcement. The self-assembly of the flame retardant coating on the fabric surface endowed the composites with self-extinguishing ability, and the treated composites can reach UL-94 V-0 rating during the vertical flame tests. Moreover, the interfacial adhesion of the treated composites has been enhanced. In consequence, its tensile and flexural properties have been improved and the treated composites show much higher strength and toughness compared with the untreated composites.

The thesis aims to provide insights into the optimization of flame retardant formulations and interfacial modifications, leading to the design

and fabrication of sustainable composites with improved fire resistance and enhanced mechanical properties. This work provides three simple, green and renewable char forming agent and bridging agent for plant fiber-epoxy resin composites. I hope this work could bring us a new thought of the improvement of interfacial properties of flame retardant ramie-epoxy resin composites through an eco-friendly manner. This work not only provides an advanced method for the efficient and integrated modification of plant fiber-reinforced composites, but also paves the way for the wider and safer application of green composite materials, which may enable potential application prospects in the files of construction, trains, and automobiles with interior trim.

5.2 Future works

The following aspects will be included in the future development directions of plant fiber reinforced composite materials:

a) Improvement of material properties: Research in the future should concentrate on improving the mechanical properties, durability, and thermal performance of plant fiber composites. To further improve the overall performance of the materials, this can be accomplished by optimizing fiber treatment methods, making interfacial alterations, and choosing reinforcing materials.

b) Development of sustainable resources: It is essential to continue developing and using plant fiber composites from sustainable sources in order to lessen dependency on finite resources. To accomplish resource recycling, researchers can investigate novel sources of plant fibers and bio-based epoxy resin, such as woody fibers and agricultural byproducts, and create appropriate extraction and processing methods.

c) Development of multifunctional composites: Expanding the functionality of plant fiber composites is a promising direction. Future research can explore the incorporation of additional functional fillers, additives, or nanomaterials to impart enhanced conductivity, flame retardancy, antimicrobial properties, and other characteristics, meeting a wider range of application needs.

d) Improvement of processing techniques: Further improvement of processing techniques for plant fiber composites is crucial for enhancing production efficiency and reducing costs. Future research can focus on developing more efficient and controllable processing techniques such as injection molding, 3D printing, and automated production, to improve the feasibility and economic viability of engineering applications.

Overall, the future development of plant fiber reinforced composite materials will continue to progress towards higher performance, sustainability, and multifunctionality. This will provide more

environmentally friendly and alternative material options across various industries, contributing to the achievement of sustainable development goals.

References

1. Maiti, S.; Islam, M. R.; Uddin, M. A.; Afroj, S.; Eichhorn, S. J.; Karim, N., Sustainable Fiber‐Reinforced Composites: A Review. *Adv. Sustain. Syst.* **2022,** *6* (11).

2. Chen, Y.; Wu, X.; Wei, J.; Wu, H., Nondestructive Modification of Catechol/Polyethyleneimine onto Polyester Fabrics by Mussel‐Inspiration for Improving Interfacial Performance. *Macromolecular Materials and Engineering* **2020,** *305* (9), 2000258.

3. Le Duigou, A.; Bourmaud, A.; Gourier, C.; Baley, C., Multi-scale shear properties of flax fiber reinforced polyamide 11 biocomposites. *Composites Part A: Applied Science and Manufacturing* **2016,** *85*, 123-129.

4. Chen, L.; Msigwa, G.; Yang, M.; Osman, A. I.; Fawzy, S.; Rooney, D. W.; Yap, P. S., Strategies to achieve a carbon neutral society: a review. *Environ. Chem. Lett.* **2022,** *20* (4), 2277-2310.

5. Ashadujjaman, M.; Saifullah, A.; Shah, D. U.; Zhang, M.; Akonda, M.; Karim, N.; Sarker, F., Enhancing the mechanical properties of natural jute yarn suitable for structural applications. *Materials Research Express* **2021,** *8* (5), 055503.

6. Tian, H.; Zhang, Y. X.; Yang, C.; Ding, Y., Recent advances in experimental studies of the mechanical behaviour of natural fiber‐reinforced cementitious composites. *Structural Concrete* **2016,** *17* (4), 564-575.

7. Samouh, Z.; Molnár, K.; Hajba, S.; Boussu, F.; Cherkaoui, O.; El Moznine, R., Elaboration and characterization of biocomposite based on polylactic acid and Moroccan sisal fiber as reinforcement. *Polymer Composites* **2021,** *42* (8), 3812-3826.

8. Azwa, Z. N.; Yousif, B. F.; Manalo, A. C.; Karunasena, W., A review on the degradability of polymeric composites based on natural fibers. *Mater. Design* **2013,** *47*, 424-442.

9. Joshi, S. V.; Drzal, L. T.; Mohanty, A. K.; Arora, S., Are natural fiber composites environmentally superior to glass fiber reinforced composites? *Composites Part A: Applied Science and Manufacturing* **2004,** *35* (3), 371-376.

10. Jang, J. Y.; Jeong, T. K.; Oh, H. J.; Youn, J. R.; Song, Y. S., Thermal stability and flammability of coconut fiber reinforced poly(lactic acid) composites. *Composites Part B: Engineering* **2012,** *43* (5), 2434-2438.
11. John, M.; Thomas, S., Biofibers and biocomposites. *Carbohydrate Polymers* **2008,** *71* (3), 343-364.
12. Mngomezulu, M. E.; John, M. J.; Jacobs, V.; Luyt, A. S., Review on flammability of biofibers and biocomposites. *Carbohydr Polym* **2014,** *111*, 149-82.
13. Oksman, K.; Skrifvars, M.; Selin, J. F., Natural fibers as reinforcement in polylactic acid (PLA) composites. *Composites Science and Technology* **2003,** *63* (9), 1317-1324.
14. Wei, Z.; Ji, C.; Yu, T.; Li, Y.; Liu, X., The unique wick effect and combustion behavior of flax fiber reinforced composites: Experiment and simulation. *Composites Part B: Engineering* **2023,** *265*, 110954.
15. Thyavihalli Girijappa, Y. G.; Mavinkere Rangappa, S.; Parameswaranpillai, J.; Siengchin, S., Natural Fibers as Sustainable and Renewable Resource for Development of Eco-Friendly Composites: A Comprehensive Review. *Front Mater* **2019,** *6*.
16. Asim, M.; Jawaid, M.; Abdan, K.; Ishak, M. R., The Effect of Silane Treated Fiber Loading on Mechanical Properties of Pineapple Leaf/Kenaf Fiber Filler Phenolic Composites. *Journal of Polymers and the Environment* **2017,** *26* (4), 1520-1527.
17. Cordeiro, E. P.; Pita, V. J. R. R.; Soares, B. G., Epoxy–Fiber of Peach Palm Trees Composites: The Effect of Composition and Fiber Modification on Mechanical and Dynamic Mechanical Properties. *Journal of Polymers and the Environment* **2016,** *25* (3), 913-924.
18. Kalia, S.; Kaith, B. S.; Kaur, I., Pretreatments of natural fibers and their application as reinforcing material in polymer composites—A review. *Polymer Engineering & Science* **2009,** *49* (7), 1253-1272.
19. Almeida, J. H. S.; Amico, S. C.; Botelho, E. C.; Amado, F. D. R., Hybridization effect on the mechanical properties of curaua/glass fiber composites. *Composites Part B: Engineering* **2013,** *55*, 492-497.
20. Venkateshwaran, N.; Elayaperumal, A.; Sathiya, G. K., Prediction of tensile properties of hybrid-natural fiber composites. *Composites Part B: Engineering* **2012,** *43* (2), 793-796.
21. Nurazzi, N. M.; Asyraf, M. R. M.; Athiyah, S. F.; Shazleen, S. S.; Rafiqah, S. A.; Harussani, M. M.; Kamarudin, S. H.; Razman, M. R.;

Rahmah, M.; Zainudin, E. S.; Ilyas, R. A.; Aisyah, H. A.; Norrrahim, M. N. F.; Abdullah, N.; Sapuan, S. M.; Khalina, A., A Review on Mechanical Performance of Hybrid Natural Fiber Polymer Composites for Structural Applications. *Polymers (Basel)* **2021,** *13* (13).

22. Liew, F. K.; Hamdan, S.; Rahman, M. R.; Rusop, M., Thermomechanical Properties of Jute/Bamboo Cellulose Composite and Its Hybrid Composites: The Effects of Treatment and Fiber Loading. *Adv Mater Sci Eng* **2017,** *2017*, 1-10.

23. Marceau, S.; Glé, P.; Guéguen-Minerbe, M.; Gourlay, E.; Moscardelli, S.; Nour, I.; Amziane, S., Influence of accelerated aging on the properties of hemp concretes. *Constr Build Mater* **2017,** *139*, 524-530.

24. Jami, T.; Karade, S. R.; Singh, L. P., A review of the properties of hemp concrete for green building applications. *Journal of Cleaner Production* **2019,** *239*, 117852.

25. Liew, F. K.; Hamdan, S.; Rahman, M. R.; Rusop, M.; Khan, A., Thermo‐mechanical properties of jute/bamboo/polyethylene hybrid composites: The combined effects of silane coupling agent and copolymer. *Polymer Composites* **2020,** *41* (11), 4830-4841.

26. Tan, W.; Hao, X.; Fan, Q.; Sun, L.; Xu, J.; Wang, Q.; Ou, R., Bamboo particle reinforced polypropylene composites made from different fractions of bamboo culm: Fiber characterization and analysis of composite properties. *Polymer Composites* **2019,** *40* (12), 4619-4628.

27. Guo, J.; Cao, M.; Ren, W.; Wang, H.; Yu, Y., Mechanical, dynamic mechanical and thermal properties of TiO2 nanoparticles treatment bamboo fiber-reinforced polypropylene composites. *J Mater Sci* **2021,** *56* (22), 12643-12659.

28. Liu, L.; Yuan, Z.; Fan, X.; Pan, C.; Li, X., A review of interfacial bonding mechanism of bamboo fiber reinforced polymer composites. *Cellulose* **2021,** *29* (1), 83-100.

29. Nabihah Rahmana, L. W. S., *, Lee Simonb, Müller Philippb, Javadian Alirezab, Enhanced bamboo composite with protective coating for structural concrete application. **2017**, 19-21.

30. Vijaya Kumar, K.; Arul Marcel Moshi, A.; Selwin Rajadurai, J., Mechanical property analysis on bamboo-glass fiber reinforced hybrid composite structures under different lamina orders. *Materials Today: Proceedings* **2021,** *45*, 1620-1625.

31. Dev, B.; Rahman, M. A.; Repon, M. R.; Rahman, M. M.; Haji, A.; Nawab, Y., Recent progress in thermal and acoustic properties of natural fiber reinforced polymer composites: Preparation, characterization, and data analysis. *Polymer Composites* **2023,** *44* (11), 7235-7297.
32. Thygesen, A.; Oddershede, J.; Lilholt, H.; Thomsen, A. B.; Ståhl, K., On the determination of crystallinity and cellulose content in plant fibers. *Cellulose* **2005,** *12* (6), 563-576.
33. Atmakuri, A.; Palevicius, A.; Vilkauskas, A.; Janusas, G., Review of Hybrid Fiber Based Composites with Nano Particles-Material Properties and Applications. *Polymers (Basel)* **2020,** *12* (9).
34. Jawaid, M.; Abdul Khalil, H. P. S., Cellulosic/synthetic fiber reinforced polymer hybrid composites: A review. *Carbohydrate Polymers* **2011,** *86* (1), 1-18.
35. Behnaz Baghaei , a. M. S., All-Cellulose Composites: A Review of Recent Studies on Structure, Properties and Applications.
36. Kaczmar, A. G. K. a. J. W., Application of Polymer Based Composite Materials in Transportation *Progress in Rubber, Plastics and Recycling T echnology* **2016,** *32*.
37. Mayank; Bardenhagen, A.; Sethi, V.; Gudwani, H., Spider-silk composite material for aerospace application. *Acta Astronaut* **2022,** *193*, 704-709.
38. Liu, J.; Wang, S.; Peng, Y.; Zhu, J.; Zhao, W.; Liu, X., Advances in sustainable thermosetting resins: From renewable feedstock to high performance and recyclability. *Progress in Polymer Science* **2021,** *113*, 101353.
39. Wang, X.; Guo, W.; Song, L.; Hu, Y., Intrinsically flame retardant bio-based epoxy thermosets: A review. *Composites Part B: Engineering* **2019,** *179*, 107487.
40. Arpitha, G. R.; Sanjay, M. R.; Senthamaraikannan, P.; Barile, C.; Yogesha, B., Hybridization Effect of Sisal/Glass/Epoxy/Filler Based Woven Fabric Reinforced Composites. *Experimental Techniques* **2017,** *41* (6), 577-584.
41. Riccio, A.; Raimondo, A.; Saputo, S.; Sellitto, A.; Battaglia, M.; Petrone, G., A numerical study on the impact behaviour of natural fibers made honeycomb cores. *Composite Structures* **2018,** *202*, 909-916.
42. Vajdova, I.; Jencova, E.; Szabo, S., Jr.; Melnikova, L.; Galanda, J.; Dobrowolska, M.; Ploch, J., Environmental Impact of Burning Composite

Materials Used in Aircraft Construction on the Air. *Int J Environ Res Public Health* **2019,** *16* (20).

43. Wernet, G.; Bauer, C.; Steubing, B.; Reinhard, J.; Moreno-Ruiz, E.; Weidema, B., The ecoinvent database version 3 (part I): overview and methodology. *The International Journal of Life Cycle Assessment* **2016,** *21* (9), 1218-1230.

44. H, S., Material intensity of advanced composite materials: Results of asudy for the Verbundwerkstofflabor Bremen. *Wuppertal Papers* **1999,** *15* (5), 700.

45. La Rosa, A. D.; Greco, S.; Tosto, C.; Cicala, G., LCA and LCC of a chemical recycling process of waste CF-thermoset composites for the production of novel CF-thermoplastic composites. Open loop and closed loop scenarios. *Journal of Cleaner Production* **2021,** *304*, 127158.

46. Koronis, G.; Silva, A.; Fontul, M., Green composites: A review of adequate materials for automotive applications. *Composites Part B: Engineering* **2013,** *44* (1), 120-127.

47. Mitsubishi-motors.com. Mitsubishi Motors develops plant-based green plastic floor mat. Tokyo: Mitsubishi Motors Co. (20.06.06). <http://www.mitsubishimotors.com/en/corporate/pressrelease/corporate/detail1475.html>

48. Saha, A.; Kumar, S.; Kumar, A., Influence of pineapple leaf particulate on mechanical, thermal and biodegradation characteristics of pineapple leaf fiber reinforced polymer composite. *J Polym Res* **2021,** *28* (2).

49. Xu, W.; Wirasaputra, A.; Liu, S.; Yuan, Y.; Zhao, J., Highly effective flame retarded epoxy resin cured by DOPO-based co-curing agent. *Polymer Degradation and Stability* **2015,** *122*, 44-51.

50. Abbas, Z.; Shahid, S.; Nawab, Y.; Shaker, K.; Umair, M., Effect of glass microspheres and fabric weave structure on mechanical performance of hemp/green epoxy composites. *Polymer Composites* **2020,** *41* (11), 4771-4787.

51. Borchers, A.; Pieler, T., Programming pluripotent precursor cells derived from Xenopus embryos to generate specific tissues and organs. *Genes (Basel)* **2010,** *1* (3), 413-26.

52. Hossen, M. F.; Hamdan, S.; Rahman, M. R.; Rahman, M. M.; Liew, F. K.; Lai, J. C., Effect of fiber treatment and nanoclay on the tensile

properties of jute fiber reinforced polyethylene/clay nanocomposites. *Fiber Polym* **2015,** *16* (2), 479-485.

53. Jeng-Yueh Shieha, C.-S. W., Synthesis of novel flame retardant epoxy hardeners and properties of cured products. *polymer* **2001,** *42*, 7617-7625.

54. Ramezanzadeh, B.; Bahlakeh, G.; Mohamadzadeh Moghadam, M. H.; Miraftab, R., Impact of size-controlled p-phenylenediamine (PPDA)-functionalized graphene oxide nanosheets on the GO-PPDA/Epoxy anti-corrosion, interfacial interactions and mechanical properties enhancement: Experimental and quantum mechanics investigations. *Chemical Engineering Journal* **2018,** *335*, 737-755.

55. Kong, Q.; Wu, T.; Zhang, J.; Wang, D.-Y., Simultaneously improving flame retardancy and dynamic mechanical properties of epoxy resin nanocomposites through layered copper phenylphosphate. *Composites Science and Technology* **2018,** *154*, 136-144.

56. Yang, P.; Ren, M.; Chen, K.; Liang, Y.; Lü, Q.-F.; Zhang, T., Synthesis of a novel silicon-containing epoxy resin and its effect on flame retardancy, thermal, and mechanical properties of thermosetting resins. *Materials Today Communications* **2019,** *19*, 186-195.

57. Wang, Y.; Zhao, J.; Yuan, Y.; Liu, S.; Feng, Z.; Zhao, Y., Synthesis of maleimido-substituted aromatic s-triazine and its application in flame-retarded epoxy resins. *Polymer Degradation and Stability* **2014,** *99*, 27-34.

58. Xu, W.; Zhang, B.; Wang, X.; Wang, G.; Ding, D., The flame retardancy and smoke suppression effect of a hybrid containing CuMoO(4) modified reduced graphene oxide/layered double hydroxide on epoxy resin. *J Hazard Mater* **2018,** *343*, 364-375.

59. Xiao, Y.; Mu, X.; Wang, B.; Hu, W.; Wang, J.; Zhou, F.; Ma, C.; Hu, Y.; Song, L., A novel phosphorous-containing polymeric compatibilizer: Effective reinforcement and flame retardancy in glass fiber reinforced polyamide 6 composites. *Composites Part B: Engineering* **2021,** *205*, 108536.

60. Saba, N.; Jawaid, M.; Alothman, O. Y.; Inuwa, I. M.; Hassan, A., A review on potential development of flame retardant kenaf fibers reinforced polymer composites. *Polymers for Advanced Technologies* **2017,** *28* (4), 424-434.

61. Saba, N.; Jawaid, M.; Paridah, M. T.; Al-othman, O. Y., A review on flammability of epoxy polymer, cellulosic and non-cellulosic fiber reinforced epoxy composites. *Polymers for Advanced Technologies* **2016,** *27* (5), 577-590.
62. Song, X.; Song, F.; Ding, X.-M.; Wu, J.-M.; Wang, X.-H.; Wang, F.; Feng, R.; Wang, X.-L.; Wang, Y.-Z., Construction of bio-based ramie fabric/epoxy resin composites with high flame retardant and mechanical performances. *Industrial Crops and Products* **2023,** *194*, 116281.
63. Liu, T.; Butaud, P.; Placet, V.; Ouisse, M., Damping behavior of plant fiber composites: A review. *Composite Structures* **2021,** *275*, 114392.
64. Mohit, H.; Mavinkere Rangappa, S.; Siengchin, S.; Gorbatyuk, S.; Manimaran, P.; Alka Kumari, C.; Khan, A.; Doddamani, M., A comprehensive review on performance and machinability of plant fiber polymer composites. *Polymer Composites* **2021,** *43* (1), 608-623.
65. George, J.; Sreekala, M. S.; Thomas, S., A review on interface modification and characterization of natural fiber reinforced plastic composites. *Polymer Engineering & Science* **2004,** *41* (9), 1471-1485.
66. Fiore, V.; Scalici, T.; Nicoletti, F.; Vitale, G.; Prestipino, M.; Valenza, A., A new eco-friendly chemical treatment of natural fibers: Effect of sodium bicarbonate on properties of sisal fiber and its epoxy composites. *Composites Part B: Engineering* **2016,** *85*, 150-160.
67. Jochen Gassan a, Voytek S. Gutowski b, Effects of corona discharge and UV treatment on the properties of jute-fiber epoxy composites. *Composites Science and Technology* **2000,** *60*, 2857-2863.
68. Liu, Y.; Lv, X.; Bao, J.; Xie, J.; Tang, X.; Che, J.; Ma, Y.; Tong, J., Characterization of silane treated and untreated natural cellulosic fiber from corn stalk waste as potential reinforcement in polymer composites. *Carbohydr Polym* **2019,** *218*, 179-187.
69. Orue, A.; Jauregi, A.; Unsuain, U.; Labidi, J.; Eceiza, A.; Arbelaiz, A., The effect of alkaline and silane treatments on mechanical properties and breakage of sisal fibers and poly(lactic acid)/sisal fiber composites. *Composites Part A: Applied Science and Manufacturing* **2016,** *84*, 186-195.
70. Zhou, S.; Chen, X.; Huang, R.; Lin, Y.; Ye, X., Interfacial treatment-induced high-strength plant fiber/phenolic resin composite. *Front Mater* **2022,** *9*.

71. Huang, G.; Chen, F., Reaction of jute fiber with isocyanate component for the production of plant fiber-reinforced polyurethane composites. *Cellulose* **2019,** *26* (12), 7297-7308.
72. Ammari, M. S.; Belhadj, B.; Bederina, M.; Ferhat, A.; Quéneudec, M., Contribution of hybrid fibers on the improvement of sand concrete properties: Barley straws treated with hot water and steel fibers. *Constr Build Mater* **2020,** *233*, 117374.
73. Sarker, F.; Uddin, M. D. Z.; Sowrov, K.; Islam, M. S.; Miah, A., Improvement of mechanical and interfacial properties of hot water and sodium bicarbonate treated jute fibers for manufacturing high performance natural composites. *Polymer Composites* **2021,** *43* (3), 1330-1342.
74. Lei, B.; Liang, Y.; Feng, Y.; He, H.; Yang, Z., Preparation and Characteristics of Biocomposites Based on Steam Exploded Sisal Fiber Modified with Amphipathic Epoxidized Soybean Oil Resin. *Materials (Basel)* **2018,** *11* (9).
75. Zaman, H. U.; Khan, R. A., Acetylation used for natural fiber/polymer composites. *J Thermoplast Compos* **2019,** *34* (1), 3-23.
76. Oladele, I. O.; Michael, O. S.; Adediran, A. A.; Balogun, O. P.; Ajagbe, F. O., Acetylation Treatment for the Batch Processing of Natural Fibers: Effects on Constituents, Tensile Properties and Surface Morphology of Selected Plant Stem Fibers. *Fibers* **2020,** *8* (12), 73.
77. Joseph, S. K., P .; Thomas, S. , The role of interfacial interactions on the mechanical properties of banana fiber reinforced phenol formaldehyde composites. , , . *Compos. Interfaces* **2005,** *12*, 581-600.
78. Robles, E.; Csóka, L.; Labidi, J., Effect of Reaction Conditions on the Surface Modification of Cellulose Nanofibrils with Aminopropyl Triethoxysilane. *Coatings* **2018,** *8* (4), 139.
79. M. Castellano, A. G., ,∗ P. Fabbri, and M.N. Belgacem Modification of cellulose fibers with organosilanes: Under what conditions does coupling occur?
80. Azizah, A. B.; Rozman, H. D.; Azniwati, A. A.; Tay, G. S., The Effect of Filler Loading and Silane Treatment on Kenaf Core Reinforced Polyurethane Composites: Mechanical and Thermal Properties. *Journal of Polymers and the Environment* **2019,** *28* (2), 517-531.
81. Pei-Yu Kuo, S.-Y. W., Jin-Hau Chen, Huei-Chin Hsueh, Ming-Jer Tsai *, Effects of material compositions on the mechanical properties of

wood–plastic composites manufactured by injection molding. *Materials and Design* **2009,** *30*, 3489-3496.

82. Zini, E.; Scandola, M., Green composites: An overview. *Polymer Composites* **2011,** *32* (12), 1905-1915.

83. Zini, E.; Baiardo, M.; Armelao, L.; Scandola, M., Biodegradable polyesters reinforced with surface-modified vegetable fibers. *Macromol Biosci* **2004,** *4* (3), 286-95.

84. Akram Bhuiyan, M. S.; Roland, J. D.; Liu, B.; Reaume, M.; Zhang, Z.; Kelley, J. D.; Lee, B. P., In Situ Deactivation of Catechol-Containing Adhesive Using Electrochemistry. *J Am Chem Soc* **2020,** *142* (10), 4631-4638.

85. Liu, Y.; Ai, K.; Lu, L., Polydopamine and its derivative materials: synthesis and promising applications in energy, environmental, and biomedical fields. *Chem Rev* **2014,** *114* (9), 5057-115.

86. Zhang, C.; Gong, L.; Xiang, L.; Du, Y.; Hu, W.; Zeng, H.; Xu, Z. K., Deposition and Adhesion of Polydopamine on the Surfaces of Varying Wettability. *ACS Appl Mater Interfaces* **2017,** *9* (36), 30943-30950.

87. Ryou, M. H.; Lee, Y. M.; Park, J. K.; Choi, J. W., Mussel-inspired polydopamine-treated polyethylene separators for high-power li-ion batteries. *Adv Mater* **2011,** *23* (27), 3066-70.

88. Zhang, C.; Ma, M. Q.; Chen, T. T.; Zhang, H.; Hu, D. F.; Wu, B. H.; Ji, J.; Xu, Z. K., Dopamine-Triggered One-Step Polymerization and Codeposition of Acrylate Monomers for Functional Coatings. *ACS Appl Mater Interfaces* **2017,** *9* (39), 34356-34366.

89. Saiz-Poseu, J.; Mancebo-Aracil, J.; Nador, F.; Busque, F.; Ruiz-Molina, D., The Chemistry behind Catechol-Based Adhesion. *Angew Chem. Int. Ed. Engl.* **2019,** *58* (3), 696-714.

90. Kiliaris, P.; Papaspyrides, C. D., Polymer/layered silicate (clay) nanocomposites: An overview of flame retardancy. *Progress in Polymer Science* **2010,** *35* (7), 902-958.

91. Laoutid, F.; Bonnaud, L.; Alexandre, M.; Lopez-Cuesta, J. M.; Dubois, P., New prospects in flame retardant polymer materials: From fundamentals to nanocomposites. *Materials Science and Engineering: R: Reports* **2009,** *63* (3), 100-125.

92. Torero, J. L.; Gerhard, J. I.; Martins, M. F.; Zanoni, M. A. B.; Rashwan, T. L.; Brown, J. K., Processes defining smouldering

combustion: Integrated review and synthesis. *Prog. Energ. Combust.* **2020,** *81*, 100869.

93. Dogan, M.; Dogan, S. D.; Savas, L. A.; Ozcelik, G.; Tayfun, U., Flame retardant effect of boron compounds in polymeric materials. *Composites Part B: Engineering* **2021,** *222*, 109088.

94. Shui-Yu Lu, I. H., Recent developments in the chemistry of halogen-free flame retardant polymers. **2002**, 1661-1712.

95. Sharkey, M.; Harrad, S.; Abou-Elwafa Abdallah, M.; Drage, D. S.; Berresheim, H., Phasing-out of legacy brominated flame retardants: The UNEP Stockholm Convention and other legislative action worldwide. *Environ. Int.* **2020,** *144*, 106041.

96. Lee, P. S.; Jung, S. M., Flame retardancy of polyurethane foams prepared from green polyols with flame retardants. *Journal of Applied Polymer Science* **2021,** *139* (17).

97. Costes, L.; Laoutid, F.; Khelifa, F.; Rose, G.; Brohez, S.; Delvosalle, C.; Dubois, P., Cellulose/phosphorus combinations for sustainable fire retarded polylactide. *European Polymer Journal* **2016,** *74*, 218-228.

98. Sener, A. A.; Demirhan, E., The investigation of using magnesium hydroxide as a flame retardant in the cable insulation material by cross-linked polyethylene. *Mater. Design* **2008,** *29* (7), 1376-1379.

99. Zou, H.; Sun, J.; Gu, X. Y.; Jiang, P.; Liu, X. S.; Zhang, S., Preparation and characterization of flame retardant and low smoke releasing oil-resistant EVA/NBR blends. *Chinese Journal of Polymer Science* **2015,** *33* (4), 554-563.

100. Guo, W.; Nie, S.; Kalali, E. N.; Wang, X.; Wang, W.; Cai, W.; Song, L.; Hu, Y., Construction of SiO2@UiO-66 core–shell microarchitectures through covalent linkage as flame retardant and smoke suppressant for epoxy resins. *Composites Part B: Engineering* **2019,** *176*, 107261.

101. Zou, J. H.; Duan, H. J.; Chen, Y. S.; Ji, S.; Cao, J. F.; Ma, H. R., A P/N/S-containing high-efficiency flame retardant endowing epoxy resin with excellent flame retardance, mechanical properties and heat resistance. *Compos. Part B-Eng.* **2020,** *199*.

102. Xin Wang, W. G., Wei Cai, Junling Wang, Lei Song , Yuan Hu Recent advances in construction of hybrid nano-structures for flame retardant polymers application. *Appl. Mater Today* **2020,** *20*.

103. Yang, S.; Wang, J.; Huo, S. Q.; Cheng, L. F.; Wang, M., Preparation and flame retardancy of an intumescent flame-retardant epoxy resin

system constructed by multiple flame-retardant compositions containing phosphorus and nitrogen heterocycle. *Polymer Degradation and Stability* **2015,** *119*, 251-259.
104. Shui-Yu Lu, I. H., Recent developments in the chemistry of halogen-free flame retardant polymers.
105. Dittenber, D. B.; GangaRao, H. V. S., Critical review of recent publications on use of natural composites in infrastructure. *Composites Part A: Applied Science and Manufacturing* **2012,** *43* (8), 1419-1429.
106. Rakotomalala, M.; Wagner, S.; Doring, M., Recent Developments in Halogen Free Flame Retardants for Epoxy Resins for Electrical and Electronic Applications. *Materials* **2010,** *3* (8), 4300-4327.
107. Wan, C.; Duan, H.; Zhang, C.; Liu, C.; Zhao, H.; Ma, H., Synthesis of a Multielement Flame Retardant and Its Application in Epoxy Resin. *ACS Applied Polymer Materials* **2023,** *5* (3), 1775-1785.
108. Luo, X.; Shen, J.; Ma, Y.; Liu, L.; Meng, R.; Yao, J., Robust, sustainable cellulose composite aerogels with outstanding flame retardancy and thermal insulation. *Carbohydr. Polym.* **2020,** *230*, 115623.
109. Ho, T.-H.; Hwang, H.-J.; Shieh, J.-Y.; Chung, M.-C., Thermal, physical and flame-retardant properties of phosphorus-containing epoxy cured with cyanate ester. *Reactive and Functional Polymers* **2009,** *69* (3), 176-182.
110. Buczko, A.; Stelzig, T.; Bommer, L.; Rentsch, D.; Heneczkowski, M.; Gaan, S., Bridged DOPO derivatives as flame retardants for PA6. *Polymer Degradation and Stability* **2014,** *107*, 158-165.
111. Sag, J.; Goedderz, D.; Kukla, P.; Greiner, L.; Schonberger, F.; Doring, M., Phosphorus-Containing Flame Retardants from Biobased Chemicals and Their Application in Polyesters and Epoxy Resins. *Molecules* **2019,** *24* (20).
112. Gaan, S.; Liang, S.; Mispreuve, H.; Perler, H.; Naescher, R.; Neisius, M., Flame retardant flexible polyurethane foams from novel DOPO-phosphonamidate additives. *Polymer Degradation and Stability* **2015,** *113*, 180-188.
113. Hu, J.; Shan, J.; Wen, D.; Liu, X.; Zhao, J.; Tong, Z., Flame retardant, mechanical properties and curing kinetics of DOPO-based epoxy resins. *Polymer Degradation and Stability* **2014,** *109*, 218-225.

114.Qian, L.; Qiu, Y.; Wang, J.; Xi, W., High-performance flame retardancy by char-cage hindering and free radical quenching effects in epoxy thermosets. *Polymer* **2015,** *68*, 262-269.
115. Li, X.; Xie, Q.; Lin, J.; Huang, J.; Xie, K.; Liu, J.; Li, X.; Wei, W., A phosphorus/silicon‐containing flame retardant based on eugenol for improving flame retardancy and smoke suppression of epoxy resin. *Journal of Applied Polymer Science* **2023,** *140* (39).
116. Zhao, J. J.; Dong, X.; Huang, S.; Tian, X. J.; Song, L.; Yu, Q.; Wang, Z. W., Performance comparison of flame retardant epoxy resins modified by DPO-PHE and DOPO-PHE. *Polymer Degradation and Stability* **2018,** *156*, 89-99.
117. Battig, A.; Müller, P.; Bertin, A.; Schartel, B., Hyperbranched Rigid Aromatic Phosphorus‐Containing Flame Retardants for Epoxy Resins. *Macromolecular Materials and Engineering* **2021,** *306* (4).
118. Wenchao Zhang, X. L., Rongjie Yang, Blowing-out effect in epoxy composites flame retarded by DOPO-POSS and its correlation with amide curing agents. *Polymer Degradation and Stability* **2012,** *97*, 1314-1324.
119. Gao, M.; Yang, S., A novel intumescent flame‐retardant epoxy resins system. *Journal of Applied Polymer Science* **2009,** *115* (4), 2346-2351.
120. Wang, X.; Hu, Y.; Song, L.; Yang, H. Y.; Xing, W. Y.; Lu, H. D., Synthesis and characterization of a DOPO-substitued organophosphorus oligomer and its application in flame retardant epoxy resins. *Progress in Organic Coatings* **2011,** *71* (1), 72-82.
121. Yang, S.; Wang, J.; Huo, S. Q.; Wang, M.; Cheng, L. F., Synthesis of a Phosphorus/Nitrogen-Containing Additive with Multifunctional Groups and Its Flame-Retardant Effect in Epoxy Resin. *Industrial & Engineering Chemistry Research* **2015,** *54* (32), 7777-7786.
122. Kumar, S. A.; Denchev, Z., Development and characterization of phosphorus-containing siliconized epoxy resin coatings. *Progress in Organic Coatings* **2009,** *66* (1), 1-7.
123. Schartel, B.; Balabanovich, A. I.; Braun, U.; Knoll, U.; Artner, J.; Ciesielski, M.; Döring, M.; Perez, R.; Sandler, J. K. W.; Altstädt, V.; Hoffmann, T.; Pospiech, D., Pyrolysis of epoxy resins and fire behavior of epoxy resin composites flame‐retarded with

9,10 - dihydro - 9 - oxa - 10 - phosphaphenanthrene - 10 - oxide additives. *Journal of Applied Polymer Science* **2007,** *104* (4), 2260-2269.
124.Tang, S.; Qian, L. J.; Liu, X. X.; Dong, Y. P., Gas-phase flame-retardant effects of a bi-group compound based on phosphaphenanthrene and triazine-trione groups in epoxy resin. *Polymer Degradation and Stability* **2016,** *133*, 350-357.
125. Qian, L. J.; Qiu, Y.; Sun, N.; Xu, M. L.; Xu, G. Z.; Xin, F.; Chen, Y. J., Pyrolysis route of a novel flame retardant constructed by phosphaphenanthrene and triazine-trione groups and its flame-retardant effect on epoxy resin. *Polymer Degradation and Stability* **2014,** *107*, 98-105.
126. Chen, R.; Hu, K.; Tang, H.; Wang, J.; Zhu, F.; Zhou, H., A novel flame retardant derived from DOPO and piperazine and its application in epoxy resin: Flame retardance, thermal stability and pyrolysis behavior. *Polymer Degradation and Stability* **2019,** *166*, 334-343.
127. Zou, B.; Qiu, S. L.; Qian, Z. Y.; Wang, J. W.; Zhou, Y. F.; Xu, Z. M.; Yang, W. H.; Xing, W. Y., Phosphorus/Nitrogen-Codoped Molybdenum Disulfide/Cobalt Borate Nanostructures for Flame-Retardant and Tribological Applications. *Acs Appl. Nano Mater.* **2021,** *4* (10), 10495-10504.
128. Zong, L. Y.; Li, L. Y.; Zhang, J. Y.; Yang, X. B.; Lu, G. X.; Tang, Z. C., Synthesis of High Dispersion and Uniform Nano-sized Flame Retardant-Used Hexagonal Mg(OH)(2). *J. Clust. Sci.* **2016,** *27* (6), 1831-1841.
129. Sain, M.; Park, S. H.; Suhara, F.; Law, S., Flame retardant and mechanical properties of natural fiber–PP composites containing magnesium hydroxide. *Polymer Degradation and Stability* **2004,** *83* (2), 363-367.
130. Jeencham, R.; Suppakarn, N.; Jarukumjorn, K., Effect of flame retardants on flame retardant, mechanical, and thermal properties of sisal fiber/polypropylene composites. *Composites Part B: Engineering* **2014,** *56*, 249-253.
131. Zou, L. Y.; Liu, J. Y.; Liu, X. Q.; Wang, X. M.; Chen, J., Synthesis and performance of star-shaped aluminum phosphinate flame retardant. *J Therm Anal Calorim* **2016,** *124* (3), 1399-1409.
132. Zhou, K.; Gao, R.; Qian, X., Self-assembly of exfoliated molybdenum disulfide (MoS(2)) nanosheets and layered double

hydroxide (LDH): Towards reducing fire hazards of epoxy. *J. Hazard Mater.* **2017,** *338*, 343-355.
133. Wang, W.; Wang, J.; Wang, X.; Wang, S.; Liu, X.; Qi, P.; Li, H.; Sun, J.; Tang, W.; Zhang, S.; Gu, X., Improving flame retardancy and self-cleaning performance of cotton fabric via a coating of in-situ growing layered double hydroxides (LDHs) on polydopamine. *Progress in Organic Coatings* **2020,** *149*, 105930.
134. Gu, L.; Qiu, J.; Yao, Y.; Sakai, E.; Yang, L., Functionalized MWCNTs modified flame retardant PLA nanocomposites and cold rolling process for improving mechanical properties. *Composites Science and Technology* **2018,** *161*, 39-49.
135. Zuo, L. Z.; Fan, W.; Zhang, Y. F.; Zhang, L. S.; Gao, W.; Huang, Y. P.; Liu, T. X., Graphene/montmorillonite hybrid synergistically reinforced polyimide composite aerogels with enhanced flame-retardant performance. *Composites Science and Technology* **2017,** *139*, 57-63.
136. Guo, Z.; Ye, R.; Zhao, L.; Ran, S.; Fang, Z.; Li, J., Fabrication of fullerene-decorated graphene oxide and its influence on flame retardancy of high density polyethylene. *Composites Science and Technology* **2016,** *129*, 123-129.
137. Chen, X.; Peng, F.; Wang, C.; Zhou, H.; Lin, X.; Liu, W.; Zhang, A., Improving the flame retardancy and mechanical properties of epoxy composites significantly with a low-loading CNT-based hierarchical hybrid decorated with reactive hyperbranched polyphosphoramide. *Applied Surface Science* **2022,** *576*, 151765.
138. Wu, Q.; Bao, J.; Zhang, C.; Liang, R.; Wang, B., The effect of thermal stability of carbon nanotubes on the flame retardancy of epoxy and bismaleimide/carbon fiber/buckypaper composites. *J. Therm. Anal. Calorim.* **2010,** *103* (1), 237-242.
139. Jiang, W., Jin, Fan-Long, Park, Soo-Jin, Synthesis of a novel phosphorus-nitrogen-containing intumescent flame retardant and its application to fabrics. *Journal of Industrial and Engineering Chemistry* **2015,** *27*, 40-43.
140. Jordanov, I.; Magovac, E.; Fahami, A.; Lazar, S.; Kolibaba, T.; Smith, R. J.; Bischof, S.; Grunlan, J. C., Flame retardant polyester fabric from nitrogen-rich low molecular weight additives within intumescent nanocoating. *Polymer Degradation and Stability* **2019,** *170*, 108998.

141. Xu, J.; Wu, Y.; Zhang, B.; Zhang, G., Synthesis and synergistic flame‐retardant effects of rigid polyurethane foams used reactive DOPO‐based polyols combination with expandable graphite. *Journal of Applied Polymer Science* **2020,** *138* (16), 50223.
142. Gao, F.; Tong, L.; Fang, Z., Effect of a novel phosphorous–nitrogen containing intumescent flame retardant on the fire retardancy and the thermal behaviour of poly(butylene terephthalate). *Polymer Degradation and Stability* **2006,** *91* (6), 1295-1299.
143. Zhang, J.; Li, Z.; Yin, G.-Z.; Wang, D.-Y., Construction of a novel three-in-one biomass based intumescent fire retardant through phosphorus functionalized metal-organic framework and β-cyclodextrin hybrids in achieving fire safe epoxy. *Composites Communications* **2021,** *23*, 100594.
144. Xu, J.; Ou, H.; Shan, X.; Liu, B.; Jiang, J.; Xu, G., Investigation of novel intumescent flame retardant low‐density polyethylene based on SiO_2@MAPP and double pentaerythritol. *Journal of Applied Polymer Science* **2020,** *137* (41), 49242.
145. Zhu, F. L.; Xin, Q.; Feng, Q. Q.; Liu, R. T.; Li, K. J., Influence of nano-silica on flame resistance behavior of intumescent flame retardant cellulosic textiles: Remarkable synergistic effect? *Surf. Coat Tech.* **2016,** *294*, 90-94.
146. Xu, J.; Li, Y.; Yu, T.; Cong, L., Reinforcement of denture base resin with short vegetable fiber. *Dent. Mater.* **2013,** *29* (12), 1273-9.
147. Dong, S.; Xian, G.; Yi, X.-S., Life Cycle Assessment of Ramie Fiber Used for FRPs. *Aerospace* **2018,** *5* (3), 81.
148. Houston, J. H. a. D., Natural-Fiber-Reinforced Polymer Composites in Automotive Applications. *JOM* **2006,** 58, 80-86.
149. Baruah, P.; Karak, N., Bio-based tough hyperbranched epoxy/graphene oxide nanocomposite with enhanced biodegradability attribute. *Polymer Degradation and Stability* **2016,** *129*, 26-33.
150. Liu, J.; Dai, J.; Wang, S.; Peng, Y.; Cao, L.; Liu, X., Facile synthesis of bio-based reactive flame retardant from vanillin and guaiacol for epoxy resin. *Composites Part B: Engineering* **2020,** *190*, 107926.
151. Subasinghe, A.; Bhattacharyya, D., Performance of different intumescent ammonium polyphosphate flame retardants in PP/kenaf fiber composites. *Compos. Part a-Appl. S.* **2014,** *65*, 91-99.

152. Rybyan, A. A.; Bilichenko, J. V.; Kireev, V. V.; Kolenchenko, A. A.; Chistyakov, E. M., Curing of DER-331 Epoxy Resin with Arylaminocyclotriphosphazenes Based on o-, m-, and p-methylanilines. *Polymers (Basel)* **2022,** *14* (24).
153. Alongi, J.; Malucelli, G., State of the art and perspectives on sol–gel derived hybrid architectures for flame retardancy of textiles. *J. Mater. Chem.* **2012,** *22* (41), 21805-21809.
154. Tai, Q.; Song, L.; Hu, Y.; Yuen, R. K. K.; Feng, H.; Tao, Y., Novel styrene polymers functionalized with phosphorus–nitrogen containing molecules: Synthesis and properties. *Materials Chemistry and Physics* **2012,** *134* (1), 163-169.
155. Nabipour, H.; Wang, X.; Batool, S.; Song, L.; Hu, Y., A phosphaphenanthrene-containing vanillin derivative as co-curing agent for flame-retardant and antibacterial epoxy thermoset. *Polymer* **2021,** *217*, 123460.
156. Wang, J.; Tang, H.; Yu, X.; Xu, J.; Pan, Z.; Zhou, H., Reactive organophosphorus flame retardant for transparency, low‐flammability, and mechanical reinforcement epoxy resin. *Journal of Applied Polymer Science* **2021,** *138* (23), 50536.
157. Wang, P.; Cai, Z., Highly efficient flame-retardant epoxy resin with a novel DOPO-based triazole compound: Thermal stability, flame retardancy and mechanism. *Polymer Degradation and Stability* **2017,** *137*, 138-150.
158. Yousif, B. F.; Ku, H., Suitability of using coir fiber/polymeric composite for the design of liquid storage tanks. *Materials & Design (1980-2015)* **2012,** *36*, 847-853.
159. Shumao, L.; Jie, R.; Hua, Y.; Tao, Y.; Weizhong, Y., Influence of ammonium polyphosphate on the flame retardancy and mechanical properties of ramie fiber-reinforced poly(lactic acid) biocomposites. *Polymer International* **2010,** *59* (2), 242-248.
160. Tang, X.-Z.; Yu, B.; Hansen, R. V.; Chen, X.; Hu, X.; Yang, J., Grafting Low Contents of Branched Polyethylenimine onto Carbon Fibers to Effectively Improve Their Interfacial Shear Strength with an Epoxy Matrix. *Adv. Mater. Interfaces* **2015,** *2* (12), 1500122.
161. Chhetri, S.; Bougherara, H., A comprehensive review on surface modification of UHMWPE fiber and interfacial properties. *Composites Part A: Applied Science and Manufacturing* **2021,** *140*, 106146.

162. Xing, L.; Liu, L.; Huang, Y.; Jiang, D.; Jiang, B.; He, J., Enhanced interfacial properties of domestic aramid fiber-12 via high energy gamma ray irradiation. *Composites Part B: Engineering* **2015,** *69*, 50-57.
163. Shih, Y.-F., Mechanical and thermal properties of waste water bamboo husk fiber reinforced epoxy composites. *Materials Science and Engineering: A* **2007,** *445-446*, 289-295.
164. Seki, Y., Innovative multifunctional siloxane treatment of jute fiber surface and its effect on the mechanical properties of jute/thermoset composites. *Materials Science and Engineering: A* **2009,** *508* (1-2), 247-252.
165. Zhou, Y.; Kang, L.; Yue, Z.; Liu, X.; Wallace, G. G., Composite Tissue Adhesive Containing Catechol-Modified Hyaluronic Acid and Poly-l-lysine. *ACS Applied Bio Materials* **2019,** *3* (1), 628-638.
166. Dai, J.; Teng, N.; Peng, Y.; Liu, Y.; Cao, L.; Zhu, J.; Liu, X., Biobased Benzoxazine Derived from Daidzein and Furfurylamine: Microwave-Assisted Synthesis and Thermal Properties Investigation. *ChemSusChem* **2018,** *11* (18), 3175-3183.
167. Yan, H.; Li, N.; Cheng, J.; Song, P.; Fang, Z.; Wang, H., Fabrication of flame retardant benzoxazine semi-biocomposites reinforced by ramie fabrics with bio-based flame retardant coating. *Polymer Composites* **2018,** *39*, E480-E488.
168. Kwak, W. G.; Oh, M. H.; Gong, M. S., Preparation of silver-coated cotton fabrics using silver carbamate via thermal reduction and their properties. *Carbohydr Polym* **2015,** *115*, 317-24.
169. Tian, C.; Wang, C.; Ren, X.; Hong, L., Synthesis of silane-modified polyphosphate esters and its application in transparent flame-retardant coatings. *Journal of Applied Polymer Science* **2019,** *136* (11), 47199.
170. Luo, Y. F.; Wang, S.; Du, X. S.; Du, Z. L.; Cheng, X.; Wang, H. B., Durable flame retardant and water repellent cotton fabric based on synergistic effect of ferrocene and DOPO. *Cellulose* **2021,** *28* (3), 1809-1826.
171. Zuo, J. D.; Liu, S. M.; Sheng, Q., Synthesis and Application in Polypropylene of a Novel of Phosphorus-Containing Intumescent Flame Retardant. *Molecules* **2010,** *15* (11), 7593-7602.
172. Teng, N.; Dai, J.; Wang, S.; Hu, J.; Liu, X., Hyperbranched flame retardant for epoxy resin modification: Simultaneously improved flame

retardancy, toughness and strength as well as glass transition temperature. *Chemical Engineering Journal* **2022,** *428*, 131226.
173. Feng, Y.; He, C.; Wen, Y.; Ye, Y.; Zhou, X.; Xie, X.; Mai, Y. W., Superior flame retardancy and smoke suppression of epoxy-based composites with phosphorus/nitrogen co-doped graphene. *J. Hazard Mater.* **2018,** *346*, 140-151.
174. Forte, C.; Alongi, J.; Beduini, A.; Borsacchi, S.; Calucci, L.; Carosio, F.; Ferruti, P.; Ranucci, E., The Thermo-Oxidative Behavior of Cotton Coated with an Intumescent Flame Retardant Glycine-Derived Polyamidoamine: A Multi-Technique Study. *Polymers (Basel)* **2021,** *13* (24).
175. Wang, J.; Guo, Y.; Zhao, S. P.; Huang, R. Y.; Kong, X. J., A novel intumescent flame retardant imparts high flame retardancy to epoxy resin. *Polymers for Advanced Technologies* **2020,** *31* (5), 932-940.
176. Lu, H.; Wilkie, C. A., Study on intumescent flame retarded polystyrene composites with improved flame retardancy. *Polymer Degradation and Stability* **2010,** *95* (12), 2388-2395.
177. Cheng, J.; Wang, J.; Yang, S.; Zhang, Q.; Huo, S.; Zhang, Q.; Hu, Y.; Ding, G., Benzimidazolyl-substituted cyclotriphosphazene derivative as latent flame-retardant curing agent for one-component epoxy resin system with excellent comprehensive performance. *Composites Part B: Engineering* **2019,** *177*, 107440.
178. Fogorasi, M. S.; Barbu, I., The potential of natural fibers for automotive sector -review. *IOP Conference Series: Materials Science and Engineering* **2017,** *252*, 012044.
179. Yu, X.; Pan, Y.; Wang, D.; Yuan, B.; Song, L.; Hu, Y., Fabrication and Properties of Biobased Layer-by-Layer Coated Ramie Fabric-Reinforced Unsaturated Polyester Resin Composites. *Industrial & Engineering Chemistry Research* **2017,** *56* (16), 4758-4767.
180. Cui, J. F.; Li, F. Y.; Li, J. Y.; Li, J. F.; Zhang, C. W.; Chen, S.; Sun, X., Effects of magnesium hydroxide on the properties of starch/plant fiber composites with foam structure. *RSC Adv.* **2019,** *9* (30), 17405-17413.
181. H.P.S.A. Khalil, H. I., H.D. Rozman, M.N. Ahmad The effect of acetylation on interfacial shear strength between plant fibers and various matrices. *European Polymer Journal* **2001,** *37*, 1037-1045.

182. Ahmad, R.; Hamid, R.; Osman, S. A., Physical and Chemical Modifications of Plant Fibers for Reinforcement in Cementitious Composites. *Advances in Civil Engineering* **2019,** *2019*, 1-18.
183. Chen, J.; Wang, J.; Ding, A.; Ni, A.; Chen, H., Flame retardancy and mechanical properties of glass fiber reinforced polyethylene composites filled with novel intumescent flame retardant. *Composites Part B: Engineering* **2019,** *179*, 107555.
184. Yu, T.; Jiang, N.; Li, Y., Functionalized multi-walled carbon nanotube for improving the flame retardancy of ramie/poly(lactic acid) composite. *Composites Science and Technology* **2014,** *104*, 26-33.
185. Zhu, Z. M.; Wang, L. X.; Dong, L. P., Influence of a novel P/N-containing oligomer on flame retardancy and thermal degradation of intumescent flame-retardant epoxy resin. *Polymer Degradation and Stability* **2019,** *162*, 129-137.
186. Zhang, X.; Liu, L.; Yu, Y.; Weng, L., Flame - Retardant Mechanism of Benzoxazine Resin with Triazine Structure. *Adv. Polym. Tech.* **2016,** *37* (2), 384-389.
187. Wang, Z. J.; Liu, Y. F.; Li, J., Regulating Effects of Nitrogenous Bases on the Char Structure and Flame Retardancy of Polypropylene/Intumescent Flame Retardant Composites. *Acs Sustainable Chemistry & Engineering* **2017,** *5* (3), 2375-2383.
188. Wang, C.; Wu, Y. C.; Li, Y. C.; Shao, Q.; Yan, X. R.; Han, C.; Wang, Z.; Liu, Z.; Guo, Z. H., Flame-retardant rigid polyurethane foam with a phosphorus-nitrogen single intumescent flame retardant. *Polymers for Advanced Technologies* **2018,** *29* (1), 668-676.
189. Chi, Z.; Guo, Z.; Xu, Z.; Zhang, M.; Li, M.; Shang, L.; Ao, Y., A DOPO-based phosphorus-nitrogen flame retardant bio-based epoxy resin from diphenolic acid: Synthesis, flame-retardant behavior and mechanism. *Polymer Degradation and Stability* **2020,** *176*, 109151.
190. Jin, D.; Dai, J.; Zhang, L.; Chen, Q.; Liu, X., Hyperbranched Phosphorus-Containing Benzoxazine for Epoxy Modification: Flame Retardant and Toughening Agent. *Ind. Eng. Chem. Res.* **2023,** *62, 18, 7262–7274*.
191. Yu, Z.; Ma, S.; Liu, Y.; Su, Y.; Feng, H.; Li, P.; Dong, Y.; Tang, Z.; Zhang, K.; Zhu, J., Facile synthesis of bio-based latent curing agent and its high-Tg epoxy network. *European Polymer Journal* **2022,** *164*, 110965.

192. Zhu, Z. M.; Shang, K.; Wang, L. X.; Wang, J. S., Synthesis of an effective bio-based flame-retardant curing agent and its application in epoxy resin: Curing behavior, thermal stability and flame retardancy. *Polymer Degradation and Stability* **2019,** *167*, 179-188.
193. Barth, A., The infrared absorption of amino acid side chains. *Progress in Biophysics & Molecular Biology* **2000,** *74*, 141-173.